Title: Islet-reactive CD8$^+$ T-cell frequencies in the pancreas but not blood distinguish type 1 diabetes from healthy donors

Authors: Slobodan Culina[1,2,3†], Ana Ines Lalanne[1,2,3†], Georgia Afonso[1,2,3], Karen Cerosaletti[4], Sheena Pinto[5], Guido Sebastiani[6], Klaudia Kuranda[1,2,3], Laura Nigi[6], Anne Eugster[7], Thomas Osterbye[8], Alicia Maugein[1,2,3], James E. McLaren[9], Kristin Ladell[9], Etienne Larger[1,2,3,10], Jean-Paul Beressi[11], Anna Lissina[12,13], Victor Appay[12,13], Howard W. Davidson[14], Soren Buus[8], David A. Price[9,15], Matthias Kuhn[16], Ezio Bonifacio[7], Manuela Battaglia[17], Sophie Caillat-Zucman[18], Francesco Dotta[6], Raphael Scharfmann[1,2,3], Bruno Kyewski[5], Roberto Mallone[1,2,3,10*] and the ImMaDiab Study Group[‡].

Affiliations:
[1]INSERM, U1016, Cochin Institute, Paris, France.
[2]CNRS, UMR8104, Cochin Institute, Paris, France.
[3]Paris Descartes University, Sorbonne Paris Cité, Paris, France.
[4]Benaroya Research Institute, Translational Research Program, Seattle, WA 98101, USA.
[5]DKFZ, Division of Developmental Immunology, Heidelberg, Germany.
[6]University of Siena, Department of Medicine, Surgery and Neuroscience, Diabetes Unit and Fondazione Umberto di Mario ONLUS, Toscana Life Sciences, Siena, Italy.
[7]CRTD-DFG Research Center for Regenerative Therapies Dresden, Medical Faculty, Technische Universität Dresden, Dresden, Germany.
[8]Panum Institute, Department of International Health, Immunology and Microbiology, Copenhagen, Denmark.
[9]Division of Infection and Immunity, Cardiff University School of Medicine, Cardiff, UK.
[10]Assistance Publique Hôpitaux de Paris, Service de Diabétologie, Cochin Hospital, Paris, France.
[11]Centre Hospitalier de Versailles André Mignot, Service de Diabétologie, Le Chesnay, France.
[12]Pierre et Marie Curie Paris 6 University, Sorbonne Paris Cité, DHU FAST, CR7, Centre d'Immunologie et des Maladies Infectieuses (CIMI-Paris), Paris, France.
[13]INSERM, U1135, CIMI-Paris, Paris, France.
[14]Barbara Davis Center for Diabetes and Integrated Department of Immunology, University of Colorado Denver Anschutz Medical Campus, Aurora, CO 80045, USA.
[15]Vaccine Research Center, National Institute of Allergy and Infectious Diseases, National Institutes of Health, Bethesda, MD 20892, USA.
[16]Institut für Medizinische Informatik und Biometrie, Medical Faculty, Technische Universität Dresden, Dresden, Germany.
[17]Diabetes Research Institute, IRCCS San Raffaele Scientific Institute, Milan, Italy.
[18]Assistance Publique Hôpitaux de Paris, Laboratoire d'Immunologie et Histocompatibilité, Hôpital Saint-Louis, Paris, France.

†S. Culina and A.I. Lalanne are co-first authors.
‡Members of the ImMaDiab Study Group are listed in Supplementary Materials

*Corresponding author: Roberto Mallone, MD PhD INSERM U1016 Cochin Institute, DcARLab – Cochin-Port Royal Hospital, Cassini Building – 123, boulevard de Port Royal, F-75014 Paris, France. Phone: +33-1-76.53.55.83. E-mail: roberto.mallone@inserm.fr

Abstract: The human leukocyte antigen (HLA)-A2-restricted zinc transporter (ZnT)$8_{186\text{-}194}$ and other islet epitopes elicit interferon-γ secretion by $CD8^+$ T cells preferentially in type 1 diabetes (T1D) patients compared with controls. Here, we show that clonal $ZnT8_{186\text{-}194}$-reactive $CD8^+$ T cells express private T-cell receptors and display equivalent functional properties in T1D and healthy subjects. *Ex-vivo* analyses further revealed that $CD8^+$ T cells reactive to $ZnT8_{186\text{-}194}$ and other islet epitopes circulate at similar frequencies and exhibit a predominantly naïve phenotype in age-matched T1D and healthy donors. Higher frequencies of $ZnT8_{186\text{-}194}$-reactive $CD8^+$ T cells with a more antigen-experienced phenotype were detected in children *vs.* adults, irrespective of disease status. Moreover, some $ZnT8_{186\text{-}194}$-reactive $CD8^+$ T-cell clonotypes were found to cross-recognize a *Bacteroides stercoris* mimotope. While ZnT8 was poorly expressed in thymic medullary epithelial cells, variable thymic expressions levels of islet antigens did not modulate the peripheral frequency of their cognate $CD8^+$ T cells. In contrast, $ZnT8_{186\text{-}194}$-reactive cells were enriched in the pancreata of T1D donors *vs.* non-diabetic and type 2 diabetic controls. Thus, islet-reactive $CD8^+$ T cells circulate in most individuals, but home to the pancreas preferentially in T1D patients. We conclude that the activation of this common islet-reactive T-cell repertoire and progression to T1D likely require defective peripheral immunoregulation and/or a pro-inflammatory islet microenvironment.

One Sentence Summary: Islet-reactive $CD8^+$ T cells are common in the periphery, but home to the pancreas preferentially in the context of type 1 diabetes.

[Main Text:]

Introduction

In the setting of type 1 diabetes (T1D), insulitic lesions are enriched for $CD8^+$ T cells, which are held as the final mediators of islet destruction. Concordantly, preproinsulin (PPI)-reactive $CD8^+$ T-cell clones can lyse β cells *in-vitro* (*1*), and β-cell-reactive $CD8^+$ T cells infiltrate the islets of T1D patients (*2*). Autoimmune $CD8^+$ T cells may therefore provide new biomarkers for disease staging complementary to auto-antibodies (aAbs). While interferon (IFN)-γ-secreting $CD8^+$ T cells detected by enzyme-linked immunospot (ELISpot) distinguish T1D patients from healthy donors (*3*), the situation is more complex when non-functional human leukocyte antigen (HLA) Class I multimer (MMr) assays are used. Although MMr^+CD8^+ T cells were often (*4*), but not invariably (*5, 6*), found at similar frequencies in both T1D and healthy subjects, they have been reported to exhibit more differentiated effector/memory phenotypes (*4, 6*) in T1D patients. A rather enigmatic state of 'benign' autoimmunity therefore exists in healthy individuals.

We therefore aimed to determine the key features of islet-reactive $CD8^+$ T cells that associate with T1D. We focused our efforts on well-defined HLA-A*02:01 (HLA-A2)-restricted immunodominant epitopes derived from PPI, glutamic acid decarboxylase (GAD), insulinoma-associated protein-2 (IA-2), and islet-specific glucose-6-phosphatase catalytic subunit-related protein (IGRP) (*3*), and on a highly immunoprevalent zinc transporter $(ZnT)8_{186\text{-}194}$ epitope that we recently described (*7*). The results indicate that incomplete central tolerance mechanisms allow the survival of an islet-reactive $CD8^+$ T-cell repertoire, which in some individuals may be primed in the presence of defective peripheral immunoregulation and/or a pro-inflammatory islet microenvironment to progress toward T1D.

Results

$ZnT8_{186-194}$-reactive $CD8^+$ T-cell clones from T1D and healthy donors display equivalent functionality

Given that $ZnT8_{186-194}$-reactive IFN-γ responses are highly prevalent in T1D patients (*7*), we started by generating $ZnT8_{186-194}$-reactive $CD8^+$ T-cell clones from a new-onset T1D patient (D222D) (*7*). Following *in-vitro* expansion with the $ZnT8_{186-194}$ peptide (*8*), HLA-A2 MMr^+ cells were labeled with two different fluorochromes (*9*) and sorted (Fig. 1A). The 3 clones thus generated stained uniformly positive with $ZnT8_{186-194}$ MMrs (Fig. 1B) and responded to $ZnT8_{186-194}$ peptide stimulation by secreting tumor necrosis factor (TNF)-α (Fig. 1C), IFN-γ, interleukin (IL)-2 and, to a lesser extent, macrophage inflammatory protein (MIP)-1β in a dose-dependent fashion (Fig. S1A-C). Cytotoxicity was then tested against an $HLA\text{-}A2^+$ Epstein-Barr virus (EBV)-transformed B-lymphoblastoid cell line (LCL) pulsed with the cognate $ZnT8_{186-194}$ peptide. Increasing numbers of clonal $CD8^+$ T cells led to the complete disappearance of $ZnT8_{186-194}$-pulsed but not control-pulsed targets, with ≥90% lysis at a 1/2 effector/target (E/T) ratio (Fig. 1D-E and S1D-F). This lytic activity was mostly perforin-mediated (Fig. 1F), as it was inhibited significantly by concanamycin A, marginally by brefeldin A (suppressing cytokine secretion) and not at all by a blocking anti-FasL mAb (suppressing Fas-dependent cytotoxicity), and it was associated with CD107a upregulation (Fig. 1G).

Additional $ZnT8_{186-194}$-reactive $CD8^+$ T-cell clones were generated from other T1D patients and healthy donors. The final panel comprised 16 clones (9 clones from 5 T1D patients and 7 clones from 5 healthy donors), most of which were isolated directly *ex-vivo* (Table S1). All but one clone (H328C 9B3) stained with HLA-A2 MMrs loaded with $ZnT8_{186-194}$ (VAANIVLTV), and several of them also with a longer $ZnT8_{185-194}$ variant (AVAANIVLTV) reported to exhibit similar immunoprevalence (Fig. S2A) (*10*). Higher staining intensities were observed with $ZnT8_{186-194}$ MMrs for all clones barring D010R 1D3. Concordantly,

$ZnT8_{186-194}$ bound to recombinant HLA-A2 molecules with higher affinity (K_D 15 nM *vs.* 207 nM) and similar stability ($t_{1/2}$ 1.8 h *vs.* 2.3 h) relative to the longer $ZnT8_{185-194}$ peptide (Fig. S2B-C). The $ZnT8_{186-194}$ epitope was therefore retained for subsequent experiments, except for clone D010R 1D3.

Clones from T1D and healthy donors were first compared for the intensity of $ZnT8_{186-194}$ MMr staining. The tyrosine kinase inhibitor dasatinib, which stabilizes T-cell receptor (TCR) interactions with peptide-HLA complexes (*11*), enhanced MMr staining, particularly for MMr^{low} clones (Fig. 2A). Heterogeneous staining patterns were observed when comparing normalized MMr fluorescence intensities (Fig. 2B). While dasatinib reduced variability, even in its absence no difference was apparent between the T1D and healthy group.

Next, we performed *in-vitro* recall assays with increasing $ZnT8_{186-194}$ peptide concentrations. Representative data are shown in Fig. 2C and results summarized in Fig. 2D-E. In line with the MMr staining profiles, the half maximal effective peptide concentration (EC50) required to elicit cytokine responses (TNF-α, IFN-γ, IL-2) and the maximal cytokine responses were again heterogeneous, but not significantly different between T1D and healthy clones (Fig. 2D-E), with one exception noted for the lower MIP-1β EC50 of T1D clones. Clones obtained after *in-vitro* expansion displayed an equivalent range of antigen (Ag) sensitivities, either high (D222D, H017N) or low (H328C), arguing against a bias compared with clones isolated directly *ex-vivo*. Moreover, the polyfunctionality index, which reflects the number of cells secreting multiple cytokines (*12*), was similar for T1D and healthy clones (Fig. 2F). As expected, EC50 values correlated negatively with MMr staining and polyfunctionality indices (Fig. S3).

Collectively, these results show that ZnT8-reactive $CD8^+$ T cells isolated from T1D and healthy subjects exhibit similar Ag avidity, sensitivity and polyfunctionality.

$ZnT8_{186-194}$-reactive $CD8^+$ T-cell clones from T1D and healthy donors display equivalent β-cell cytotoxicity

To determine if $ZnT8_{186-194}$-reactive $CD8^+$ T cells can recognize naturally processed ZnT8 epitopes, we performed cytotoxicity assays using ZnT8-transduced K562-A2 targets (K562-A2/ZnT8). High avidity $ZnT8_{186-194}$-reactive clones lysed unpulsed K562-A2/ZnT8 targets almost as efficiently as targets pulsed with the $ZnT8_{186-194}$ peptide, while unpulsed K562-A2 control targets remained largely intact (Fig. 3A-B). In contrast, low avidity $ZnT8_{186-194}$-reactive clones were unable to lyse K562-A2/ZnT8 targets in the absence of exogenous $ZnT8_{186-194}$ peptide (Fig. 3C).

We then evaluated cytotoxicity against T1D-relevant targets by employing HLA-$A2^+$ ECN90 and control HLA-$A2^-$ EndoC-βH2 human β-cell lines. Although the ECN90 but not the EndoC-βH2 line expressed HLA Class I in the unstimulated state, expression levels were similarly upregulated by pretreatment with different cocktails of inflammatory cytokines, without inducing significant β-cell death (Fig. S4A-B). IFN-γ was chosen as the single cytokine that upregulated HLA Class I expression to comparable levels in both lines, and pretreatment was carried out for 18 h prior to a real-time cytotoxicity assay. As observed with K562-A2/ZnT8 targets, high avidity clones lysed unpulsed HLA-$A2^+$ ECN90 cells presenting naturally processed ZnT8-derived epitopes (Fig. 3D-E), while low avidity clones displayed marginal lytic activity (Fig. 3F). Cytotoxicity increased in all cases with the addition of $ZnT8_{186-194}$ peptide, suggesting more limited natural presentation compared with ZnT8-transduced targets. Lysis of HLA-A2 EndoC-βH2 cells was negligible, and a control clone reactive to the melanocyte self-epitope $MelanA_{26-35}$ only lysed ECN90 cells in the presence of exogenous $MelanA_{26-35}$ peptide (Fig. 3G). Microscopic inspection confirmed the lysis measured in real-time cytotoxicity assays (Fig. S4C). β-cell lysis was not different between T1D and healthy clones, either in the absence or presence of exogenous $ZnT8_{186-194}$ peptide (Fig. 3H). Moreover, IFN-γ-pretreatment of HLA-$A2^+$ ECN90 cells neither upregulated ZnT8

protein expression (Fig. S4D) nor increased the functional activation of co-incubated $CD8^+$ T-cell clones (Fig. S4E-F). Collectively, these results demonstrate that $ZnT8_{186-194}$-reactive $CD8^+$ T cells display similar cytotoxicity in T1D and healthy subjects and that ZnT8 expression is not modulated by inflammation.

$ZnT8_{186-194}$-reactive $CD8^+$ T cells display private TCR gene usage but public CDR3β aminoacid sequences

Molecular analysis of expressed TCRα (*TRA*) and TCRβ (*TRB*) gene transcripts revealed that no sequences were shared (public) among $ZnT8_{186-194}$-reactive clones isolated from T1D or healthy subjects (Fig. S5). Of note, the 3 clones from patient D222D harbored an identical TCR. However, this observation did not affect our previous functional comparisons, because the measured parameters were even more similar between T1D and healthy donors when only one D222D clone was considered.

We then interrogated an *in-silico* database of *TRB* sequences compiled by high-throughput sequencing of naïve/terminal effector ($CD45RA^+CD45RO^-$) or central memory ($CD45RO^+CD45RA^-CD62L^{hi}$) $CD4^+$ and $CD8^+$ T cells obtained from HLA-$A2^+$ recent-onset T1D patients, at-risk aAb^+ and healthy subjects (Table S2). The D010R 1E2, H328C 8E8 and H034O 141B9 complementarity-determining region (CDR)3β aminoacid sequences were found among $CD8^+$ and $CD4^+$ T cells isolated from several individuals (Fig. 4A-C), mostly within the $CD45RA^+CD45RO^-$ pool for $CD8^+$ T cells. Several different *TRBV* genes were used in conjunction with these identical CDR3β loops to generate 'mosaic' sequences. The same CDR3β aminoacid sequences were detected *in-silico* among the polyclonal TCR repertoires compiled from conventional and regulatory $CD4^+$ and $CD8^+$ T cells isolated from pancreatic lymph node (PLN) and spleen samples by the Network for Pancreatic Organ Donors (nPOD) (Fig. 4D; n=67 identical CDR3β, n=6 identical TCRβ). Most of the $CD8^+$ T-

cell hits in PLNs (11/15, 73%) were from HLA-A2$^+$ subjects, but with no obvious association with T1D.

To extend these findings, we developed D010R 1E2, H328C 8E8 and D222D *TRA* and *TRB* clonotype-specific TaqMan real-time quantitative PCR (qPCR) assays (Fig. S6A-B). Applied to CD4$^+$ and CD8$^+$ T-cell cDNA preparations from two independent cohorts of T1D (n=97 and n=53) and healthy subjects (n=97 and n=38), these assays detected the D010R and H328C *TRB* among CD8$^+$ T cells from a single HLA-A2$^+$ T1D patient in each case (Fig. S6C-D).

Collectively, these results show that ZnT8$_{186\text{-}194}$ recognition is mediated primarily by private clonotypes, some of which share CDR3β aminoacid sequences among individuals to form 'mosaic' TCRs.

Circulating islet-reactive CD8$^+$ T cells display similar ex-vivo frequencies and a predominantly naïve phenotype in T1D and healthy subjects

In further experiments, we used *ex-vivo* combinatorial HLA-A2 MMr assays (*9*) to analyze ZnT8$_{186\text{-}194}$-reactive CD8$^+$ T cells in 39 HLA-A2$^+$ recent-onset T1D patients (16 children, 23 adults) and 39 age/sex-matched healthy donors (17 children, 22 adults) (Table S3, Fig. S7). Control specificities included MelanA$_{26\text{-}35}$, which is recognized by a large naïve pool in humans (*13*), and Flu MP$_{58\text{-}66}$, to which most individuals harbor Ag-experienced CD8$^+$ T cells reflecting prior viral exposure. Donors yielding <3x10^5 total CD8$^+$ T cells or <5 MMr$^+$ cells were excluded from the analysis to avoid undersampling. Parallel ELISpot assays confirmed that ZnT8$_{186\text{-}194}$-reactive IFN-γ responses were more frequent in T1D *vs.* healthy donors (Fig. S8) (*7*). In contrast, similar frequencies of ZnT8$_{186\text{-}194}$ and MelanA$_{26\text{-}35}$ MMr$^+$CD8$^+$ T cells were detected in age-stratified T1D and healthy donors (Fig. 5A). Healthy chidren and adults displayed higher frequencies of Flu MP$_{58\text{-}66}$ MMr$^+$CD8$^+$ T cells compared with their age/sex-matched T1D counterparts, while children displayed ~4-fold higher

frequencies of $ZnT8_{186-194}$ and $MelanA_{26-35}$ MMr^+CD8^+ T cells compared with adults, irrespective of T1D status.

Among $ZnT8_{186-194}$ MMr^+CD8^+ cells, the Ag-experienced fraction ($CD45RA^+CCR7^-$ or $CD45RA^-CCR7^{+/-}$) was similarly limited (generally ≤25% of all $ZnT8_{186-194}$ MMr^+ events) in T1D and healthy adults (Fig. 5B). In contrast, higher proportions of Ag-experienced $ZnT8_{186-194}$ MMr^+ cells were present in T1D children *vs.* adults, although these values were not different in healthy children. T1D children also harbored significantly higher proportions of Ag-experienced $ZnT8_{186-194}$ *vs.* $MelanA_{26-35}$ MMr^+ cells. $MelanA_{26-35}$-reactive $CD8^+$ T cells were mostly naïve, while Flu MP_{58-66}-reactive $CD8^+$ T cells were mostly Ag-experienced in all groups. Comparable results were obtained using the absolute frequencies of Ag-experienced MMr^+CD8^+ T cells (Fig. 5C).

Single-cell gene expression analysis of sorted $ZnT8_{186-194}$ MMr^+ cells (Fig. S9A) revealed few differences, with T1D patients displaying higher expression of the Th17-related aryl hydrocarbon receptor (*AHR*) and the mitotic aurora kinase A (*AURKA*) and lower expression of the transcriptional activator RAR related orphan receptor A (*RORA*). In line with our *in-vitro* data, clonotypic analyses of individual $ZnT8_{186-194}$ MMr^+CD8^+ T cells sorted *ex-vivo* yielded unique CDR3α and CDR3β sequences (Fig. S9B). Of the 21 CDR3β aminoacid sequences obtained, 7 (33%) were found in our *in-silico TRB* database across all subject groups (Fig. S9C). Among $CD8^+$ T cells, these 7 sequences were again most frequent within the $CD45RA^+CD45RO^-$ compartment, and predominantly found in T1D *vs.* healthy subjects. Preferential usage of certain *TRBV* (mostly *TRBV19*, 25%) and *TRAV* (mostly *TRAV12-2*, 38%) genes was observed (Fig. S9D-E), with *TRBV19* also shared among the $ZnT8_{186-194}$-reactive clones. However, only 8 out of 63 matching sequences (13%) expressed the *TRBV* gene of the corresponding $ZnT8_{186-194}$-reactive T cell. Thus, despite biased *TRAV* and *TRBV* gene usage, the *ex-vivo* data confirmed that $ZnT8_{186-194}$ recognition is mediated primarily by private clonotypes expressing 'mosaic' TCRs.

Next, we used an extended combinatorial MMr panel to compare $ZnT8_{186-194}$-reactive $CD8^+$ T cells with those recognizing other immunodominant β-cell epitopes in adult donors (Fig. S10A). Assay reproducibility across panels was confirmed using separate blood draws from the same individuals (Fig. S10B). As observed for $ZnT8_{186-194}$, other β-cell-reactive $CD8^+$ T-cell populations displayed similar frequencies (typically 1-50 MMr^+ cells/10^6 $CD8^+$ T cells) in T1D and healthy adults (Fig. 5D). An exception was noted for PPI_{15-24}-reactive $CD8^+$ T cells, whose frequencies were lower than for other β-cell-reactive fractions, and higher in T1D *vs.* healthy donors. In all instances, the Ag-experienced fraction among MMr^+CD8^+ T cells was limited in both subject groups (Fig. 5E–F). The few children included in this extended analysis harbored β-cell-reactive $CD8^+$ T cells with a more Ag-experienced phenotype. $CD45RA^+CCR7^+$ islet-reactive cells were *bona fide* naïve, as they were largely $CD27^+CD28^+$ and $CD95^-$ (Fig. S11).

Collectively, these results show that circulating $CD8^+$ T cells reactive to $ZnT8_{186-194}$ and other β-cell epitopes occur at similar frequencies and exhibit a predominantly naïve phenotype in T1D and healthy adults, while higher frequencies of total and Ag-experienced $ZnT8_{186-194}$-reactive $CD8^+$ T cells are present in children, irrespective of T1D status.

Poor promiscuous ZnT8 gene expression in human thymic medullary epithelial cells (mTECs)

The combined observations that $CD8^+$ T cells reactive to $ZnT8_{186-194}$ and other β-cell epitopes are predominantly naïve and circulate at similar frequencies in T1D and healthy donors are compatible with frequent escape from thymic deletion due to poor islet Ag expression in mTECs (*14*). We tested this hypothesis by examining ZnT8 (*SLC30A8*) gene expression in total or immature (*AIRE*$^-$HLA Class II^{low}) *vs.* mature (*AIRE*$^+$HLA Class II^{high}) human mTECs from 5 children undergoing heart surgery. As mis-initiated mRNA transcription is described in mTECs (*13, 15*), forward primers were designed to identify potential alternative start sites *via* hybridization with exons 5, 6, 7 and 8 of the *SLC30A8* gene (Fig. 6A). The $ZnT8_{186-194}$

region is encoded by exons 7-8, with the exon 8 primer located just downstream. Combinations of these forward primers with reverse primers located either in exon 11 (Fig. 6B) or in the 3'-UTR (Fig. 6C) yielded the expected bands using human islet mRNA. However, mTECs did not express *SLC30A8*. One sample (#64) displayed a faint band amplified with the exon 8 forward primer, which matched *SLC30A8* by sequencing, suggesting low-level mis-initiated transcription starting at exon 8 (i.e. downstream of the $ZnT8_{186-194}$ region). Collectively, these results demonstrate that ZnT8 is poorly expressed in mTECs, and that *SLC30A8* transcription is limited to a mis-initiated mRNA isoform skipping the $ZnT8_{186-194}$ sequence.

Islet-reactive CD8$^+$ T cells circulate at similar frequencies irrespective of thymic expression of their cognate epitopes

In contrast to ZnT8, other β-cell Ags are expressed by mTECs, including PPI (*16, 17*), IA-2 (*17, 18*) and IGRP (*19*), or by thymic Ag-presenting cells, including GAD65 (*20*). Moreover, circulating PPI_{6-14}-reactive CD8$^+$ T cells displayed higher frequencies than PPI_{15-24}-reactive CD8$^+$ T cells, despite the fact that the complete *INS* transcript incorporating both epitopes was detected in the thymus (Fig. 6D-E). In conjunction with the finding that circulating CD8$^+$ T cells reactive to $ZnT8_{186-194}$ and other islet epitopes also occur at similar frequencies (Fig. 5D), these observations suggest a limited role of thymic Ag gene expression in setting such frequencies.

Potential confounders in this scenario include the efficiency of epitope presentation and the odds of encountering cognate peptide-HLA complexes in the thymic environment. Accordingly, we compared the frequencies of islet-reactive CD8$^+$ T cells in age/sex-matched HLA-A2$^+$ and HLA-A2$^-$ healthy adults, reasoning that thymic deletion cannot occur in the absence of the appropriate HLA-A2 restriction (*21*). To exclude promiscuous presentation by non-HLA-A2 molecules, donors were selected based on HLA-A and HLA-B molecules

incapable of binding the selected islet epitopes (Table S4). Moreover, all subjects were seronegative for Ebola (EboV) and hepatitis C virus (HCV). Representative flow cytometry plots are shown in Fig. S12. Except for PPI_{6-14}, HLA-A2-restricted islet-reactive $CD8^+$ T cells occurred at largely equivalent frequencies in HLA-$A2^+$ and HLA-$A2^-$ donors (Fig. 6F). Although higher overall relative to most islet specificities, the frequencies of MMr^+CD8^+ cells recognizing the HLA-A2-restricted foreign epitopes EboV $NP_{202-210}$ and HCV $PP_{1406-1415}$ were also similar between HLA-$A2^+$ and HLA-$A2^-$ groups. No significant phenotypic differences were observed between groups for any of these MMr^+CD8^+ T-cell populations (Fig. 6G). As expected, control Flu MP_{58-66} MMr^+CD8^+ cells were more prevalent and more Ag-experienced in HLA-$A2^+$ donors.

Collectively, these findings suggest that thymic presentation of these islet epitopes does not trigger significant clonal deletion in HLA-$A2^+$ donors.

$ZnT8_{186-194}$-reactive $CD8^+$ T cells cross-recognize a Bacteroides stercoris mimotope

Although islet-reactive $CD8^+$ T cells were predominantly naïve in T1D and healthy adults, substantial Ag-experienced fractions were noted in some individuals, irrespective of disease status (Fig. 5B-5E). Moreover, $CD8^+$ T-cell frequencies correlated with the size of the Ag-experienced fraction for some individual ($ZnT8_{186-194}$, $IGRP_{265-273}$) and pooled islet epitopes (Fig. S13A-C), consistent with the patterns observed for Flu MP_{58-66}-reactive $CD8^+$ T cells (Fig. S13D). These observations raise the possibility of cross-priming by unrelated homologous epitopes (mimotopes). Indeed, sequence homology was observed between the $ZnT8_{186-194}$ epitope (VAANIVLTV) and a peptide (KAANIVLTV) derived from protein WP_060386636.1 of the intestinal commensal *Bacteroides stercoris*. To assess potential cross-reactivity, we performed *ex-vivo* MMr assays on duplicate PBMC samples. One sample was stained with pairs of $ZnT8_{186-194}$ MMrs, while the other was stained with one $ZnT8_{186-194}$ MMr and one *B. stercoris* MMr. Similar frequencies were detected for $ZnT8_{186-194}$-$ZnT8_{186-}$

$_{194}$ and ZnT8$_{186-194}$-*B. stercoris* double-MMr$^+$CD8$^+$ T cells in 3 of 4 donors (Fig. 7A). As a negative control, ZnT8$_{186-194}$-EboV NP$_{202-210}$ double-MMr$^+$CD8$^+$ T cells were undetectable (Fig. 7B), while EboV NP$_{202-210}$-EboV NP$_{202-210}$ double-MMr$^+$CD8$^+$ T cells were present at similar frequencies in duplicate samples (Fig. 7C). Cross-reactivity with the *B. stercoris* mimotope was confirmed for 1 of 4 ZnT8$_{186-194}$-reactive CD8$^+$ T-cell clones *via* MMr co-staining (Fig. 7D) and *in-vitro* recall (Fig. 7E), with the *B. stercoris* mimotope displaying stronger agonist potency than the native ZnT8$_{186-194}$ peptide. Collectively, these results show that ZnT8$_{186-194}$-reactive CD8$^+$ T cells can cross-recognize a bacterial mimotope.

ZnT8$_{186-194}$-reactive cells are enriched in the pancreas of T1D donors

To reconcile the finding that equivalent frequencies of predominantly naïve islet-reactive CD8$^+$ T cells circulate in most individuals, we hypothesized that the T1D-relevant fraction may be sequestered in the pancreas. We therefore performed *in-situ* ZnT8$_{186-194}$ MMr staining on frozen pancreatic sections from HLA-A2$^+$ T1D (n=9), aAb$^+$ (n=9), non-diabetic (n=11) and type 2 diabetes (T2D) cases (n=3) from nPOD (Table S5). Representative images are shown in Fig. 8A-E, with scattered ZnT8$_{186-194}$ MMr$^+$ cells either within islets or the exocrine tissue. Consecutive sections from ZnT8$_{186-194}$ MMr$^+$ pancreata were probed with MelanA$_{26-35}$ MMrs, which, in conjunction with positive control vitiligo skin sections, confirmed staining specificity (Fig. 8F). Donor-matched PLN sections were stained in parallel (Fig. 8G-H). While ZnT8$_{186-194}$ MMr$^+$ cells were significantly more abundant than MelanA$_{26-35}$ MMr$^+$ cells in T1D, aAb$^+$ and non-diabetic cases, ZnT8$_{186-194}$ MMr$^+$ cells were enriched in the pancreata of T1D *vs.* non-diabetic and T2D cases (Fig. 8I). In contrast, ZnT8$_{186-194}$ MMr$^+$ cell were present at similar densities across all groups in PLN sections (Fig. 8J). Several of these nPOD cases were previously analyzed *in-silico* for the presence of ZnT8$_{186-194}$ CDR3β sequences in PLNs (Fig. 4D). These sequences were present in 4/5 cases with ZnT8 MMr$^+$ pancreata and 3/5 cases with ZnT8 MMr$^+$ PLNs (Table S5). A donor with chronic pancreatitis (#6288) and

very high $ZnT8_{186-194}$-reactive CD3Rβ counts among spleen and PLN $CD8^+$ T cells also displayed high densities of ZnT8 MMr^+ cells in the pancreas. Collectively, these results show that ZnT8-reactive cells are preferentially enriched in the pancreas of T1D donors.

Discussion

In this study, we found that $ZnT8_{186-194}$-reactive $CD8^+$ T-cell clones exhibited heterogeneous functional profiles, but no consistent differences between T1D and healthy subjects. Most $ZnT8_{186-194}$-reactive clones originated from naïve precursors and expressed private TCRs. *Ex-vivo* analyses on larger donor cohorts revealed that the frequency of circulating $ZnT8_{186-194}$-reactive $CD8^+$ T cells was similar in age-matched T1D *vs.* healthy donors, but higher in children *vs.* adults, irrespective of T1D status. A similar pattern was noted for $CD8^+$ T cells recognizing the extra-pancreatic self-epitope $MelanA_{26-35}$, but the corresponding $ZnT8_{186-194}$-reactive populations were more Ag-experienced in T1D children. Thus, while most children harbor a larger autoimmune repertoire not restricted to islet Ags, the activation of the islet-reactive fraction occurs preferentially in T1D children, which may reflect a more aggressive islet autoimmunity leading to earlier disease onset. On the other hand, some Ag-experienced β-cell-reactive $CD8^+$ T cells were invariably detected in healthy donors, supporting the possibility that foreign epitopes may prime autoreactive clonotypes expressing promiscuous TCRs (*22-24*). Indeed, some $ZnT8_{186-194}$-reactive $CD8^+$ T-cell clonotypes were able to cross-recognize a *B. stercoris* mimotope. It is noteworthy that *B. stercoris* belongs to the *Bacteroidetes* phylum, which is enriched in the gut microbiome of T1D (*25*) and at-risk aAb^+ subjects (*26*). Circulating $CD8^+$ T cells reactive to other HLA-A2-restricted β-cell epitopes were also detected at equivalent frequencies (1-50 MMr^+ cells/10^6 $CD8^+$ T cells) and with a predominantly naïve phenotype in T1D and healthy adults. This coherent pattern across islet specificities suggests that Ag-driven recruitment involves a limited fraction of naïve precursors, which fits with the paucity of public clonotypes found for $ZnT8_{186-194}$-reactive $CD8^+$ T cells, as reported for PPI_{15-24} (*4*). Interestingly, the lower frequency of Flu-reactive $CD8^+$ T cells observed in T1D *vs.* healthy donors may reflect impaired anti-viral responses (*27*).

One strength of our *ex-vivo* studies is the highly specific and reproducible quantification of MMr^+ cells. The observed frequencies of β-cell-reactive $CD8^+$ T cells fall below previous estimates obtained without enrichment (*4, 5*), but mirror those described using stringent MMr-based magnetic enrichment (*22*). Although higher frequencies of β-cell-reactive $CD8^+$ T cells have been observed in T1D *vs.* healthy donors (*5*), our data align with another study reporting no difference (*4*). Importantly, this study validates comparisons based on dasatinib-enhanced MMr staining. Although the T1D children in our cohort had a longer disease duration than T1D adults, comparable age-related differences were observed in healthy donors, and similar trends remained when restricting the analysis to more recently diagnosed T1D children. Other studies reporting higher Ag-experienced β-cell-reactive $CD8^+$ T-cell fractions in T1D *vs.* healthy donors are potentially limited by undersampling and single MMr labeling (*4*). Moreover, such differences were not observed for all islet epitopes (*4*), and significant naïve fractions (~40%) were also present in T1D patients (*4, 6*).

T-cell precursors can escape thymic negative selection due to 'blindspots' that result from poor or incomplete expression of certain tissue Ags (*13, 17, 28-30*), due to alternative splicing and promoter usage and mis-initiated transcription (*13-15, 30*). These features favor the generation of truncated transcripts lacking certain T-cell epitopes, as observed for ZnT8. However, $ZnT8_{186-194}$-reactive $CD8^+$ T cells circulated at similar frequencies relative to other islet-reactive populations. Together with the finding that HLA-A2-restricted islet-reactive $CD8^+$ T cells circulated at similar frequencies in HLA-$A2^+$ and HLA-A2 donors, these results show that the thymus does not eliminate all autoreactive $CD8^+$ T cells. Nonetheless, thymic self-Ag expression may 'prune' autoreactive clonotypes bearing high-affinity TCRs (*22, 31*).

Perhaps the most outstanding question raised by our findings relates to the 'benign' state of islet autoimmunity 'licensed' by incomplete central tolerance. Evidence for such thymic defects in human T1D has been limited to *INS* polymorphisms, which rank second among

T1D susceptibility loci after DQB1 and modulate thymic *INS* expression (*16*). Given the ongoing debate surrounding the role of thymic negative selection for autoreactive T cells (*22, 32, 33*), it is not altogether surprising that even this insulin paradigm does not fully explain T1D development. Indeed, homozygous *INS* susceptibility alleles are present in ~55% of Caucasians (*34*), yet very few develop T1D. We propose that incomplete clonal deletion of autoreactive T cells involves several other β-cell Ags besides insulin and is not restricted to T1D patients.

So what distinguishes benign from pathogenic autoimmune T cells? The evidence suggests that neither their blood frequency nor their phenotype are at play. However, naïve T cells circulate perpetually, in contrast to memory T cells. The body load of Ag-experienced autoreactive T cells may therefore be underestimated in the blood of diseased individuals due to tissue sequestration (*35*). In line with this, the number of $ZnT8_{186-194}$-reactive cells was higher than for Melan-A_{26-35}-reactive ones in the pancreas, similar between aAb$^+$ and non-diabetic donors, and enriched in the pancreas of T1D donors. Moreover, $ZnT8_{186-194}$-reactive $CD8^+$ T-cell clones displayed potent lytic activity, much higher than other islet specificities (*1*). While these findings suggest a pathogenic role for ZnT8-reactive $CD8^+$ T cells, their precise localization and Ag-experienced status within the pancreas and whether their numbers are inversely correlated with age as observed in the blood remain to be verified.

The second possibility is that autoimmune T cells may be differentially regulated in T1D and healthy donors (*33, 36*), either intrinsically (e.g. anergy or exhaustion) or extrinsically by regulatory T cells. In support of this notion, T1D-specific islet-reactive $CD8^+$ T cells have been repeatedly detected using functional IFN-γ ELISpot readouts (*3, 7, 10*), which employ unfractionated PBMCs, thus preserving regulatory networks. This observation also argues that peripheral blood can be informative under appropriate assay conditions. $ZnT8_{186-194}$-reactive $CD8^+$ T cells from T1D patients also expressed higher levels of aurora A kinase, which might hint at increased mitotic activity in the T1D setting. Mirroring this observation,

an anergic phenotype has been reported for self-reactive $CD8^+$ T cells in non-autoimmune subjects (*22, 36*), which may be at least partially imprinted in the thymus (*33, 37*).

The third possibility is that the central diabetogenic ingredient may be enhanced β-cell vulnerability caused by islet inflammation in the face of similar autoimmune T-cell repertoires across individuals. In this scenario, tolerance to β-cell Ags may depend primarily on T-cell ignorance (*32, 37*). Three observations are noteworthy in this respect. First, the higher T1D risk at younger age contrasts with the lower risk of other autoimmune diseases, which may indicate greater β-cell vulnerability due to childhood stressors, such as islet-tropic enteroviruses and the metabolic demands imposed by growth. Second, high densities of $ZnT8_{186\text{-}194}$ MMr^+ cells were detected in the pancreas of an organ donor with chronic pancreatitis, suggesting that islet-reactive $CD8^+$ T cells can expand under inflammatory conditions that are not autoimmune *ab initio*. Third, $PPI_{15\text{-}24}$-reactive $CD8^+$ T cells were more frequent in T1D *vs.* healthy donors, with similar results reported for $PPI_{2\text{-}10}$ (*22*). These epitopes map to the PPI leader sequence, which may undergo enhanced processing and presentation under metabolic stress (*1*).

Collectively, the present data pose new challenges toward development of circulating T-cell biomarkers for T1D staging and suggest novel therapeutic strategies based on mimicking 'benign' autoimmunity or complementing incomplete central tolerance (*38*).

Supplementary Materials:

Materials and Methods.

Fig. S1. Cytokine secretion and cytotoxicity of $ZnT8_{186-194}$-reactive $CD8^+$ T cells from T1D patient D222D.

Fig. S2. $CD8^+$ T-cell recognition and HLA-A2 binding of $ZnT8_{186-194}$ and $ZnT8_{185-194}$ epitope variants.

Fig. S3. Ag sensitivity correlates with Ag avidity and polyfunctionality in $ZnT8_{186-194}$-reactive $CD8^+$ T-cell clones.

Fig. S4. Modulation of HLA Class I and ZnT8 expression in human β-cell lines.

Fig. S5. TCR sequences of $ZnT8_{186-194}$-reactive $CD8^+$ T-cell clones.

Fig. S6. $ZnT8_{186-194}$-reactive clonotype-specific TaqMan assays.

Fig. S7. Gating strategy for the analysis of $ZnT8_{186-194}$, $MelanA_{26-35}$ and Flu MP_{58-66} MMr^+CD8^+ T cells.

Fig. S8. IFN-γ secretion by $ZnT8_{186-194}$-reactive $CD8^+$ T cells.

Fig. S9. Gene expression in *ex-vivo* single-sorted $ZnT8_{186-194}$ MMr^+CD8^+ T cells.

Fig. S10. Extended combinatorial MMr panel for the analysis of multiple islet-reactive $CD8^+$ T-cell populations, and reproducibility of *ex-vivo* MMr assays.

Fig. S11. CD27, CD28 and CD95 expression on $ZnT8_{186-194}$-reactive $CD8^+$ T cells.

Fig. S12. Representative MMr and CD45RA/CCR7 dot plots for HLA-$A2^+$ and HLA-$A2^-$ healthy donors depicted in Fig. 6F-G.

Fig. S13. Correlation between the frequency of MMr^+CD8^+ T cells and the Ag-experienced fraction within the same MMr^+CD8^+ population.

Table S1. Summary of $ZnT8_{186-194}$-reactive $CD8^+$ T-cell clones.

Table S2. Characteristics of study subjects for *in-silico TRB* analyses.

Table S3. Characteristics of HLA-$A2^+$ study subjects for *ex-vivo* MMr studies.

Table S4. Characteristics of HLA-$A2^+$ and HLA-$A2^-$ healthy donors for *ex-vivo* MMr studies.

Table S5. Characteristics of nPOD cases for *in-situ* $ZnT8_{186-194}$ MMr staining.

Table S6. Primers used for gene expression analysis of the individual $ZnT8_{186-194}$ MMr^+CD8^+ T cells depicted in Fig. S9A.

Members of the ImMaDiab Study Group.

Excel file. Raw data from figure graphs.

References and Notes

1. A. Skowera, R. J. Ellis, R. Varela-Calvino, S. Arif, G. C. Huang, C. Van-Krinks, A. Zaremba, C. Rackham, J. S. Allen, T. I. Tree, M. Zhao, C. M. Dayan, A. K. Sewell, W. Unger, J. W. Drijfhout, F. Ossendorp, B. O. Roep, M. Peakman, CTLs are targeted to kill beta cells in patients with type 1 diabetes through recognition of a glucose-regulated preproinsulin epitope. *J. Clin. Invest.* **118**, 3390-3402 (2008).

2. K. T. Coppieters, F. Dotta, N. Amirian, P. D. Campbell, T. W. Kay, M. A. Atkinson, B. O. Roep, M. G. von Herrath, Demonstration of islet-autoreactive CD8 T cells in insulitic lesions from recent onset and long-term type 1 diabetes patients. *J. Exp. Med.* **209**, 51-60 (2012).

3. R. Mallone, E. Martinuzzi, P. Blancou, G. Novelli, G. Afonso, M. Dolz, G. Bruno, L. Chaillous, L. Chatenoud, J. M. Bach, P. van Endert, CD8+ T-cell responses identify beta-cell autoimmunity in human type 1 diabetes. *Diabetes* **56**, 613-621 (2007).

4. A. Skowera, K. Ladell, J. E. McLaren, G. Dolton, K. K. Matthews, E. Gostick, D. Kronenberg-Versteeg, M. Eichmann, R. R. Knight, S. Heck, J. Powrie, P. J. Bingley, C. M. Dayan, J. J. Miles, A. K. Sewell, D. A. Price, M. Peakman, Beta-cell-specific CD8 T cell phenotype in type 1 diabetes reflects chronic autoantigen exposure. *Diabetes* **64**, 916-925 (2015).

5. J. H. Velthuis, W. W. Unger, J. R. Abreu, G. Duinkerken, K. Franken, M. Peakman, A. H. Bakker, S. Reker-Hadrup, B. Keymeulen, J. W. Drijfhout, T. N. Schumacher, B. O. Roep, Simultaneous Detection of Circulating Autoreactive CD8+ T-Cells Specific for Different Islet Cell-Associated Epitopes Using Combinatorial MHC Multimers. *Diabetes* **59**, 1721-1730 (2010).

6. S. Luce, F. Lemonnier, J. P. Briand, J. Coste, N. Lahlou, S. Muller, E. Larger, B. Rocha, R. Mallone, C. Boitard, Single insulin-specific CD8+ T cells show characteristic gene expression profiles in human type 1 diabetes. *Diabetes* **60**, 3289-3299 (2011).

7. M. Scotto, G. Afonso, E. Larger, C. Raverdy, F. A. Lemonnier, J. C. Carel, D. Dubois-Laforgue, B. Baz, D. Levy, J. F. Gautier, O. Launay, G. Bruno, C. Boitard, L. A. Sechi, J. C. Hutton, H. W. Davidson, R. Mallone, Zinc transporter (ZnT)8(186-194) is an immunodominant CD8+ T cell epitope in HLA-A2+ type 1 diabetic patients. *Diabetologia* **55**, 2026-2031 (2012).

8. E. Martinuzzi, G. Afonso, M. C. Gagnerault, G. Naselli, D. Mittag, B. Combadiere, C. Boitard, N. Chaput, L. Zitvogel, L. C. Harrison, R. Mallone, acDCs enhance human antigen-specific T-cell responses. *Blood* **118**, 2128-2137 (2011).

9. S. R. Hadrup, A. H. Bakker, C. J. Shu, R. S. Andersen, V. J. van, P. Hombrink, E. Castermans, S. P. Thor, C. Blank, J. B. Haanen, M. H. Heemskerk, T. N. Schumacher, Parallel detection of antigen-specific T-cell responses by multidimensional encoding of MHC multimers. *Nat. Methods* **6**, 520-526 (2009).

10. E. Enee, R. Kratzer, J. B. Arnoux, E. Barilleau, Y. Hamel, C. Marchi, J. Beltrand, B. Michaud, L. Chatenoud, J. J. Robert, P. van Endert, ZnT8 Is a Major CD8+ T Cell-Recognized Autoantigen in Pediatric Type 1 Diabetes. *Diabetes* **61**, 1779-1784 (2012).

11. A. Lissina, K. Ladell, A. Skowera, M. Clement, E. Edwards, R. Seggewiss, H. A. van den Berg, E. Gostick, K. Gallagher, E. Jones, J. J. Melenhorst, A. J. Godkin, M. Peakman, D. A. Price, A. K. Sewell, L. Wooldridge, Protein kinase inhibitors substantially improve the

physical detection of T-cells with peptide-MHC tetramers. *J. Immunol. Methods* **340**, 11-24 (2009).

12. M. Larsen, D. Sauce, L. Arnaud, S. Fastenackels, V. Appay, G. Gorochov, Evaluating cellular polyfunctionality with a novel polyfunctionality index. *PLoS One* 7, e42403 (2012).

13. S. Pinto, D. Sommermeyer, C. Michel, S. Wilde, D. Schendel, W. Uckert, T. Blankenstein, B. Kyewski, Misinitiation of intrathymic MART-1 transcription and biased TCR usage explain the high frequency of MART-1-specific T cells. *Eur. J. Immunol.* **44**, 2811-2821 (2014).

14. L. Klein, B. Kyewski, P. M. Allen, K. A. Hogquist, Positive and negative selection of the T cell repertoire: what thymocytes see (and don't see). *Nat. Rev. Immunol.* **14**, 377-391 (2014).

15. J. Villasenor, W. Besse, C. Benoist, D. Mathis, Ectopic expression of peripheral-tissue antigens in the thymic epithelium: probabilistic, monoallelic, misinitiated. *Proc. Natl. Acad. Sci. U.S.A.* **105**, 15854-15859 (2008).

16. A. Pugliese, M. Zeller, A. Fernandez, Jr., L. J. Zalcberg, R. J. Bartlett, C. Ricordi, M. Pietropaolo, G. S. Eisenbarth, S. T. Bennett, D. D. Patel, The insulin gene is transcribed in the human thymus and transcription levels correlated with allelic variation at the INS VNTR-IDDM2 susceptibility locus for type 1 diabetes. *Nat. Genet.* **15**, 293-297 (1997).

17. J. Gotter, B. Brors, M. Hergenhahn, B. Kyewski, Medullary epithelial cells of the human thymus express a highly diverse selection of tissue-specific genes colocalized in chromosomal clusters. *J. Exp. Med.* **199**, 155-166 (2004).

18. J. Diez, Y. Park, M. Zeller, D. Brown, D. Garza, C. Ricordi, J. Hutton, G. S. Eisenbarth, A. Pugliese, Differential splicing of the IA-2 mRNA in pancreas and lymphoid organs as a permissive genetic mechanism for autoimmunity against the IA-2 type 1 diabetes autoantigen. *Diabetes* **50**, 895-900 (2001).

19. R. S. Dogra, P. Vaidyanathan, K. R. Prabakar, K. E. Marshall, J. C. Hutton, A. Pugliese, Alternative splicing of G6PC2, the gene coding for the islet-specific glucose-6-phosphatase catalytic subunit-related protein (IGRP), results in differential expression in human thymus and spleen compared with pancreas. *Diabetologia* **49**, 953-957 (2006).

20. A. Pugliese, D. Brown, D. Garza, D. Murchison, M. Zeller, M. Redondo, J. Diez, G. S. Eisenbarth, D. D. Patel, C. Ricordi, Self-antigen-presenting cells expressing diabetes-associated autoantigens exist in both thymus and peripheral lymphoid organs. *J. Clin. Invest.* **107**, 555-564 (2001).

21. H. G. Rammensee, M. J. Bevan, Evidence from in vitro studies that tolerance to self antigens is MHC-restricted. *Nature* **308**, 741-744 (1984).

22. W. Yu, N. Jiang, P. J. Ebert, B. A. Kidd, S. Muller, P. J. Lund, J. Juang, K. Adachi, T. Tse, M. E. Birnbaum, E. W. Newell, D. M. Wilson, G. M. Grotenbreg, S. Valitutti, S. R. Quake, M. M. Davis, Clonal deletion prunes but does not eliminate self-specific alphabeta CD8(+) T lymphocytes. *Immunity* **42**, 929-941 (2015).

23. N. Tai, J. Peng, F. Liu, E. Gulden, Y. Hu, X. Zhang, L. Chen, F. S. Wong, L. Wen, Microbial antigen mimics activate diabetogenic CD8 T cells in NOD mice. *J. Exp. Med.* **213**, 2129-2146 (2016).

24. D. K. Cole, A. M. Bulek, G. Dolton, A. J. Schauenberg, B. Szomolay, W. Rittase, A. Trimby, P. Jothikumar, A. Fuller, A. Skowera, J. Rossjohn, C. Zhu, J. J. Miles, M. Peakman, L. Wooldridge, P. J. Rizkallah, A. K. Sewell, Hotspot autoimmune T cell receptor binding

underlies pathogen and insulin peptide cross-reactivity. *J. Clin. Invest.* **126**, 2191-2204 (2016).

25. M. C. de Goffau, S. Fuentes, B. van den Bogert, H. Honkanen, W. M. de Vos, G. W. Welling, H. Hyoty, H. J. Harmsen, Aberrant gut microbiota composition at the onset of type 1 diabetes in young children. *Diabetologia* **57**, 1569-1577 (2014).

26. M. C. de Goffau, K. Luopajarvi, M. Knip, J. Ilonen, T. Ruohtula, T. Harkonen, L. Orivuori, S. Hakala, G. W. Welling, H. J. Harmsen, O. Vaarala, Fecal microbiota composition differs between children with beta-cell autoimmunity and those without. *Diabetes* **62**, 1238-1244 (2013).

27. R. J. Diepersloot, K. P. Bouter, W. E. Beyer, J. B. Hoekstra, N. Masurel, Humoral immune response and delayed type hypersensitivity to influenza vaccine in patients with diabetes mellitus. *Diabetologia* **30**, 397-401 (1987).

28. M. Giraud, R. Taubert, C. Vandiedonck, X. Ke, M. Levi-Strauss, F. Pagani, F. E. Baralle, B. Eymard, C. Tranchant, P. Gajdos, A. Vincent, N. Willcox, D. Beeson, B. Kyewski, H. J. Garchon, An IRF8-binding promoter variant and AIRE control CHRNA1 promiscuous expression in thymus. *Nature* **448**, 934-937 (2007).

29. H. Lv, E. Havari, S. Pinto, R. V. Gottumukkala, L. Cornivelli, K. Raddassi, T. Matsui, A. Rosenzweig, R. T. Bronson, R. Smith, A. L. Fletcher, S. J. Turley, K. Wucherpfennig, B. Kyewski, M. A. Lipes, Impaired thymic tolerance to alpha-myosin directs autoimmunity to the heart in mice and humans. *J. Clin. Invest.* **121**, 1561-1573 (2011).

30. L. Klein, M. Klugmann, K. A. Nave, V. K. Tuohy, B. Kyewski, Shaping of the autoreactive T-cell repertoire by a splice variant of self protein expressed in thymic epithelial cells. *Nat. Med.* **6**, 56-61 (2000).

31. S. Enouz, L. Carrie, D. Merkler, M. J. Bevan, D. Zehn, Autoreactive T cells bypass negative selection and respond to self-antigen stimulation during infection. *J. Exp. Med.* **209**, 1769-1779 (2012).

32. F. P. Legoux, J. B. Lim, A. W. Cauley, S. Dikiy, J. Ertelt, T. J. Mariani, T. Sparwasser, S. S. Way, J. J. Moon, CD4+ T Cell Tolerance to Tissue-Restricted Self Antigens Is Mediated by Antigen-Specific Regulatory T Cells Rather Than Deletion. *Immunity* **43**, 896-908 (2015).

33. M. M. Davis, Not-So-Negative Selection. *Immunity* **43**, 833-835 (2015).

34. S. T. Bennett, J. A. Todd, Human type 1 diabetes and the insulin gene: principles of mapping polygenes. *Annu. Rev. Genet.* **30**, 343-370 (1996).

35. J. J. Thome, N. Yudanin, Y. Ohmura, M. Kubota, B. Grinshpun, T. Sathaliyawala, T. Kato, H. Lerner, Y. Shen, D. L. Farber, Spatial map of human T cell compartmentalization and maintenance over decades of life. *Cell* **159**, 814-828 (2014).

36. Y. Maeda, H. Nishikawa, D. Sugiyama, D. Ha, M. Hamaguchi, T. Saito, M. Nishioka, J. B. Wing, D. Adeegbe, I. Katayama, S. Sakaguchi, Detection of self-reactive CD8(+) T cells with an anergic phenotype in healthy individuals. *Science* **346**, 1536-1540 (2014).

37. D. Malhotra, J. L. Linehan, T. Dileepan, Y. J. Lee, W. E. Purtha, J. V. Lu, R. W. Nelson, B. T. Fife, H. T. Orr, M. S. Anderson, K. A. Hogquist, M. K. Jenkins, Tolerance is established in polyclonal CD4(+) T cells by distinct mechanisms, according to self-peptide expression patterns. *Nat. Immunol.* **17**, 187-195 (2016).

38. S. Culina, N. Gupta, R. Boisgard, G. Afonso, M. C. Gagnerault, J. Dimitrov, T. Osterbye, S. Justesen, S. Luce, M. Attias, B. Kyewski, S. Buus, F. S. Wong, S. Lacroix-

Desmazes, R. Mallone, Materno-fetal transfer of preproinsulin through the neonatal Fc receptor protects from autoimmune diabetes. *Diabetes* **64**, 3532-3542 (2015).

39. C. Leisner, N. Loeth, K. Lamberth, S. Justesen, C. Sylvester-Hvid, E. G. Schmidt, M. Claesson, S. Buus, A. Stryhn, One-pot, mix-and-read peptide-MHC tetramers. *PLoS One* **3**, e1678 (2008).

40. P. Ravassard, Y. Hazhouz, S. Pechberty, E. Bricout-Neveu, M. Armanet, P. Czernichow, R. Scharfmann, A genetically engineered human pancreatic beta cell line exhibiting glucose-inducible insulin secretion. *J. Clin. Invest.* **121**, 3589-3597 (2011).

41. M. F. Quigley, J. R. Almeida, D. A. Price, D. C. Douek, Unbiased molecular analysis of T cell receptor expression using template-switch anchored RT-PCR. *Curr. Protoc. Immunol.* **Chapter 10**, Unit 10.33 (2011).

42. G. C. Wang, P. Dash, J. A. McCullers, P. C. Doherty, P. G. Thomas, T cell receptor alphabeta diversity inversely correlates with pathogen-specific antibody levels in human cytomegalovirus infection. *Sci. Transl. Med.* **4**, 128ra142 (2012).

43. E. Bonifacio, A. G. Ziegler, G. Klingensmith, E. Schober, P. J. Bingley, M. Rottenkolber, A. Theil, A. Eugster, R. Puff, C. Peplow, F. Buettner, K. Lange, J. Hasford, P. Achenbach, P.-P. S. Group, Effects of high-dose oral insulin on immune responses in children at high risk for type 1 diabetes: the Pre-POINT randomized clinical trial. *JAMA* **313**, 1541-1549 (2015).

Acknowledgments: We thank C. Maillard, M. Scotto and S. Rozlan for technical assistance; Univercell Biosolutions for providing the ECN90 β-cell line; K. Kedzierska and her laboratory (University of Melbourne) for help with single-cell TCR sequencing; T. Brusko (University of Florida, Gainesville) for help with the nPOD TCR database; the CyBio platform of the Cochin Institute and DKFZ Flow Cytometry Core Facility for assistance with flow cytometry; T. Loukanov (University of Heidelberg) for providing human thymic tissue; K. Boniface and J. Seneschal (INSERM U1035, Bordeaux) for providing vitiligo skin sections; and S. You for reviewing the manuscript. Members of the ImMaDiab Study Group are listed in the Supplemental Acknowledgments. **Funding:** This work was performed within the *Département Hospitalo-Universitaire* (DHU) AutHorS, supported by the *Programme Hospitalier de Recherche Clinique* ImMaDiab, Lilly France, the INSERM-Transfert Proof-of-Concept program acDC, the *Ile-de-France* CORDDIM, and by grants from the JDRF (1-PNF-2014-155-A-V, 2-SRA-2016-164-Q-R), the Aviesan/Astra Zeneca 'Diabetes and the Vessel Wall Injury' program, the *Société Francophone du Diabète*, the *Agence Nationale de la Recherche* (ANR-2015-CE17-0018-01), and the *Fondation pour la Recherche Médicale* (Equipe FRM DEQ20140329520), to RM; a JDRF Biomarkers grant (17-2012-598), to KC; an NIH R01 grant (DK052068), to HWD; Lilly and *Fondation Bettencourt-Schueller* funds, to RS; a European Research Council grant (ERC-2012-AdG), to BK; and funds from JDRF, the Wellcome Trust and the National Institute for Health Research (NIHR) Cambridge Biomedical Research Centre, to the JDRF/Wellcome Trust Diabetes and Inflammation Laboratory (CIMR, University of Cambridge), which provided PBMC samples from the JDRF D-GAP study. Samples from at-risk subjects were obtained through a TrialNet ancillary study to the TN-01 Pathway to Prevention study funded by NIH grants U01 DK061010, U01 DK061034, U01 DK061042, U01 DK061058, U01 DK085465, U01 DK085453, U01 DK085461, U01 DK085463, U01 DK085466, U01 DK085499, U01 DK085504, U01 DK085505, U01 DK085509, U01 DK103180, U01-DK103153, U01-

DK085476, U01-DK103266 and by JDRF. DAP is a Wellcome Trust Senior Investigator (100326Z/12/Z). This research was performed with the support of the Network for Pancreatic Organ Donors with Diabetes (nPOD), a collaborative T1D research project funded by JDRF. Organ Procurement Organizations partnering with nPOD to provide research resources are listed at www.jdrfnpod.org/our-partners.php. This project has received funding from the Innovative Medicines Initiative 2 Joint Undertaking (INNODIA, no. 115797). This Joint Undertaking receives support from the Union's Horizon 2020 research and innovation programme and the European Federation of Pharmaceutical Industries and Associations, JDRF, and The Leona M. and Harry B. Helmsley Charitable Trust. **Author contributions:** S.C. A.I.L., G.A., K.C., S.P., G.S., K.K., L.N., A.E., T.Ø., J.E.M. and M.K. performed experiments and analyzed data; A.M., K.L., E.L., J.P.B., A.L., V.A., H.W.D., S.B., D.A.P., E.B., M.B., S.C.Z., F.D. and R.S. provided critical reagents, experimental assistance and intellectual input; M.K. and R.M. performed statistical analyses; S.C., A.I.L., G.A., K.C., S.P., D.A.P., B.K. and R.M. designed and interpreted experiments, and wrote the paper; the ImMaDiab Study Group recruited patients and performed clinical phenotyping. **Competing interests**: The authors declare that no conflict of interest exists. Some T-cell receptor sequences described herein are covered by Inserm-Transfert patent WO/2017/046335. **Data and materials availability:** available materials will be provided with the appropriate material transfer agreement.

Figures Legends

Fig. 1. $ZnT8_{186-194}$-reactive $CD8^+$ T-cell clones from patient D222D. (**A**) Frozen-thawed PBMCs were cultured with $ZnT8_{186-194}$ or no peptide and stained with PE/APC-labeled $ZnT8_{186-194}$ MMrs. (**B**) $ZnT8_{186-194}$ and control MMr stains for one clone obtained from single-sorted $ZnT8_{186-194}$/$ZnT8_{186-194}$ double-MMr^+ cells. (**C**) Percent intracellular TNF-α^+ D222D clone 1 cells stimulated for 6 h with K562-A2 cells pulsed with $ZnT8_{186-194}$ or Flu MP_{58-66} peptide. (**D**) Percent lysis of FarRed-labeled LCL targets pulsed with $ZnT8_{186-194}$ (top) or Flu MP_{58-66} peptide (bottom) and cultured for 24 h with CFSE-labeled D222D clone 3 at increasing E/T ratios. (**E**) Percent lysis of LCL targets cultured with D222D clones 1, 2 or 3 (mean±SEM; each clone is depicted in Fig. S1D-F). (**F**) Lysis of cognate peptide-pulsed LCLs cultured for 4 h with D222D clone 2 or a $MelanA_{26-35}$-reactive clone (E/T 1/1) in the presence of concanamycin A (CMA), brefeldin A (BFA), CMA and BFA, anti-FasL or control IgG1. *p=0.015, **p=0.009, ***p<0.001 by Student's t test. Results are mean+SEM of triplicate measurements from one of three experiments. (**G**) Percent surface $CD107a^+$ D222D clone 1 cells stimulated as in (C). For panels A, C, G, gate is on viable $CD8^+$ cells.

Fig. 2. Ag avidity, Ag sensitivity and polyfunctionality of $ZnT8_{186-194}$-reactive $CD8^+$ T-cell clones. (**A**) $ZnT8_{186-194}$ MMr staining in the absence (light grey) or presence (dark grey) of dasatinib. The dotted profile indicates the unstained control. (**B**) $ZnT8_{186-194}$ MMr median fluorescence intensity (MFI) for the indicated clones in the absence (left) or presence (right) of dasatinib. Bars indicate median values. Results are representative of two separate experiments. (**C**) The indicated clones were stimulated for 6 h with $ZnT8_{186-194}$-pulsed K562-A2 cells and percent $cytokine^+$ cells out of viable $CD8^+$ cells calculated. Results are representative of three independent experiments. (**D-E**) Half maximal effective peptide concentration (EC50; D) and maximal cytokine response (percent $cytokine^+$ cells at optimal

peptide concentrations; E) for clones stimulated as above. Bars indicate median values. Results are representative of two to four separate experiments. *p=0.014 by Mann-Whitney test. (**F**) Polyfunctionality distribution of T1D (left) and healthy clones (right). Percent T cells producing 0 to 4 cytokines among TNF-α, IFN-γ, IL-2 and MIP-1β upon exposure to $ZnT8_{186-194}$-pulsed K562-A2 cells (100 μM) are shown.

Fig. 3. Target cell lysis by $ZnT8_{186-194}$-reactive $CD8^+$ T-cell clones. (**A-C**) Lysis of K562-A2 cells transfected (open triangles) or not (open circles) with a full-length ZnT8 plasmid and cultured for 24 h with clones D222D 2 (A), H017N A1 (B) or H314C 6C4 (C). Filled symbols indicate $ZnT8_{186-194}$-pulsed target cells (10 μM). Results are presented as mean±SEM of triplicate wells from two separate experiments. (**D-G**) Real-time cytotoxicity for the indicated clones *vs.* HLA-$A2^+$ ECN90 (white triangles) or control HLA-$A2^-$ EndoC-βH2 β-cell targets (white circles) (E/T 2/1). Black and grey symbols indicate the corresponding targets pulsed with 10 μM $ZnT8_{186-194}$ or $GAD_{114-122}$ peptide, respectively. Mean±SEM of triplicate measurements are shown at each time point. Results are representative of at least two separate experiments. (**H**) Percent maximal HLA-$A2^+$ ECN90 and HLA-$A2^-$ EndoC-βH2 β-cell lysis by the indicated clones (T1D, grey symbols; healthy, white symbols; control, horizontal dotted line) in the absence or presence of $ZnT8_{186-194}$ peptide. Bars indicate median values. Lysis was calculated from the cytotoxicity profiles as in panels D-G.

Fig. 4. *In-silico* search for CDR3β aminoacid sequences from $ZnT8_{186-194}$-reactive $CD8^+$ T-cell clones. (**A-C**) Prevalence of the CDR3β aminoacid sequences from clones D010R 1E2 (A), H328C 8E8 (B) and H034O 141B9 (C) among HLA-$A2^+$ T1D (n=5), aAb^+ (n=5) and healthy subjects (n=10), as assessed by *in-silico* analysis of TCRβ repertoires obtained from the indicated $CD8^+$ and $CD4^+$ T-cell subsets. (**D**) *In-silico* search for the same CDR3β

aminoacid sequences in the repertoire of $CD8^+$, conventional $CD4^+$ (Tconv; $CD127^+$) and regulatory $CD4^+$ (Treg; $CD25^+CD127^-$) T cells obtained from nPOD PLN, spleen and inguinal lymph node (ILN) samples *via* the online database http://clonesearch.jdrfnpod.org. For each cell type and tissue, the first, second and third columns refer to clones D010R 1E2, H034O 141B9 and H328C 8E8, respectively. Dark and light grey cells indicate negative and positive samples, respectively. Frequencies per 10^6 TCRs are annotated, and underlining indicates samples with a nucleotide sequence match. White cells indicate unavailable samples. Pancreatic NET, neuro-endocrine tumor.

Fig. 5. *Ex-vivo* frequencies and Ag-experienced phenotypes of circulating islet-reactive $CD8^+$ T cells. (**A**) $ZnT8_{186\text{-}194}$, $MelanA_{26\text{-}35}$ and Flu $MP_{58\text{-}66}$ MMr^+CD8^+ cells were stained *ex-vivo* and counted (see Fig. S7). Frequencies out of total $CD8^+$ T cells are depicted for T1D adults (red circles), T1D children (crossed red circles), age/sex-matched healthy adults (blue circles) and children (crossed blue circles). $*p\leq0.05$, $**p=0.002$, $***p\leq0.0003$. (**B**) Percent Ag-experienced cells out of total MMr^+ cells. $*p\leq0.03$, $**p=0.004$, $***p=0.0007$. (**C**) Absolute frequencies of the corresponding Ag-experienced fractions. $*p\leq0.03$, $**p\leq0.01$, $***p\leq0.0001$. (**D**) MMr^+CD8^+ cells reactive to the indicated islet epitopes were stained *ex-vivo* and counted (see Fig. S10A). Frequencies out of total $CD8^+$ T cells are depicted as in panel A. $*p=0.02$. (**E**) Percent Ag-experienced cells out of total MMr^+ cells. (**F**) Absolute frequencies of the corresponding Ag-experienced fractions. Bars display median values. The median number of MMr^+ events and total $CD8^+$ T cells analyzed are indicated for each distribution. Significance was determined using the Mann-Whitney test. For panels A and D, data-points with <300,000 $CD8^+$ T cells and <5 MMr^+ cells were excluded. For panels B-C and E-F, data-points with <5 MMr^+ cells were excluded.

Fig. 6. *SLC30A8* and *INS* gene expression in mTECs and circulating islet-reactive CD8$^+$ T-cell frequencies in HLA-A2$^+$ and HLA-A2$^-$ healthy donors. (**A**) *SLC30A8* RT-PCR strategy. Forward primers spanned exons 5 to 8, reverse primers spanned either exon 11 or the 3'-UTR. The position of the ZnT8$_{186-194}$-coding region is shown. (**B**) *SLC30A8* expression in mTECs, using the indicated forward primers and the exon 11 reverse primer. (**C**) *SLC30A8* expression in mTECs from donor #64 (previously testing positive with the exon 8 forward primer) and #211 (previously testing negative), using the 3'-UTR reverse primer. (**D**) *INS* RT-PCR strategy. Forward primers spanned both or neither of the PPI$_{6-14}$ and PPI$_{15-24}$ regions, reverse primers spanned either the 3'-UTR or exon 2 (PCR products 1 and 2, respectively). (**E**) *INS* expression in thymuses pooled from 5-8 donors. (**F**) *Ex-vivo* MMr$^+$CD8$^+$ cell frequencies in age/sex-matched, EboV- and HCV-seronegative HLA-A2$^+$ and HLA-A2$^-$ healthy donors. (**G**) Percent Ag-experienced MMr$^+$ cells. Bars indicate median values. The median number of MMr$^+$ events is indicated, with a median of 1x10^6 total CD8$^+$ T cells analyzed. *$p\leq0.03$, **$p=0.008$, ***$p\leq0.0004$ by Mann-Whitney test. For panels G, data points with <5 MMr$^+$ cells were excluded. NA, not available.

Fig. 7. ZnT8$_{186-194}$-reactive CD8$^+$ T cells cross-recognize a *B. stercoris* mimotope. (**A-C**) Four donors with sizable ZnT8$_{186-194}$ MMr$^+$CD8$^+$ T-cell fractions were selected. A first PBMC aliquot received PE/BV786-labeled ZnT8$_{186-194}$ MMrs and PE/BV711-labeled EboV NP$_{202-210}$ MMrs. For the second aliquot, PE-labeled *B. stercoris* MMrs replaced the PE-labeled ZnT8$_{186-194}$ MMrs. (**A**) Overlay of ZnT8$_{186-194}$/ZnT8$_{186-194}$ MMr$^+$ (blue) and ZnT8$_{186-194}$/*B. stercoris* MMr$^+$ cells (red). (**B**) Negative control staining of ZnT8$_{186-194}$/EboV NP$_{202-210}$ MMr$^+$ cells. (**C**) Positive control staining of EboV NP$_{202-210}$/EboV NP$_{202-210}$ MMr$^+$ cells from the first and second aliquot. The frequencies of MMr$^+$ out of total CD8$^+$ T cells are indicated. (**D**) Four ZnT8$_{186-194}$-reactive CD8$^+$ T-cell clones (D222D 2, D349D 178B9, H017N A1, H328C 9C8) were stained with BV786/PE-labeled ZnT8$_{186-194}$, PE-labeled *B. stercoris* and

BV650-labeled MelanA$_{26-35}$ MMrs. The ZnT8$_{186-194}$/*B. stercoris* cross-reactive clone H017N is shown, from left to right: ZnT8$_{186-194}$/*B. stercoris* MMr$^+$; ZnT8$_{186-194}$/ZnT8$_{186-194}$ MMr$^+$; and negative control ZnT8$_{186-194}$/MelanA$_{26-35}$ and *B. stercoris*/MelanA$_{26-35}$ MMr$^+$ cells. (**E**) The H017N clone was stimulated with peptide-pulsed LCLs (0.1 μM, 6 h). Percent cytokine$^+$ cells are shown as mean±SEM of two experiments. p=0.008 for Wilcoxon signed-rank comparison of pooled cytokine responses between *B. stercoris* and ZnT8$_{186-194}$, MelanA$_{26-35}$ or no peptide, and between ZnT8$_{186-194}$ and MelanA$_{26-35}$ or no peptide.

Fig. 8. *In-situ* ZnT8$_{186-194}$ MMr staining of nPOD pancreas and PLN sections. (**A-E**) Representative pancreas images (20X magnification; scale bar 100 μm) from cases T1D #6161 (A), aAb$^+$ #6347 (B) and non-diabetic (ND) #6289 (C). Red arrows indicate MMr$^+$ cells and the dotted areas of panels A-B are magnified in panels D (scale bar 80 μm) and E (scale bar 50 μm), respectively. (**F**) Consecutive sections from ZnT8$_{186-194}$ MMr$^+$ pancreata were probed with negative control MelanA$_{26-35}$ MMrs. A representative image from T1D case #6211 is shown on the left, and a positive control staining on skin sections from a vitiligo patient is shown on the right (20X; scale bar 100 μm). (**G**) Representative PLN image (20X; scale bar 100 μm) from T1D case #6161. (**H**) Magnification of the dotted area of panel G (scale bar 40 μm). (**I-J**) Number of ZnT8$_{186-194}$ and MelanA$_{26-35}$ MMr$^+$ cells/mm^2 section area of pancreas (I) and PLNs (J). Each point represents an individual case (detailed in Table S5). Bars indicate median values. *$p\leq0.05$, **$p\leq0.009$ by Mann-Whitney test. NA, not assessed.

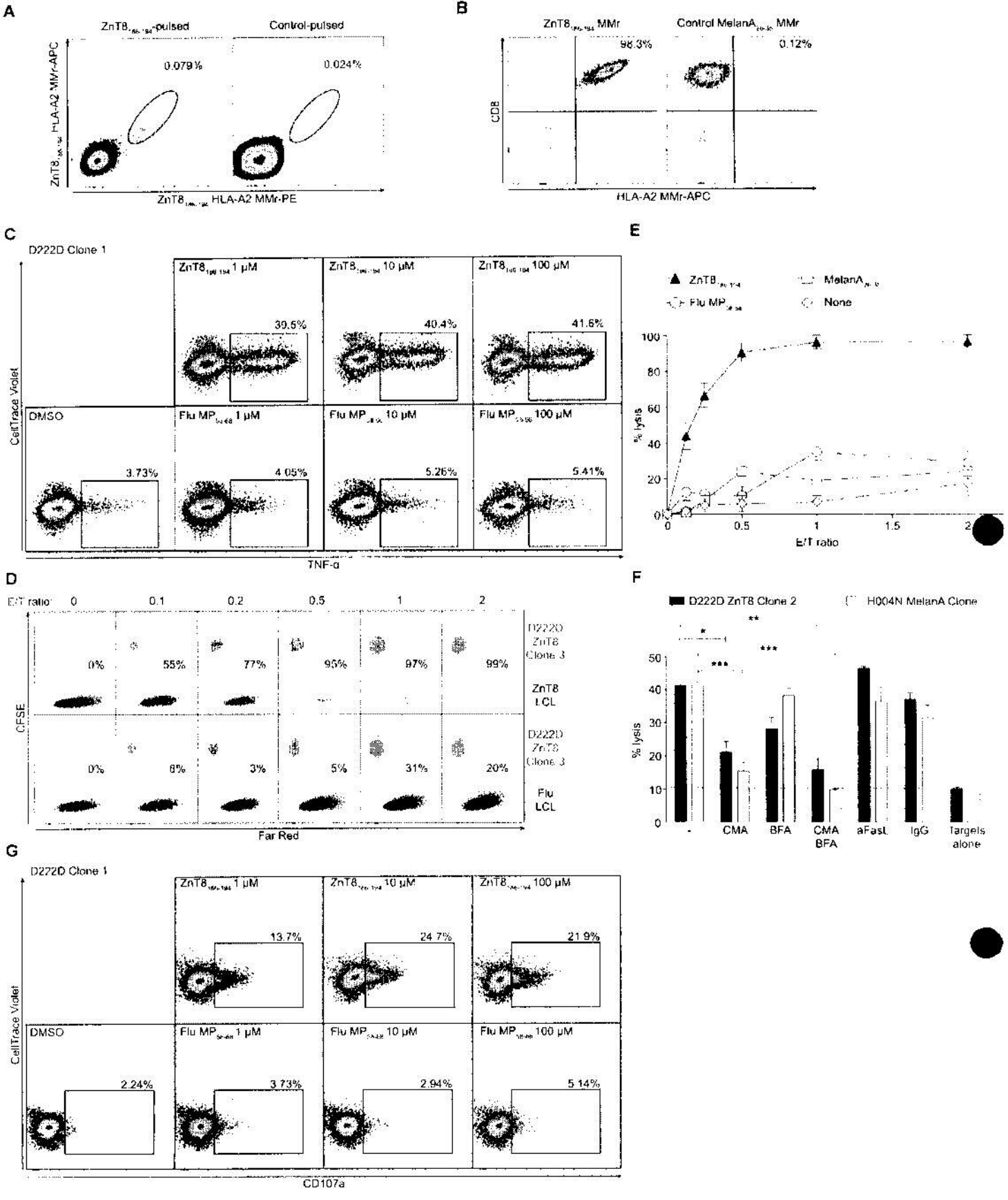
A
ZnT8 pulsed
Control-pulsed
0.079%
0.024%
HLA-A2 MMr-APC
HLA-A2 MMr-PE
B
ZnT8 MMr
Control MelanA MMr
98.3%
0.12%
CD8
HLA-A2 MMr-APC
C
D222D Clone 1
ZnT8 1 µM
ZnT8 10 µM
ZnT8 100 µM
39.6%
40.4%
41.6%
DMSO
Flu MP 1 µM
Flu MP 10 µM
Flu MP 100 µM
3.73%
4.05%
5.26%
5.41%
CellTrace Violet
TNF-α
D
E/T ratio 0 0.1 0.2 0.5 1 2
D222D ZnT8 Clone 3
ZnT8 LCL
D222D ZnT8 Clone 3
Flu LCL
0% 55% 77% 95% 97% 99%
0% 8% 3% 5% 31% 20%
CFSE
Far Red
E
ZnT8
MelanA
Flu MP
None
% lysis
E/T ratio
F
D222D ZnT8 Clone 2
H004N MelanA Clone
% lysis
-
CMA
BFA
CMA BFA
aFasL
IgG
Targets alone
G
D222D Clone 1
ZnT8 1 µM
ZnT8 10 µM
ZnT8 100 µM
13.7%
24.7%
21.9%
DMSO
Flu MP 1 µM
Flu MP 10 µM
Flu MP 100 µM
2.24%
3.73%
2.94%
5.14%
CellTrace Violet
CD107a

Figure 1.

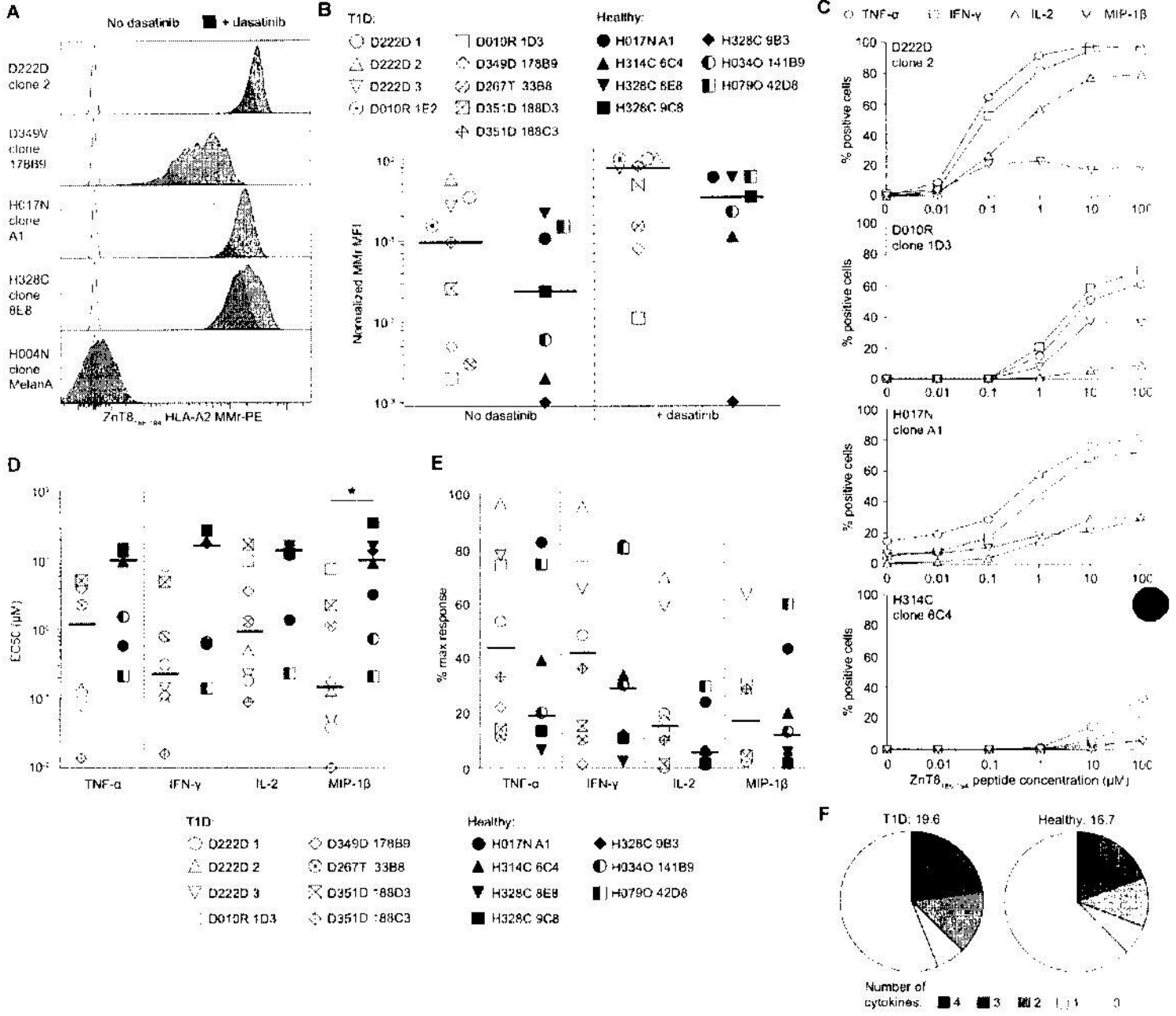
A
No dasatinib
+ dasatinib
D222D clone 2
D349V clone 17B89
H017N clone A1
H328C clone 8E8
H004N clone MelanA
ZnT8 HLA-A2 MMr-PE
B
T1D:
D222D 1
D222D 2
D222D 3
D010R 1E2
D010R 1D3
D349D 178B9
D267T 33B8
D351D 188D3
D351D 188C3
Healthy:
H017N A1
H314C 6C4
H328C 8E8
H328C 9C8
H328C 9B3
H034O 141B9
H079O 42D8
Normalized MMr MFI
No dasatinib
+ dasatinib
C
TNF-α
IFN-γ
IL-2
MIP-1β
D222D clone 2
D010R clone 1D3
H017N clone A1
H314C clone 6C4
% positive cells
ZnT8 peptide concentration (μM)
D
EC50 (μM)
TNF-α
IFN-γ
IL-2
MIP-1β
E
% max response
F
T1D: 19.6
Healthy: 16.7
Number of cytokines:

Figure 2.

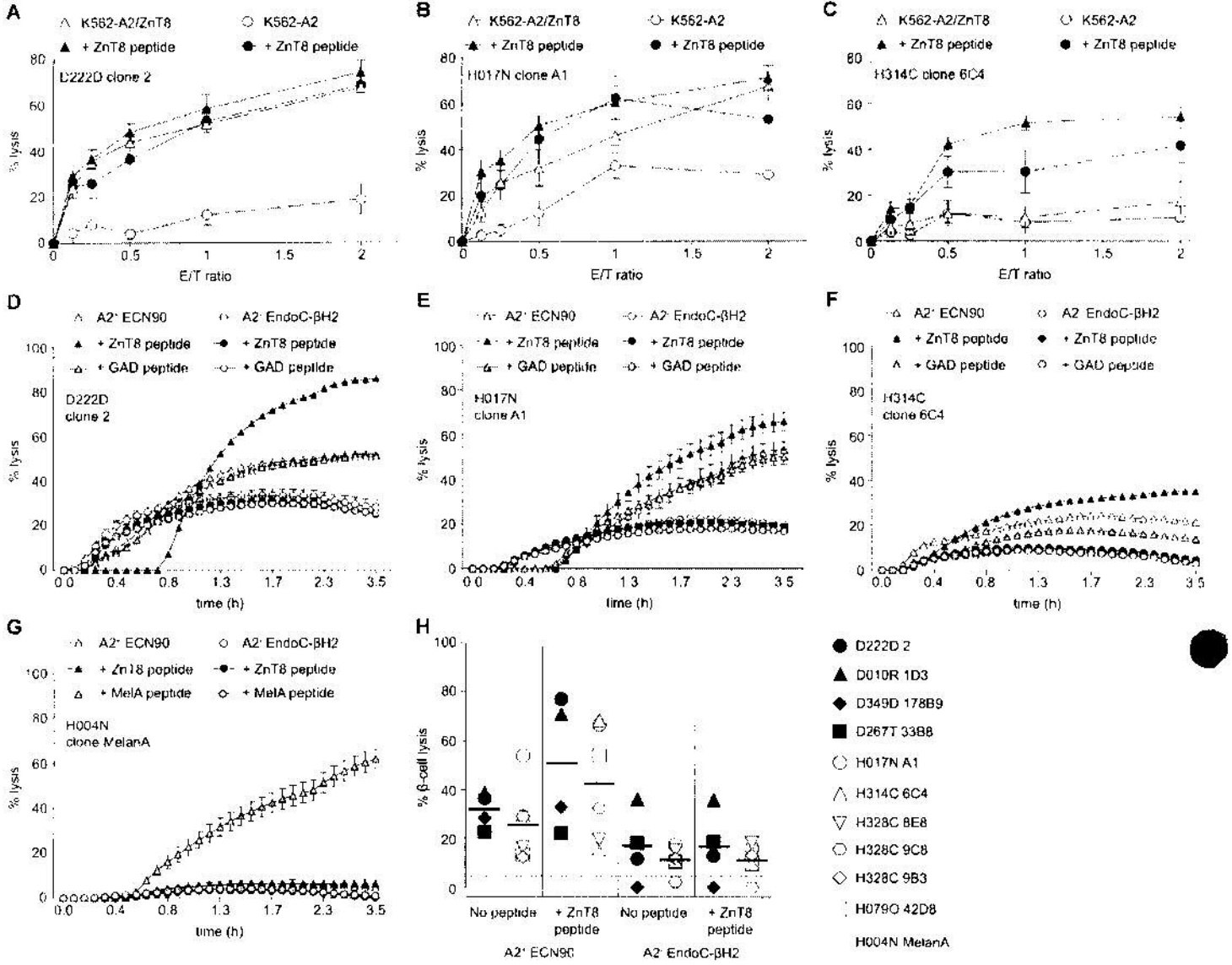
A
K562-A2/ZnT8
+ ZnT8 peptide
K562-A2
+ ZnT8 peptide
D222D clone 2
% lysis
E/T ratio
B
K562-A2/ZnT8
+ ZnT8 peptide
K562-A2
+ ZnT8 peptide
H017N clone A1
% lysis
E/T ratio
C
K562-A2/ZnT8
+ ZnT8 peptide
K562-A2
+ ZnT8 peptide
H314C clone 6C4
% lysis
E/T ratio
D
A2+ ECN90
+ ZnT8 peptide
+ GAD peptide
A2+ EndoC-βH2
+ ZnT8 peptide
+ GAD peptide
D222D
clone 2
% lysis
time (h)
E
A2+ ECN90
+ ZnT8 peptide
+ GAD peptide
A2+ EndoC-βH2
+ ZnT8 peptide
+ GAD peptide
H017N
clone A1
% lysis
time (h)
F
A2+ ECN90
+ ZnT8 peptide
+ GAD peptide
A2+ EndoC-βH2
+ ZnT8 peptide
+ GAD peptide
H314C
clone 6C4
% lysis
time (h)
G
A2+ ECN90
+ ZnT8 peptide
+ MelA peptide
A2+ EndoC-βH2
+ ZnT8 peptide
+ MelA peptide
H004N
clone MelanA
% lysis
time (h)
H
% β-cell lysis
No peptide
+ ZnT8 peptide
No peptide
+ ZnT8 peptide
A2+ ECN90
A2+ EndoC-βH2
D222D 2
D010R 1D3
D349D 178B9
D267T 33B8
H017N A1
H314C 6C4
H328C 8E8
H328C 9C8
H328C 9B3
H079O 42D8
H004N MelanA

Figure 3.

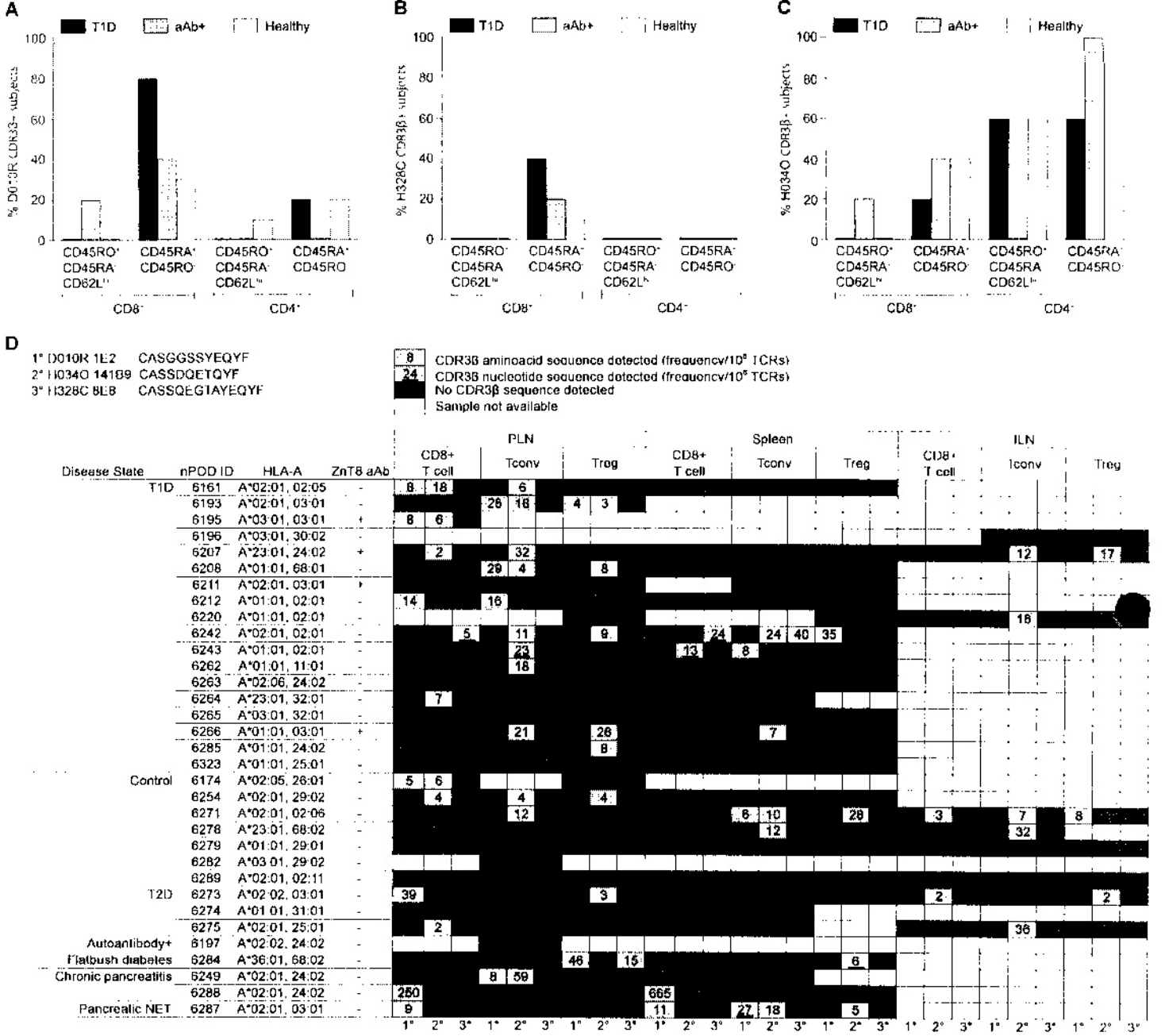
A
T1D
aAb+
Healthy
% D010R CDR3β+ subjects
CD45RO+ CD45RA- CD62L++
CD45RA+ CD45RO-
CD45RO+ CD45RA- CD62L++
CD45RA+ CD45RO
CD8+
CD4+
B
% H328C CDR3β+ subjects
CD45RO- CD45RA+ CD62L++
CD45RA- CD45RO-
CD45RO+ CD45RA- CD62L++
CD45RA- CD45RO-
C
% H034O CDR3β+ subjects
CD45RO+ CD45RA- CD62L++
CD45RA- CD45RO-
CD45RO+ CD45RA CD62L++
CD45RA- CD45RO-
D
1° D010R 1E2 CASGGSSYEQYF
2° H034O 14189 CASSDQETQYF
3° H328C 8E8 CASSQEGTAYEQYF
8
24
CDR3β aminoacid sequence detected (frequency/10^6 TCRs)
CDR3β nucleotide sequence detected (frequency/10^6 TCRs)
No CDR3β sequence detected
Sample not available
PLN
Spleen
ILN
CD8+ T cell
Tconv
Treg
Disease State
nPOD ID
HLA-A
ZnT8 aAb
T1D
Control
T2D
Autoantibody+
Flatbush diabetes
Chronic pancreatitis
Pancreatic NET

Figure 4.

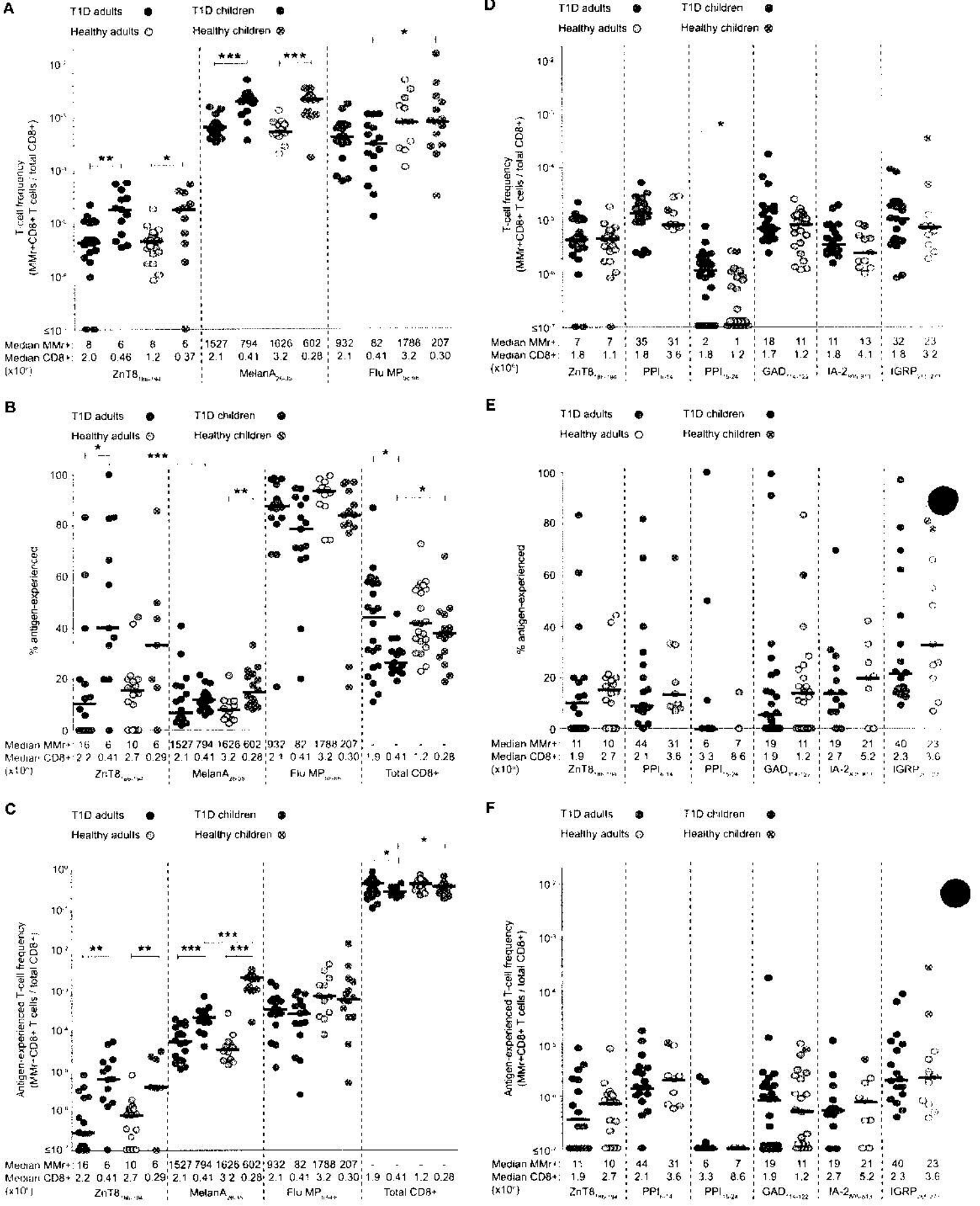
A
T1D adults
T1D children
Healthy adults
Healthy children
T-cell frequency (MMr+CD8+ T cells / total CD8+)
Median MMr+: 8 6 8 6 1527 794 1626 602 932 82 1788 207
Median CD8+ (x10⁶): 2.0 0.46 1.2 0.37 2.1 0.41 3.2 0.28 2.1 0.41 3.2 0.30
ZnT8 MelanA Flu MP
B
% antigen-experienced
Median MMr+: 16 6 10 6 1527 794 1626 602 932 82 1788 207 - - - -
Median CD8+ (x10⁶): 2.2 0.41 2.7 0.29 2.1 0.41 3.2 0.28 2.1 0.41 3.2 0.30 1.9 0.41 1.2 0.28
ZnT8 MelanA Flu MP Total CD8+
C
Antigen-experienced T-cell frequency (MMr+CD8+ T cells / total CD8+)
Median MMr+: 16 6 10 6 1527 794 1626 602 932 82 1788 207 - - - -
Median CD8+ (x10⁶): 2.2 0.41 2.7 0.29 2.1 0.41 3.2 0.28 2.1 0.41 3.2 0.30 1.9 0.41 1.2 0.28
ZnT8 MelanA Flu MP Total CD8+
D
T1D adults
T1D children
Healthy adults
Healthy children
T-cell frequency (MMr+CD8+ T cells / total CD8+)
Median MMr+: 7 7 35 31 2 1 18 11 11 13 32 23
Median CD8+ (x10⁶): 1.8 1.1 1.8 3.6 1.8 1.2 1.7 1.2 1.8 4.1 1.8 3.2
ZnT8 PPI PPI GAD IA-2 IGRP
E
% antigen-experienced
Median MMr+: 11 10 44 31 6 7 19 11 19 21 40 23
Median CD8+ (x10⁶): 1.9 2.7 2.1 3.6 3.3 8.6 1.9 1.2 2.7 5.2 2.3 3.6
ZnT8 PPI PPI GAD IA-2 IGRP
F
Antigen-experienced T-cell frequency (MMr+CD8+ T cells / total CD8+)
Median MMr+: 11 10 44 31 6 7 19 11 19 21 40 23
Median CD8+ (x10⁶): 1.9 2.7 2.1 3.6 3.3 8.6 1.9 1.2 2.7 5.2 2.3 3.6
ZnT8 PPI PPI GAD IA-2 IGRP

Figure 5.

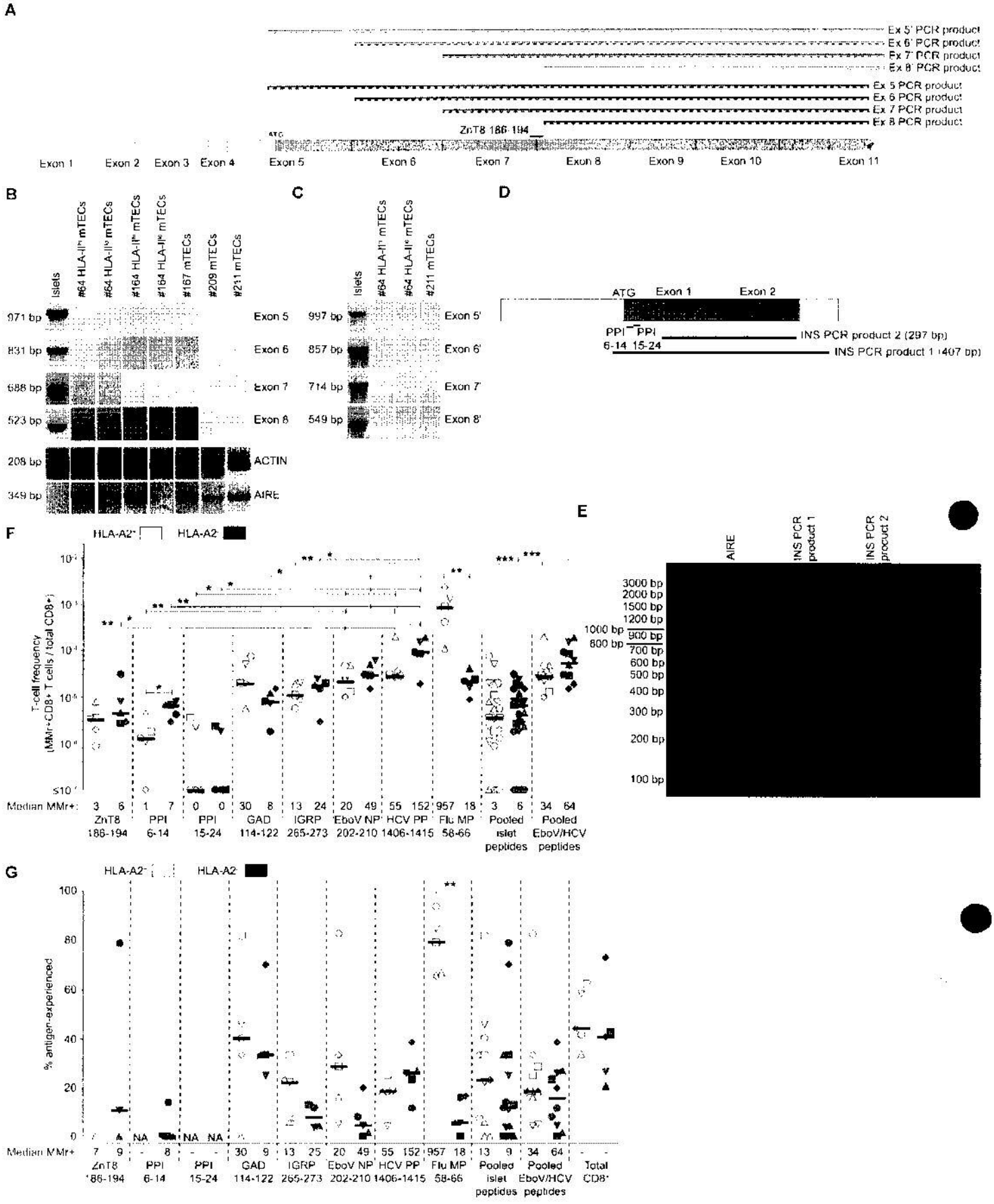
A
Ex 5' PCR product
Ex 6' PCR product
Ex 7' PCR product
Ex 8' PCR product
Ex 5 PCR product
Ex 6 PCR product
Ex 7 PCR product
Ex 8 PCR product
ZnT8 186-194
Exon 1
Exon 2
Exon 3
Exon 4
Exon 5
Exon 6
Exon 7
Exon 8
Exon 9
Exon 10
Exon 11
B
Islets
#64 HLA-II^hi mTECs
#64 HLA-II^lo mTECs
#164 HLA-II^hi mTECs
#164 HLA-II^lo mTECs
#167 mTECs
#209 mTECs
#211 mTECs
971 bp
831 bp
688 bp
523 bp
208 bp
349 bp
Exon 5
Exon 6
Exon 7
Exon 8
ACTIN
AIRE
C
997 bp
857 bp
714 bp
549 bp
Exon 5'
Exon 6'
Exon 7'
Exon 8'
D
ATG
Exon 1
Exon 2
PPI
PPI
6-14
15-24
INS PCR product 2 (297 bp)
INS PCR product 1 (407 bp)
E
AIRE
INS PCR product 1
INS PCR product 2
3000 bp
2000 bp
1500 bp
1200 bp
1000 bp
900 bp
800 bp
700 bp
600 bp
500 bp
400 bp
300 bp
200 bp
100 bp
F
HLA-A2-
HLA-A2
T-cell frequency (MMr+CD8+ T cells / total CD8+)
Median MMr+: 3 6 1 7 0 0 30 8 13 24 20 49 55 152 957 18 3 6 34 64
ZnT8 186-194
PPI 6-14
PPI 15-24
GAD 114-122
IGRP 265-273
EboV NP 202-210
HCV PP 1406-1415
Flu MP 58-66
Pooled islet peptides
Pooled EboV/HCV peptides
G
HLA-A2-
HLA-A2
% antigen-experienced
Median MMr+ 7 9 NA 8 NA NA 30 9 13 25 20 49 55 152 957 18 13 9 34 64 - -
ZnT8 186-194
PPI 6-14
PPI 15-24
GAD 114-122
IGRP 265-273
EboV NP 202-210
HCV PP 1406-1415
Flu MP 58-66
Pooled islet peptides
Pooled EboV/HCV peptides
Total CD8+

Figure 6.

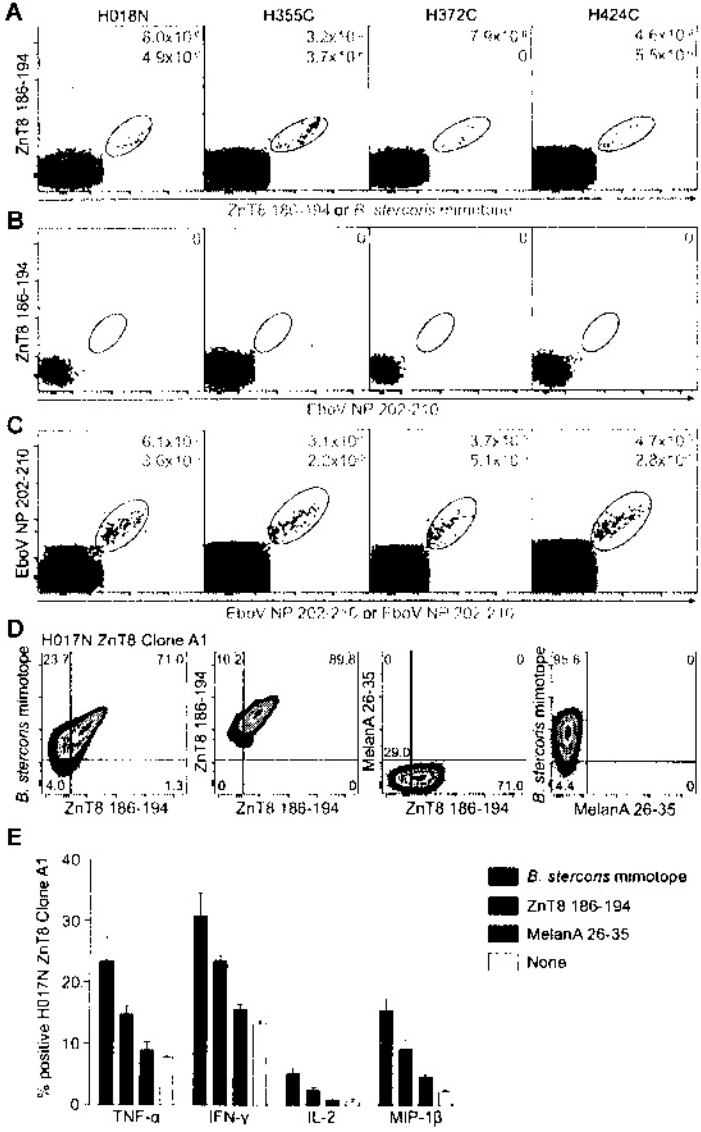
A
H018N
H355C
H372C
H424C
ZnT8 186-194
B
ZnT8 186-194
EboV NP 202-210
C
EboV NP 202-210
D
H017N ZnT8 Clone A1
B. stercoris mimotope
ZnT8 186-194
MelanA 26-35
E
% positive H017N ZnT8 Clone A1
B. stercoris mimotope
ZnT8 186-194
MelanA 26-35
None
TNF-α
IFN-γ
IL-2
MIP-1β

Figure 7.

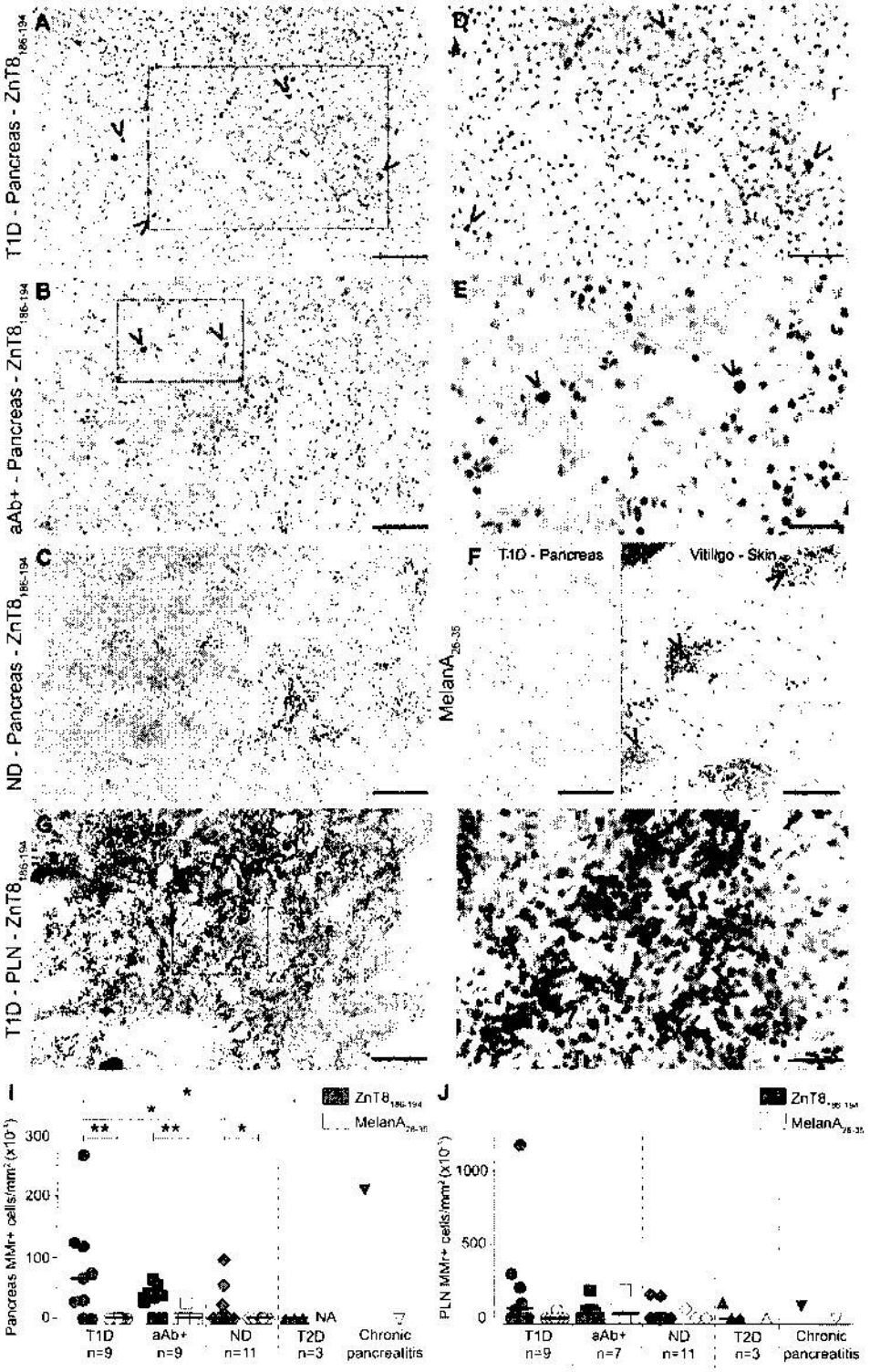
A
B
C
D
E
F
G
T1D - Pancreas - ZnT8186-194
aAb+ - Pancreas - ZnT8186-194
ND - Pancreas - ZnT8186-194
T1D - PLN - ZnT8186-194
T1D - Pancreas
Vitiligo - Skin
MelanA26-35
I
J
ZnT8186-194
MelanA26-35
Pancreas MM+ cells/mm² (x10⁻³)
PLN MM+ cells/mm² (x10⁻³)
300
200
100
0
1000
500
NA
T1D n=9
aAb+ n=9
ND n=11
T2D n=3
Chronic pancreatitis
T1D n=9
aAb+ n=7
ND n=11
T2D n=3
Chronic pancreatitis

Figure 8.

S. Culina, A.I. Lalanne et al., Islet-reactive CD8$^+$ T-cell frequencies in the pancreas but not blood distinguish type 1 diabetes from healthy donors.

Supplementary Materials

Materials and Methods

Study design. The objective of this study was to identify the features of islet-reactive $CD8^+$ T cells that associate with T1D. Hypotheses were formulated on a prospective basis guided by the data. Based on a detailed analysis of $ZnT8_{186-194}$-reactive $CD8^+$ T-cell clones (listed in Table S1), we initially hypothesized that peripheral autoreactivity occurs independently of disease status. This hypothesis was substantiated using HLA-A2 MMrs to quantify and characterize islet-reactive $CD8^+$ T cells directly *ex-vivo* (donors listed in Table S3). Next, we hypothesized that this widespread autoimmune repertoire stems from a universal leakiness of central tolerance, which was verified by thymic gene expression studies and by comparing HLA-A2-restricted Ag-reactive $CD8^+$ T-cell population frequencies in $HLA\text{-}A2^+$ vs. $HLA\text{-}A2^-$ donors (listed in Table S4). Finally, we hypothesized that the lack of distinguishing features in the periphery reflects sequestration of the disease-relevant subset in the pancreas. This hypothesis was confirmed by *in-situ* MMr staining of pancreatic sections (donors listed in Table S5). Following power analysis, age/sex-matched, unblinded case-control sets were selected from donors recruited at affiliated Diabetology Units. Samples were processed in batch, and no outliers were excluded. All *in-vitro* experiments were performed on at least two separate occasions. For *ex-vivo* MMr analyses, undersampled data-points were excluded, as detailed in Fig. 5-6.

Study approval. All subjects provided written informed consent. Ethical approval was granted by the Comité de Protection des Personnes Ile de France 1-2 (AOR10049, K091101, A01094-53) and by the Institutional Review Boards of the Cambridge Royal Free Hospital (08/H0720/25), the Benaroya Research Institute (7109-147), the University of Heidelberg (367/2002) and the University of Florida Health Center (nPOD Project). The ImMaDiab study is registered at www.clinicaltrials.gov (NCT01747967).

Peptides, MMrs and HLA-A2 binding measurements. Peptides $ZnT8_{186-194}$ (VAANIVLTV) and its *B. stercoris* WP_060386636.1 mimotope (KAANIVLTV), $ZnT8_{185-194}$ (AVAANIVLTV), $MelanA_{26-35}$ (A27L variant; ELAGIGILTV), Flu MP_{58-66} (GILGFVFTL), PPI_{6-14} (RLLPLLALL), PPI_{15-24} (ALWGPDPAAA), $GAD_{114-122}$ (VMNILLQYV), $IA\text{-}2_{805-813}$ (VIVMLTPLV), $IGRP_{265-273}$ (VLFGLGFAI), EboV $NP_{202-210}$ (RLMRTNFLI) and HCV $PP_{1406-1415}$ (KLVALGINAV) were synthesized at >85% purity (ChinaPeptides). Peptide-HLA-A2 affinity and stability assays were performed as detailed in Fig. S2. HLA-A2 MMrs were produced as described (*39*), and staining was performed in the presence of 50 nM dasatinib (*11*). For Fig. 2B, MMr MFIs were normalized to that of D222D clone 2 in the presence of dasatinib.

Cloning of $ZnT8_{186-194}$-reactive $CD8^+$ T cells. Frozen-thawed PBMCs ($2\text{-}10x10^6$) were stained with dual fluorochrome-labeled $ZnT8_{186-194}$ MMrs, either directly *ex-vivo* or after 10 days of acDC culture (*8*) in the absence or presence of 1 µM peptide ($ZnT8_{186-194}$ or $ZnT8_{185-194}$). Double-positive events were then sorted as single cells into individual wells of a U-bottom 96-well plate. Each sort well contained 200,000 irradiated PBMCs, 5% Cellkines (Zeptometrix), 200 IU/ml Proleukin, 25 ng/ml IL-15, 1 µg/ml phytohemagglutinin (PHA)-L (Sigma), penicillin/streptomycin and amphotericin B. Medium was replenished every 3 days

without PHA-L. Expanding clones were selected by visual inspection, transferred into 48-well plates for specificity testing and restimulated as above every 2-3 weeks.

Antigen recall assays. Peptide-pulsed HLA-A2$^+$ LCLs or K562 cells transduced with HLA-A2, CD80 and 4-1BBL (a kind gift from Dr. J. Riley, University of Pennsylvania, Philadelphia, PA) were labeled with CellTrace Violet (Life Technologies) and incubated with T cells at an E/T ratio of 2/1 for 6 h in the presence of 10 µg/ml brefeldin A. Intracellular cytokine staining was performed using BD Cytofix/Cytoperm reagents and analyzed using a BD LSR Fortessa cytometer. CD107a staining was performed with a FITC-labeled mAb (clone H4A3, BD). Polyfunctionality indices were calculated as described (*12*).

Cytotoxicity assays. LCL, K562-A2 or K562-A2/ZnT8 target cells were labeled with CellTrace FarRed (Life Technologies), dispensed into 96-well flat-bottom plates at 10^5 cells/well and co-cultured with different numbers of CFSE-labeled T cells for 6-24 h. After staining with Live/Dead Aqua (Life Technologies) and fixation, a set number of CompBeads (BD) was added to each well. Flow cytometric analysis was performed by counting the numbers of CFSE$^-$FarRed$^+$Live/Dead$^-$ targets for each condition, normalized to equal numbers of CompBeads. Percent lysis was calculated as 100 × (live targets cultured alone) - (live targets in the presence of T cells) / (live targets cultured alone). Blocking experiments were conducted with concanamycin A (100 nM; Sigma), brefeldin A (5 µg/ml; Sigma) and the anti-FasL antibody NOK-1 (5 µg/ml; BD).
The EndoC-βH2 cell line (HLA-A*01/03, -B*07/08, -C*07/07) was described previously (*40*), and the ECN90 cell line (HLA-A*02:01/03, -B*40/49, -C*03/07) was derived from a human neonatal pancreas using similar protocols. Real-time cytotoxicity assays on β-cell lines were performed using the xCELLigence system (ACEA Biosciences). Briefly, β cells were dispensed into 96-well E-plates and pretreated as indicated. After resting for 20 h and pulsing with 10 µM peptide or DMSO for 2 h, T cells were added at an E/T ratio of 2/1, and impedance was recorded every 5-15 min for 4 h. Cell indices were normalized to values at the time of T-cell addition (t=0) and transformed to percent lysis.

TCR sequencing, in-silico analyses and clonotype-specific TaqMan assays. TRA and *TRB* gene expression was analyzed using a template-switch anchored RT-PCR (*41*) for T-cell clones and a multiplex nested PCR (*42*) for single-sorted cells. Gene usage was determined according to the ImMunoGeneTics (IMGT) nomenclature.
The *TRB* database (Adaptive Biotechnologies) used for *in-silico* analyses was derived from the donors listed in Table S2. TaqMan assays (Life Technologies; Fig. S6) were applied to cDNA samples from naïve (CD45RA$^+$CCR7$^+$) and Ag-experienced (CD45RA$^+$CCR7$^-$ or CD45RA$^-$CCR7$^{+/-}$) CD4$^+$ and CD8$^+$ T cells bulk-sorted from age/sex-matched cohorts incorporating 83 T1D patients [age 34 years (17-59), 51% females, T1D duration 8 years (0.1-55), 51% HLA-A2$^+$] and 93 healthy donors [age 34 years (17-60), 47% females, 41% HLA-A2$^+$]. cDNA samples were amplified using clonotype-specific TaqMan primers for 18 cycles, followed by real-time qPCR using clonotype-specific TaqMan assays on Fluidigm 96.96 microfluidic chips with a BioMark HD qPCR system. Amplification curves for

individual assays were examined and compared with curves from a *TRB* constant region assay as a control for *TRB* templates in each reaction.

Ex-vivo analysis of $ZnT8_{186-194}$-reactive $CD8^+$ T cells. Cryopreserved PBMCs from T1D and healthy donors (Table S3) were magnetically depleted of $CD8^-$ cells (StemCell Technologies), stained with the combinatorial MMr panels (*9*) detailed in Fig. S7 and S10 and acquired using a BD FACSAria III cytometer. IFN-γ ELISpot assays were performed as described (*7*). Single-cell gene expression analysis is detailed in Fig. S9A and Table S6.

Gene expression in human mTECs. Human thymus samples were obtained from children undergoing corrective cardiac surgery at the University of Heidelberg, Germany. mTECs were purified as described (*13*). Sorted total, immature and mature mTECs ($CD45^-$ $EpCAM^+CDR2^-$) were independently validated for gene expression of the tissue-restricted Ags β-casein and MelanA (*13*). Amplified bands were sequences to confirm identity with the expected *SLC30A8* and *INS* regions. *SLC30A8* exons were annotated with reference to Ensembl ID ENST00000427715. The *INS* PCR covered all *INS* transcripts except ENST00000512523 (product 1) and ENST00000421783 (product 2).

In-situ $ZnT8_{186-194}$ MMr staining. In-situ staining was performed as described (*2*). Briefly, unfixed, frozen sections were dried for 2 h, loaded with 1 μg of MMrs overnight at 4°C, washed gently with phosphate-buffered saline and fixed in 2% paraformaldehyde for 10 min. After a further wash, endogenous peroxidase activity was blocked with 0.3% H_2O_2. Sections were then incubated serially with rabbit anti-phycoerythrin, horseradish peroxidase-conjugated swine anti-rabbit and 3,3'-diaminobenzidine tetrahydrochloride substrate (Thermo Scientific). After a final wash, sections were counterstained with hematoxylin, dehydrated *via* sequential passages in 95-100% ethanol and xylene, mounted and analyzed using a Nikon Eclipse Ni microscope with NIS-Elements Analysis D software v4.40.

Statistical analysis. Data are shown as median (range) or mean±SEM. Significance was assessed using two-tailed tests with a cut-off value of $\alpha=0.05$, as detailed for each figure.

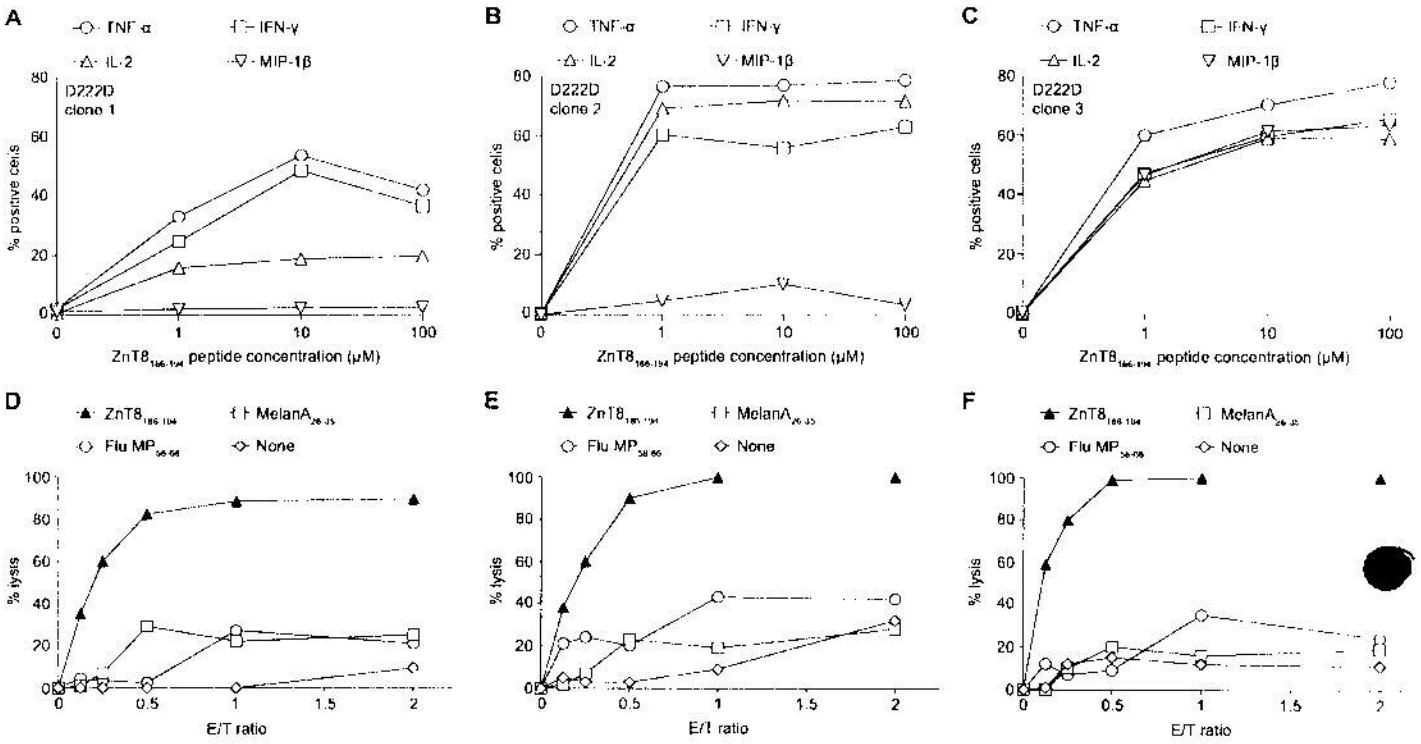

Fig. S1. Cytokine secretion and cytotoxicity of ZnT8$_{186-194}$-reactive CD8$^+$ T cells from T1D patient D222D. (**A-C**) D222D clone 1 (A), 2 (B) or 3 (C) were stimulated for 6 h with K562-A2 cells pulsed with the indicated peptide concentrations. Graphs display percent intracellular cytokine$^+$ cells calculated after gating on viable CD8$^+$ cells, as shown in Fig. 1C. The following antibodies were used: anti-TNF-α-APC (clone MAb11, BD), anti-IFN-γ-PE (clone 4S.B3, eBioscience), anti-IL-2-PE/Cy7 (clone MQ1-17H12, eBioscience) and anti-MIP-1β-FITC (clone 24006, R&D). (**D-F**) FarRed-labeled HLA-A2$^+$ LCL target cells were pulsed with the indicated peptides and cultured with CFSE-labeled D222D clones 1 (D), 2 (E) or 3 (F) at increasing E/T ratios. Live FarRed$^+$ target cells were counted at 24 h and normalized to a fixed number of beads added to each well. Percent lysis is plotted for each graph, calculated as 100 × (live targets cultured alone) – (live targets in the presence of T cells) / (live targets cultured alone). Results are representative of three independent experiments. For panels A-C, results are shown from a separate experiment than depicted in Fig. 1C. For panels D-F, results are shown from the three separate clones, with raw data for D222D clone 3 depicted in Fig. 1D, and pooled data for all three clones depicted in Fig. 1E.

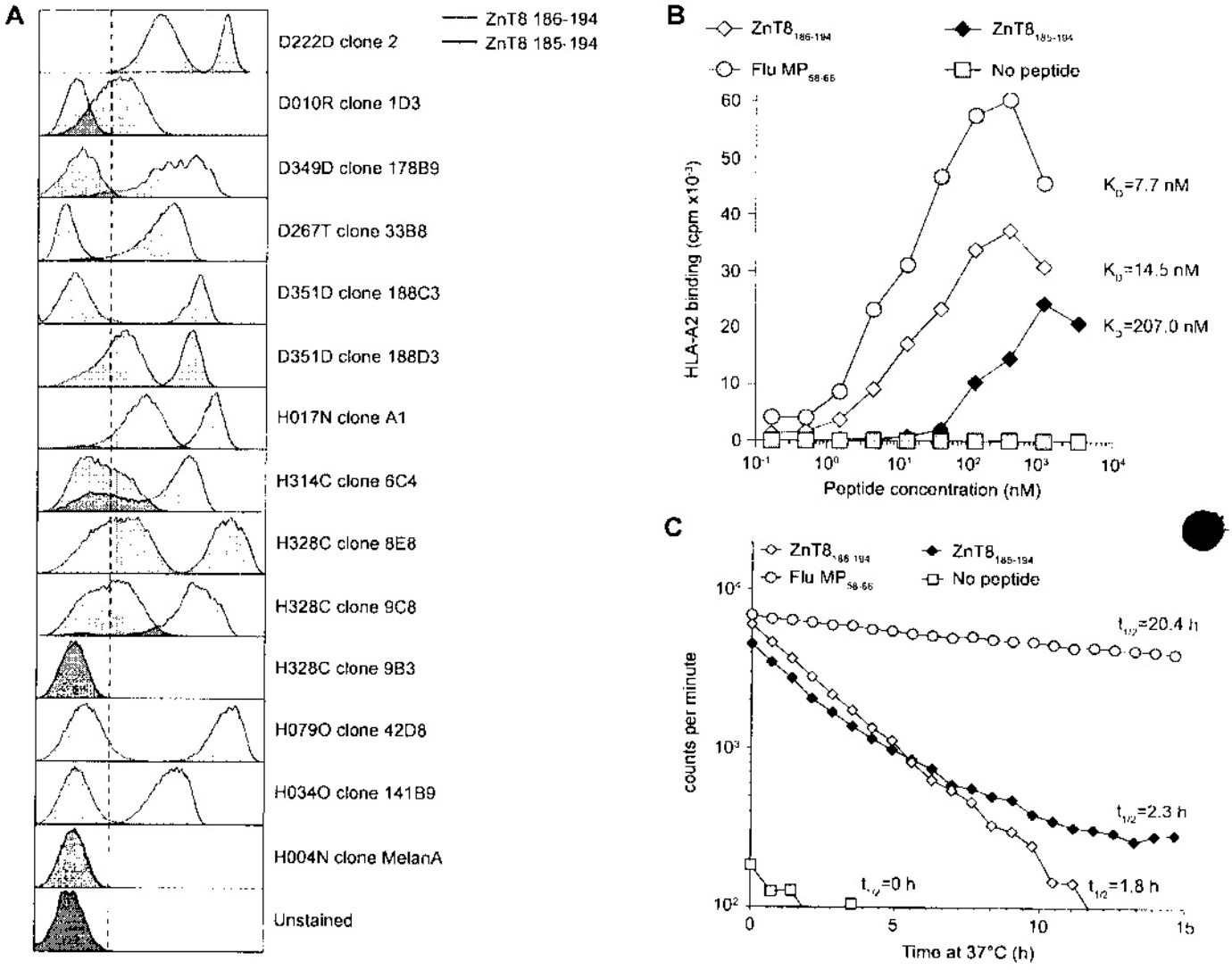

Fig. S2. CD8$^+$ T-cell recognition and HLA-A2 binding of ZnT8$_{186\text{-}194}$ and ZnT8$_{185\text{-}194}$ epitope variants. (**A**) The indicated clones were stained with HLA-A2 MMrs loaded with either ZnT8$_{186\text{-}194}$ (VAANIVLTV; blue profiles) or ZnT8$_{185\text{-}194}$ (AVAANIVLTV; red profiles) in the presence of dasatinib. MMr fluorescence intensities registered in separate runs were made comparable by using the same flow cytometer settings, by recalibrating the cytometer for each run using Spherotech Rainbow Calibration particles, and by including a reference D222D clone (thawed cryovials from the same freeze) in all experiments. The MMr fluorescence registered in each run for the reference D222D clone was also used to further normalize the median fluorescence intensities plotted in Fig. 2B. (**B**) *In-vitro* HLA-A2 binding affinity measurements for the ZnT8$_{186\text{-}194}$ (white diamonds) and ZnT8$_{185\text{-}194}$ peptides (black diamonds). Recombinant HLA-A2 (0.7 nM) was mixed in 96-well polypropylene plates (Nunc) with β_2-microglobulin (β_2M; 25-50 nM) and the indicated peptide (5-fold titrations) in phosphate-buffered saline supplemented with 0.1% Lutrol F-68 and allowed to form complexes at 18°C for 48 h. Amounts of each peptide-HLA complex were determined using an AlphaScreen assay (Perkin Elmer) with streptavidin-conjugated donor beads and W6/32 anti-HLA Class I antibody-conjugated acceptor beads. Peptide-HLA complexes (10 µl) were transferred to 384-well OptiPlates (Perkin Elmer) in duplicates, mixed with 30 µl each of streptavidin-conjugated donor beads and W6/32-conjugated acceptor beads, and

incubated in the dark for 6-8 h at room temperature. Plates were analyzed using an Envision reader (Perkin Elmer). (**C**) *In-vitro* HLA-A2 stabilization assays with the $ZnT8_{186-194}$ and $ZnT8_{185-194}$ peptides. Recombinant HLA-A2 molecules were incubated with the indicated peptides and the corresponding dissociation rates were monitored over time. Briefly, biotinylated recombinant HLA-A2 (30 nM) was mixed with peptide (10 mM) and ^{125}I-labeled β_2M (25,000 cpm/well), transferred to a 96-well FlashPlatePlus (Perkin Elmer), and allowed to form complexes overnight at 18°C. Dissociation was initiated by adding unlabeled β_2M at a final concentration of 360 nM and monitored by consecutively reading the microplates in a TopCount NXT scintillation counter (Perkin Elmer) at 37°C for 15 h. K_D affinity (B) and half-life ($t_{1/2}$) values (C) are displayed, as calculated using a non-linear regression fit (GraphPad Prism 5). Results are representative of three independent experiments.

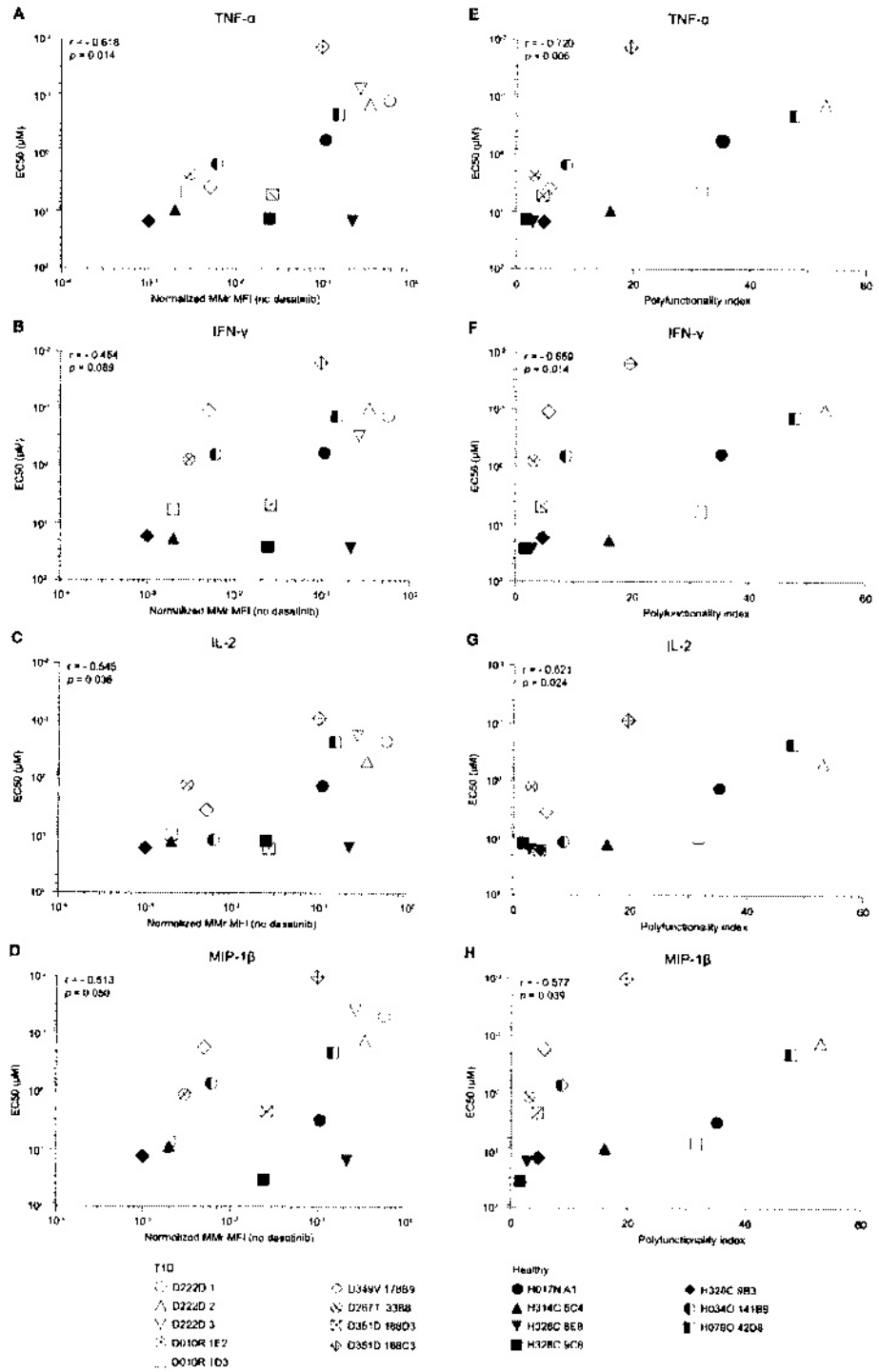

Fig. S3. Ag sensitivity correlates with Ag avidity and polyfunctionality in ZnT8$_{186\text{-}194}$-reactive CD8$^+$ T-cell clones. (A-D) The indicated CD8$^+$ T-cell clones generated from T1D and healthy subjects (white and black symbols, respectively, as in Fig. 2) were compared for normalized MMr MFI in the absence of dasatinib (from Fig. 2B; x-axis) *vs.* ZnT8$_{186\text{-}194}$ peptide EC50 for the indicated cytokine responses (from Fig. 2D; y-axis). EC50 values are plotted from higher to lower, corresponding to increasing Ag sensitivity. **(E-H)** The same clones were compared for polyfunctionality index (from Fig. 2F; x-axis) *vs.* ZnT8$_{186\text{-}194}$ peptide EC50 (as in panels A-D). The corresponding Spearman r and *p* values are displayed for each panel.

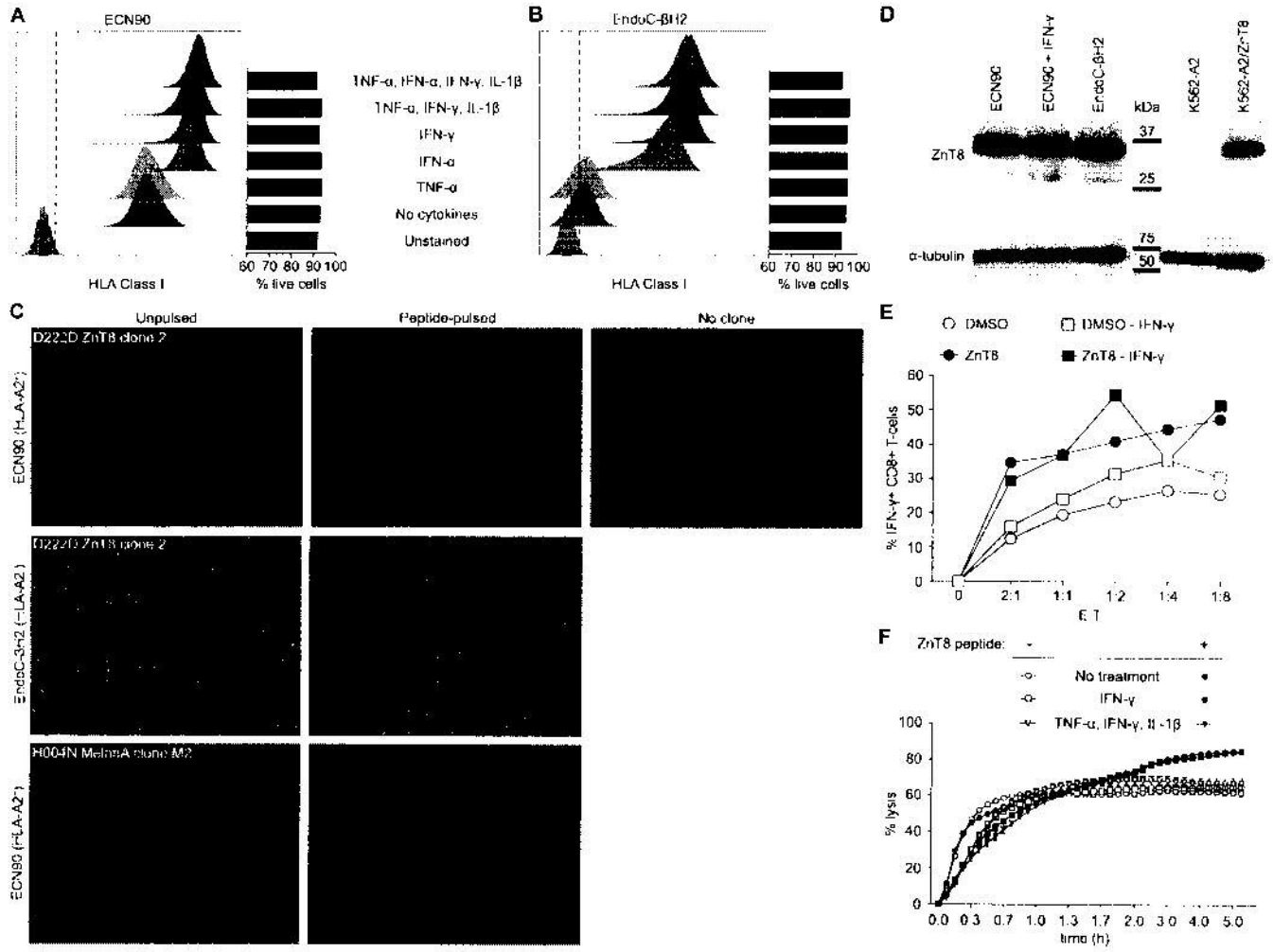

Fig. S4. Modulation of HLA Class I and ZnT8 expression in human β-cell lines. (A-B) Surface HLA Class I expression (anti-HLA-A, B, C antibody W6/32, labeled in-house with AlexaFluor647) and Live/Dead Red viability of HLA-A2$^+$ ECN90 (A) and HLA-A2$^-$ EndoC-βH2 cell lines (B) with and without exposure to the indicated cytokines for 18 h. The following cytokine cocktails were used: TNF-α alone (1,100 U/ml); IFN-α alone (500 U/ml); IFN-γ alone (500 U/ml); TNF-α, IFN-γ and IL-1β (1,100 U/ml, 2,000 U/ml and 1,000 U/ml, respectively); TNF-α, IFN-α, IFN-γ and IL-1β (2,500 U/ml, 1,000 U/ml, 500 U/ml and 50 U/ml, respectively). Results are representative of three independent experiments. **(C)** Representative optical microscopy images (10X magnification) of wells in which $ZnT8_{186-194}$-reactive D222D clones or $MelanA_{26-35}$-reactive clones were co-cultured with HLA-A2$^+$ ECN90 or HLA-A2$^-$ EndoC-βH2 cells for the cytotoxicity assays depicted in Fig. 3D-G. T cells were removed by gentle washing and the remaining cells were stained with Trypan Blue. Two independent experiments were performed. **(D)** ZnT8 expression in ECN90 and EndoC-βH2 β-cell lines pretreated with or without IFN-γ (500 U/ml, 18 h), as assessed by Western blot using an anti-ZnT8 antibody (clone 17H2.4, produced in-house). K562-A2 cells transduced or not with a full-length ZnT8 plasmid are shown as positive and negative controls, respectively. α-tubulin expression is shown as a loading control. **(E)** IFN-γ recall

assay for D222D clone 2 on ECN90 cells pretreated with or without IFN-γ (500 U/ml, 18 h), washed and pulsed with DMSO or 10 μM $ZnT8_{186-194}$ peptide for 2 h. A fixed number of T-cell effectors was co-cultured with increasing numbers of ECN90 targets for 6 h. Percent IFN-γ^+ cells was calculated from plots gated on viable $CD8^+$ cells. (**F**) Real-time cytotoxicity assays for D222D clone 2 in the presence of ECN90 cells (E/T ratio 2/1) pretreated with or without the indicated cytokines for 18 h. Results in panels D-F are representative of at least two independent experiments.

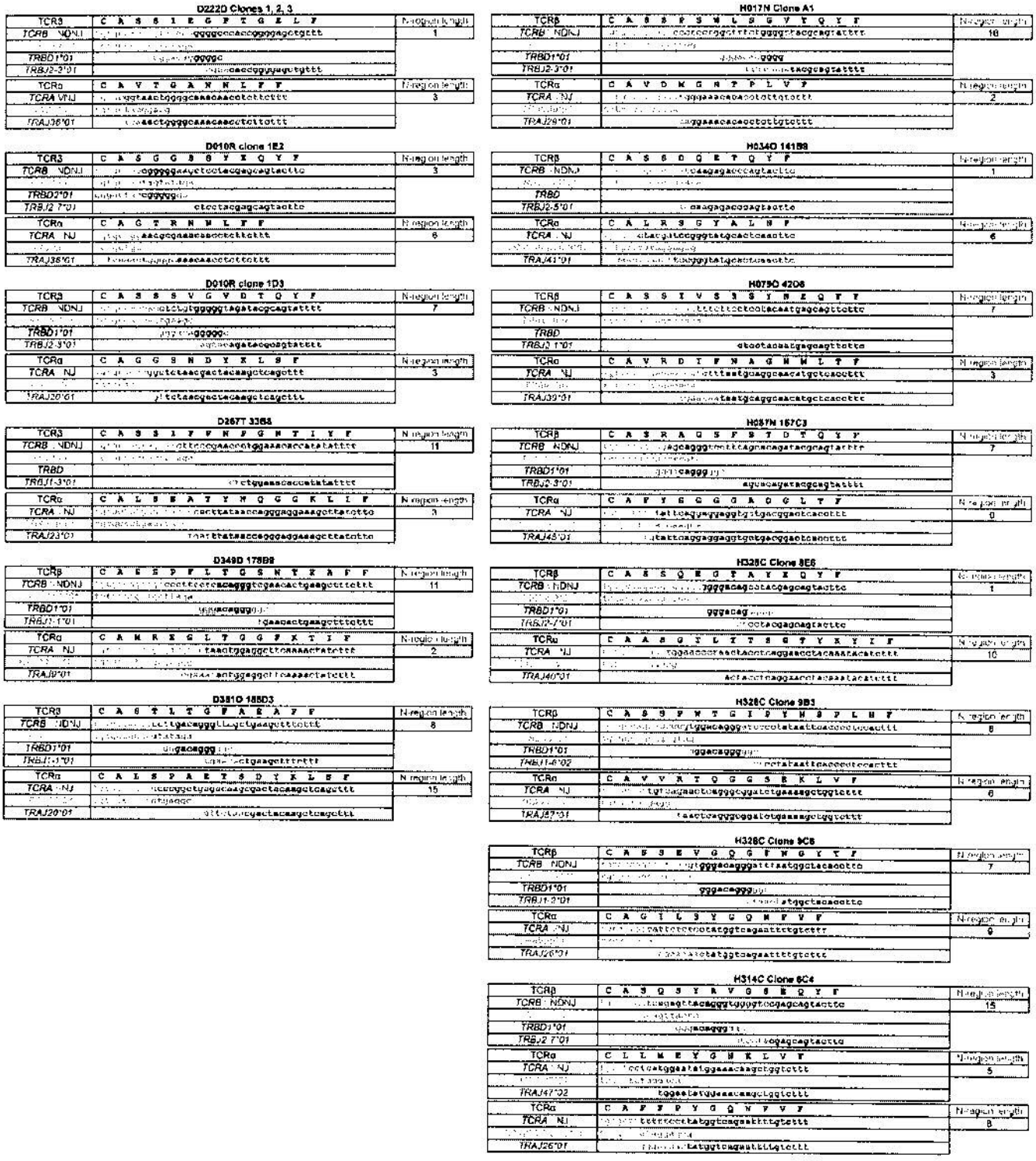

Fig. S5. TCR sequences of ZnT8$_{186\text{-}194}$-reactive CD8$^+$ T-cell clones. Clones isolated from T1D patients are shown on the left and clones isolated from healthy donors are shown on the right. Nucleotide sequences rearranged from the indicated V (green), D (black) and J (blue) genes are shown for each clone. Nucleotide additions at the V-D, D-J and V-J junctions are shown in red and the corresponding N-region length is indicated (right column).

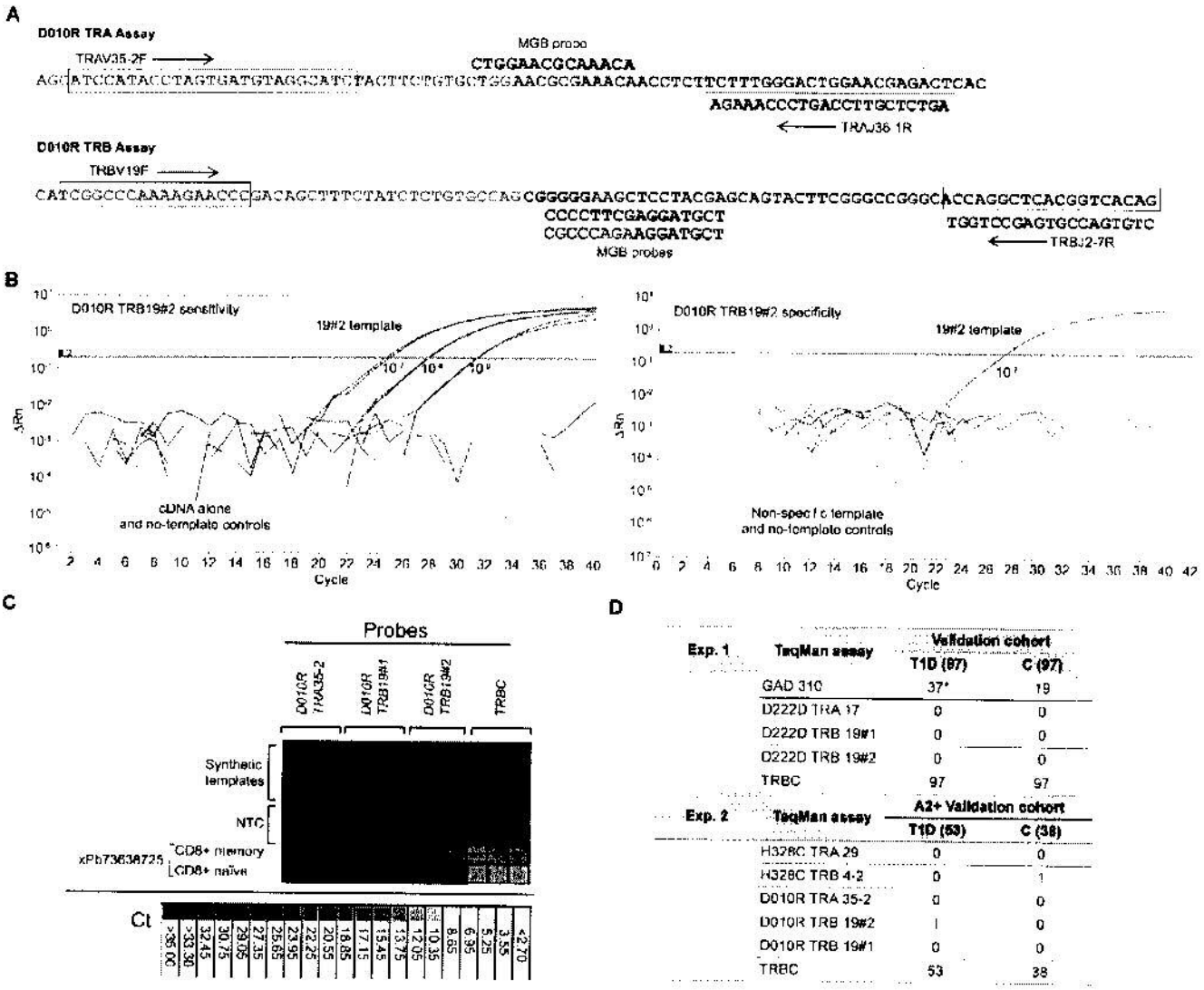

Exp. 1	TaqMan assay	Validation cohort T1D (97)	C (97)
	GAD 310	37*	19
	D222D TRA 17	0	0
	D222D TRB 19#1	0	0
	D222D TRB 19#2	0	0
	TRBC	97	97

Exp. 2	TaqMan assay	A2+ Validation cohort T1D (53)	C (38)
	H328C TRA 29	0	0
	H328C TRB 4-2	0	1
	D010R TRA 35-2	0	0
	D010R TRB 19#2	1	0
	D010R TRB 19#1	0	0
	TRBC	53	38

Fig. S6. ZnT8$_{186\text{-}194}$-reactive clonotype-specific TaqMan assays. (**A**) TaqMan assays were designed for the ZnT8$_{186\text{-}194}$-reactive CDR3 regions of the rearranged *TRA* (top) and *TRB* genes (bottom) from clones D010R 1E2, H328C 8E8 and D222D by placing forward primers in the V region and reverse primers in the J region of each transcript (black fonts). A 6-carboxyfluorescein (FAM)-labeled minor groove binder (MGB) probe was designed to cover the unique N(D)N region of each chain. For *TRBV19*$^+$ CDR3β regions (clones D010R and D222D), two unique nucleotide sequences were screened using two different probes (TRB19#1 and TRB19#2). Sequences corresponding to the V, D, N and J regions are shown in green, black, red and blue, respectively. The example shows TaqMan assays for the D010R clonotype. (**B**) Clonotype-specific TaqMan assays were validated using synthetic DNA templates (Life Technologies) for clonotype-specific or irrelevant *TRA* and *TRB* sequences. Ten-fold dilutions of the templates (from 10^{-7} to 10^{-9}; left panel, purple profiles) were spiked into naïve CD8$^+$ T-cell cDNA and amplified by qPCR. As shown for the D010R TRB19#2 probe, the sensitivity was 10^{-9}, equivalent to 100 copies of template (equivalent to ~1 T cell). The right panel shows that non-specific DNA templates and no-template controls (colored profiles) were not amplified. The blue line marks the detection threshold, set at a change in normalized reporter value (ΔRn) of 0.2. (**C**) Clonotype-specific TaqMan assays were used to screen cDNA from pooled naïve (CD45RA$^+$CCR7$^+$) or Ag-experienced (CD45RA$^+$CCR7$^-$ or

$CD45RA^-CCR7^{+/-}$) $CD4^+$ or $CD8^+$ T cells isolated from T1D or age/sex-matched healthy donors. Samples were pre-amplified with the pooled clonotype assays, and the products were used for real-time qPCR on a Fluidigm platform. Representative results are shown for the D010R *TRA* and *TRB* probes depicted in panels A-B, along with a *TRBC* probe included as a positive control for *TRB* templates in each sample. Results are shown for T1D patient xPb73638725 testing positive on memory and negative on naïve $CD8^+$ T cells. NTC, no-template controls. **(D)** Summary of the results obtained by screening T1D and control (C) healthy donors (number of subjects indicated in parentheses) with the D222D ZnT8 and control GAD clonotype-specific probes (experiment 1, top panel) and with the H328C and D010R clonotype-specific probes (experiment 2, bottom panel; only $HLA\text{-}A2^+$ subjects were analyzed). The number of subjects with ≥1 positive sample for each of the indicated assays is reported.

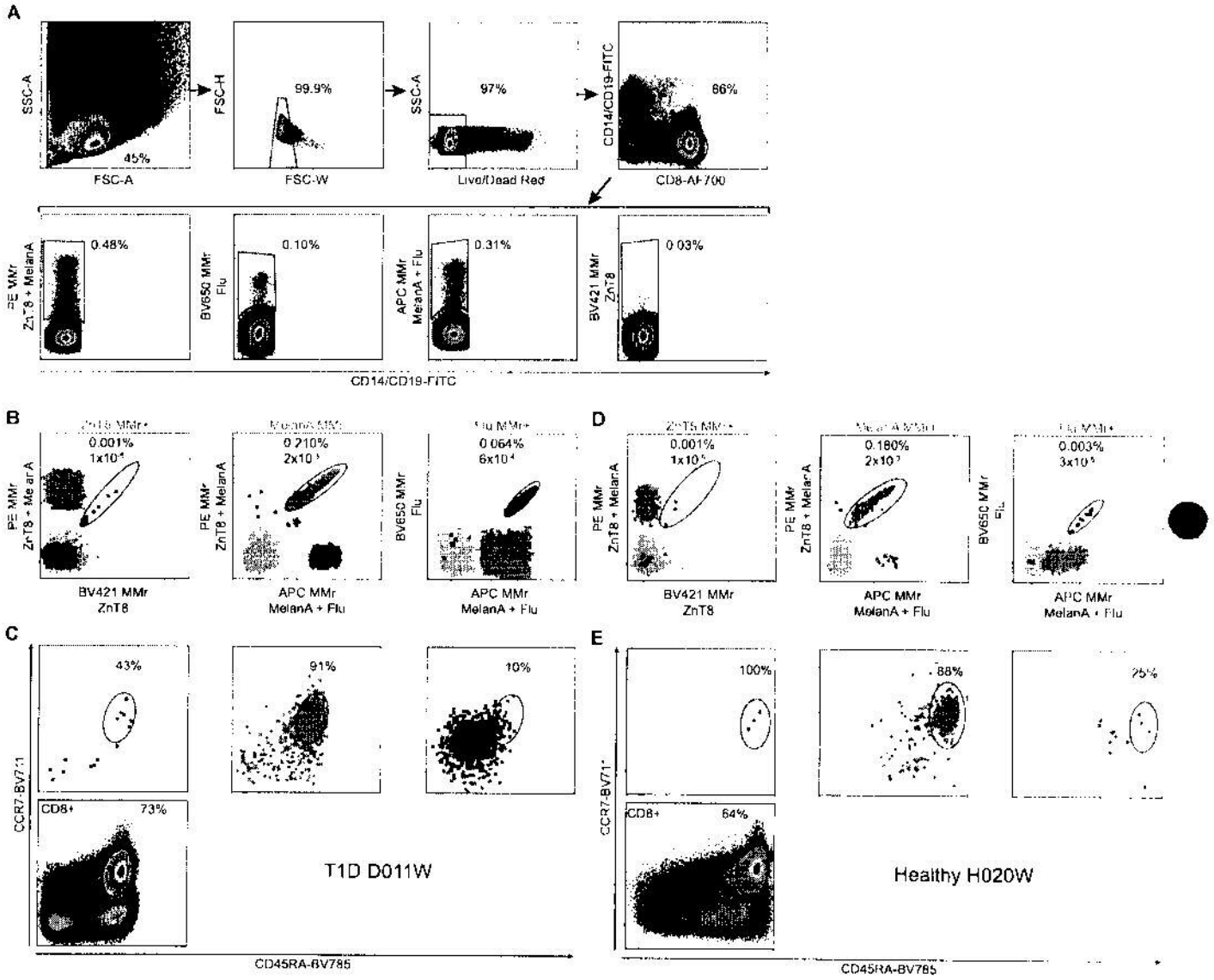

Fig. S7. Gating strategy for the analysis of $ZnT8_{186-194}$, $MelanA_{26-35}$ and Flu MP_{58-66} MMr^+CD8^+ T cells. (**A**) After magnetic depletion of $CD8^+$ cells in frozen-thawed PBMCs from T1D patient #D011W, cells were sequentially gated on small lymphocytes, singlets, live cells (Live/Dead Red^-), $CD8^+$ T cells (FITC-CD14/CD19$^-$, AlexaFluor700-$CD8^+$; clones 61D3, HIB19, RPA-T8, respectively; eBioscience) and total PE^+, $BV650^+$, APC^+ and $BV421^+$ MMr^+ T cells. $ZnT8_{186-194}$ MMr-PE/$BV421^+$, $MelanA_{26-35}$ MMr-PE/APC^+ and Flu MP_{58-66} MMr-APC/$BV650^+$ events were visualized using the gating strategy previously detailed for combinatorial MMr staining (*9*) and FlowJo v10 software (Tree Star). The staining panel also included anti-CD45RA-BV785 (clone HI100, BioLegend) and anti-CCR7-BV711 (clone 150503, BD). (**B**) The final readout obtained for T1D patient #D011W after gating out events positive for <2 or >2 MMr fluorochromes is shown, with events corresponding to each epitope-reactive population depicted in different colors within each plot, and MMr^- events depicted in grey. (**C**) Percent naïve ($CD45RA^+CCR7^+$) cells is shown after gating on the corresponding MMr^+ fractions, with the distribution of total $CD8^+$ T cells shown for comparison. Percent Ag-experienced fractions displayed in Fig. 5 included all cells not falling into the naïve gate (i.e. $CD45RA^+CCR7^-$ and $CD45RA^-CCR7^{+/-}$). (**D-E**) The final readout of MMr^+ cells and naïve fractions is shown for healthy donor #H020W.

A

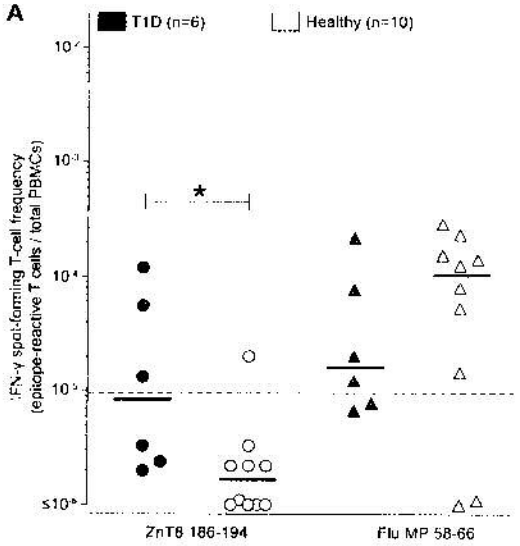

B

	% positive		T1D (n=6)						Healthy (n=10)									
	T1D	Healthy	D001W	D004W	D008W	D014W	D027W	D028W	H005W	H006W	H015W	H015T	H017T	H314C	H316C	H297S	H356C	H372C
ZnT8 186-194	50.0% (3/6)	10.0% (1/10)			3.3		2.2	2.2	1.1	2.2	3.3	1.1	2.2	0.0	0.0	2.2		0.0
Flu MP 58-66	66.7% (4/6)	80.0% (8/10)			6.7	7.8		12.2					1.1					0.0
PHA	100% (6/6)	100% (10/10)																
Basal+3SD			5.8	10.0	10.0	5.8	5.8	20.8	20.8	15.3	5.8	20.8	5.8	10.0	5.8	17.3	10.0	30.0
Basal+4SD			7.7	13.3	13.3	7.7	7.7	27.7	27.7	20.3	7.7	27.7	7.7	13.3	7.7	23.1	13.3	40.0
			9.6	16.7	16.7	9.6	9.6	34.7	34.7	25.4	9.6	34.7	9.6	16.7	9.6	28.8	16.7	50.0
Basal			1.1	3.3	3.3	7.8	2.2	7.8	11.1	4.4	1.1	12.2	1.1	3.3	4.4	6.7	3.3	13.3

Fig. S8. IFN-γ secretion by ZnT8$_{186-194}$-reactive CD8$^+$ T cells. (**A**) T1D and healthy donors previously analyzed by *ex-vivo* MMr staining for whom sufficient PBMCs remained were further analyzed by IFN-γ ELISpot as described (*7*). Briefly, unfractionated PBMCs ($3x10^5$/well) were plated in triplicate in anti-IFN-γ antibody-coated ELISpot PVDF plates in the presence of 10 μM ZnT8$_{186-194}$ or Flu MP$_{58-66}$ peptide or DMSO vehicle diluted in AIM-V medium supplemented with 0.5 U/ml IL-7. After 18 h, plates were revealed with biotin-conjugated anti-IFN-γ antibodies (U-CyTech), alkaline phosphatase-conjugated streptavidin and NBT-BCIP substrate, and counted on a BioSys Bioreader 5000 Pro-SF. Results are expressed as frequencies of epitope-reactive T cells out of total PBMCs after subtraction of background responses in the presence of DMSO alone (which were $\leq 10^{-5}$ in all cases). The dotted line represents the median cut-off for a positive response, which was set at 3 SDs above the average background for each individual, as previously determined by receiver-operator characteristics analysis (*3*). **p*=0.03 by Mann-Whitney test. (**B**) The corresponding raw IFN-γ ELISpot counts. All values, including basal + nSD cutoffs, are expressed as spot-forming cells/10^6 PBMCs with baseline subtraction. Non-subtracted basal values (reactivities to DMSO) are shown in the last row of each column. Reactivities are ranked as low (between 3 and 4 SD, yellow), intermediate (between 4 and 5 SD, orange), and high (>5 SD, red). The percentage of T1D and healthy subjects positive for each epitope is indicated in the second and third column, respectively. PHA was used as a polyclonal positive control. +++, off-scale ELISpot reading.

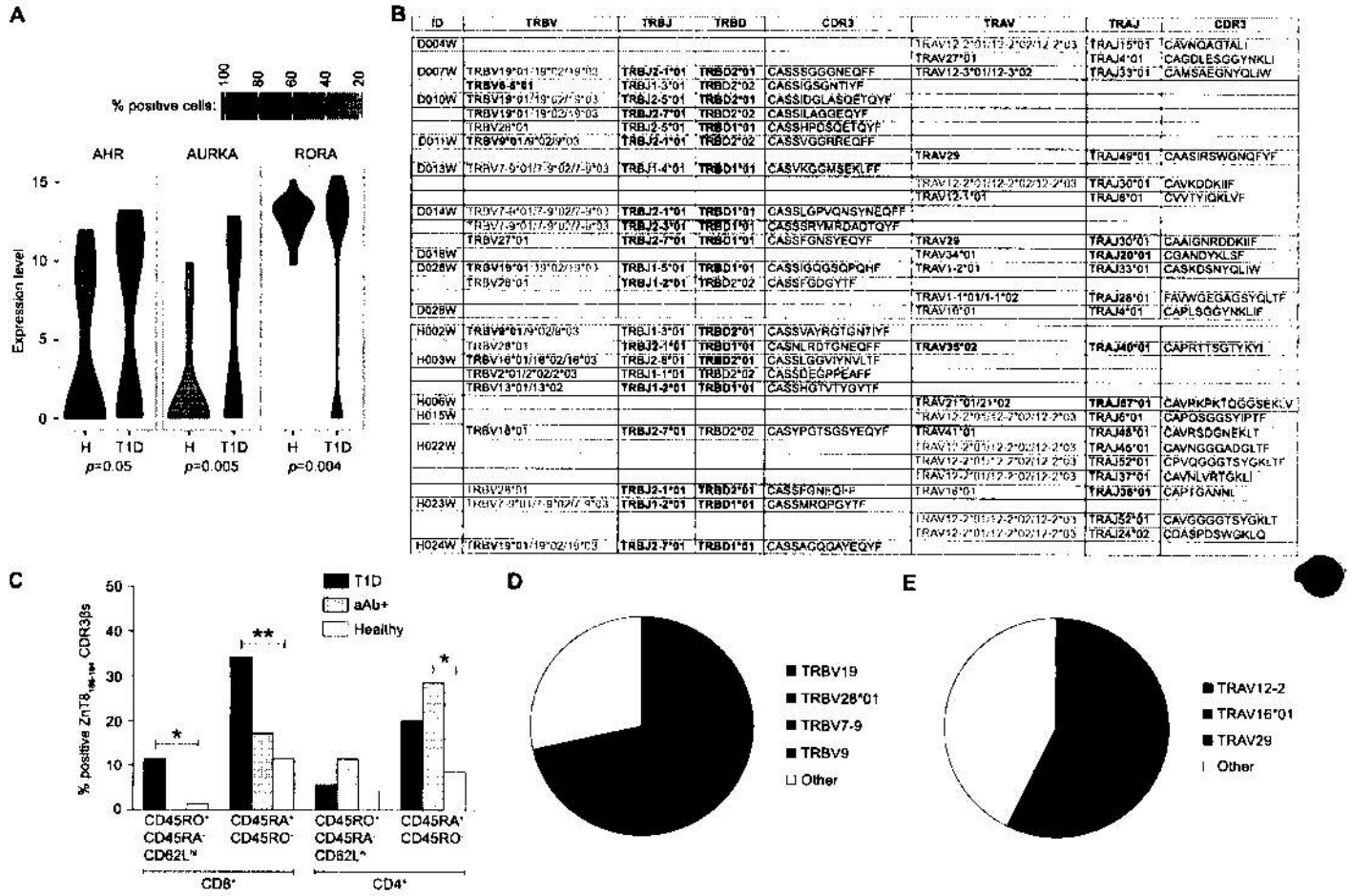

Fig. S9. Gene expression in *ex-vivo* single-sorted $ZnT8_{186\text{-}194}$ MMr^+CD8^+ T cells. (**A**) Genes differentially expressed in individual $ZnT8_{186\text{-}194}$ MMr^+CD8^+ T cells from T1D and healthy subjects. Single cells were sorted into empty PCR wells, cDNA synthesized with a Superscript VILO RT Kit (Invitrogen) was preamplified for 16 cycles with TATAA GrandMaster Mix and 61 primer pairs (Table S6) as follows: 1x [95°C 8 min], 16x [95°C 45 sec, 49°C 1 min (with 0.3°C increment/cycle), 72°C 1.5 min], 1x [72°C 7 min]. RT-PCR was carried out on a Fluidigm BioMark HD with the 96.96 Dynamic Array IFC, the GE 96x96 Fast PCR+ Melt protocol and SsoFast EvaGreen Supermix with Low ROX (Biorad), with 5 μM primers per assay. Data were analyzed using Fluidigm Real-Time PCR software followed by KNIME 2.5.2 and R 3.2.2 (www.r-project.org). Pre-processing *via* a linear model to correct for confounding effects was performed as described (*43*). The semi-continuous Hurdle model was subsequently applied to account for bimodal gene expression in single cells, allowing assessment of differential expression with respect to both the frequency of expression and the positive expression means *via* a likelihood ratio test. Violin plots display the density of expression (max.Ct–Ct) of genes that differ significantly between T1D and healthy donors (n=32 and n=25 $ZnT8_{186\text{-}194}$ MMr^+CD8^+ T cells from 11 and 6 individuals, respectively). Blue shading illustrates the proportion of positive cells. *p* values were calculated with the Hurdle model. (**B**) *TRB* and *TRA* gene usage and the corresponding CDR3 aminoacid sequences of single-sorted cells from T1D (top, D-coded IDs) and healthy donors (bottom, H-coded IDs). Each line corresponds to an individual T cell. *TRBV* and *TRAV* genes shared with $ZnT8_{186\text{-}194}$-reactive clones obtained from separate subjects are shown in bold; repeatedly used genes are shown in color. (**C**) Prevalence of the CDR3β aminoacid sequences obtained from single-sorted cells among HLA-$A2^+$ T1D (n=5), aAb^+ (n=5) and healthy subjects (n=10), as assessed by *in-silico* analysis of CDRβ repertoires obtained from the indicated $CD8^+$ and $CD4^+$ T-cell subsets. *$p \leq 0.04$, **$p=0.008$ by Fisher's exact test. (**D-E**) Distribution of *TRBV* (D) and *TRAV* (E) gene usage among $ZnT8_{186\text{-}194}$ MMr^+CD8^+ T cells. Color codes are matched to panel B.

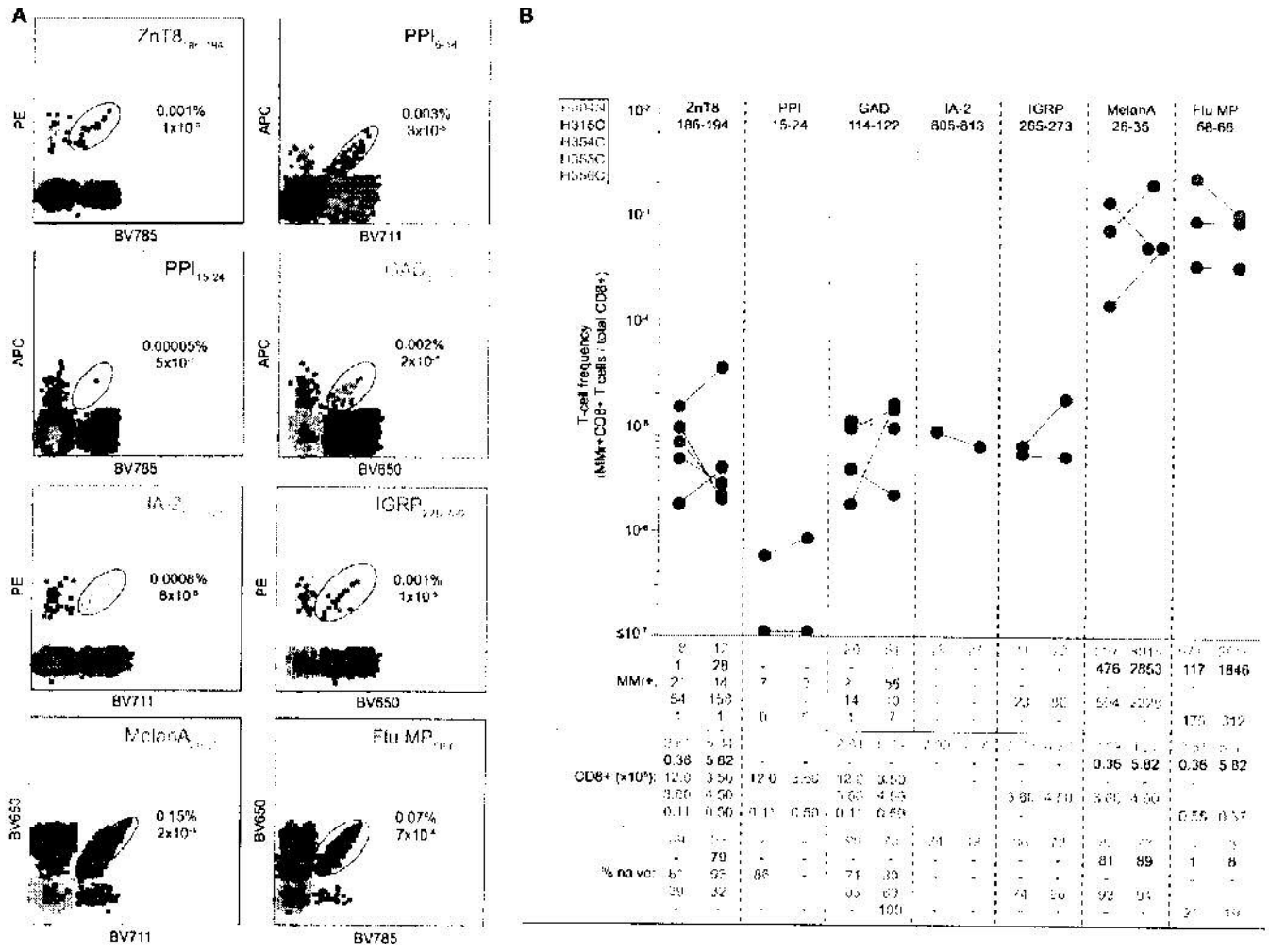

Fig. S10. Extended combinatorial MMr panel for the analysis of multiple islet-reactive CD8$^+$ T-cell populations, and reproducibility of *ex-vivo* MMr assays. (**A**) After magnetic depletion of CD8$^-$ cells, PBMCs were sequentially gated as depicted in Fig. S7 and the indicated MMr$^+$ populations were visualized using the gating strategy previously detailed for combinatorial MMr staining (*9*) and the FlowJo v10 software. The staining panel also included Live/Dead Aqua, anti-CD3-APC-H7 (clone SK7, BD), anti-CD8-PE-Cy7 (clone SK1, eBioscience), anti-CD45RA-FITC (clone HI100, eBioscience) and anti-CCR7-BV421 (clone 150503, BD). The final readout obtained for T1D patient D322D after gating out events positive for <2 or >2 MMr fluorochromes is shown, with events corresponding to each epitope-reactive population depicted in different colors within each plot, and MMr$^-$ events depicted in grey. (**B**) Reproducibility between the 3-MMr panel depicted in Fig. S7 and the extended 8-MMr panel presented here. Separate blood draws from 5 subjects (H004N, green; H315C, black; H354C, red; H355C, grey; H356C, blue) were analyzed with both panels and the frequency counts were compared. The corresponding MMr$^+$ and total CD8$^+$ T-cell counts (x10^6) are indicated with the same color code below each distribution, together with the percentage of naïve (CD45RA$^+$CCR7$^+$) cells in each MMr$^+$ fraction (for fractions ≥5 MMr$^+$ cells).

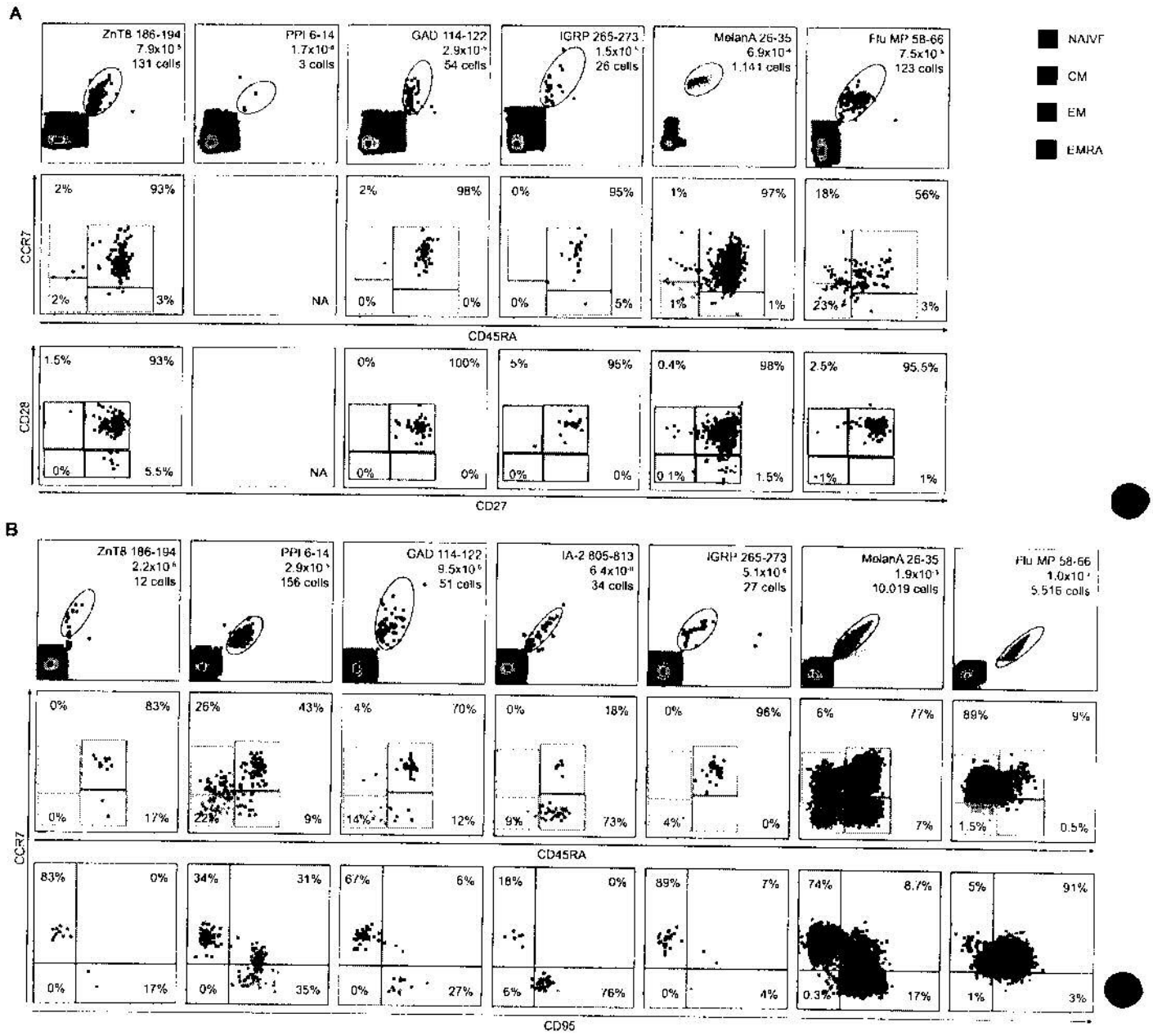

Fig. S11. CD27, CD28 and CD95 expression on ZnT8$_{186-194}$-reactive CD8$^+$ T cells. (A) Representative CD27/CD28 staining of MMr$^+$CD8$^+$ T cells from subject H372C. The first row depicts the fraction of MMr$^+$ cells for each of the indicated epitopes. The corresponding frequency out of the total 1.7x10^6 CD8$^+$ T cells acquired and the number of MMr$^+$ events counted are indicated. The second row shows the percent distribution of naïve (CD45RA$^+$CCR7$^+$; grey), central memory (CM, CD45RA$^-$CCR7$^+$; blue), effector memory (EM, CD45RA$^-$CCR7$^-$; green) and terminally differentiated EM CD45RA$^+$ cells (EMRA, CD45RA$^+$CCR7$^-$; red) within each MMr$^+$ fraction. The third row depicts CD27 (AlexaFluor700-labeled clone O323, eBioscience) and CD28 expression (BV421-labeled clone CD28.2, BioLegend) within each of these subsets, using the same color code, with total percent cells indicated in each quadrant. NA, not available (<5 MMr$^+$ events counted). **(B)** Representative CD95 staining (PE/CF594-labeled clone DX2, BD) for MMr$^+$CD8$^+$ T cells from subject H004N. A total of 5.3x10^6 CD8$^+$ T cells was acquired, and data are represented as in panel A. Results are representative of 4 subjects tested.

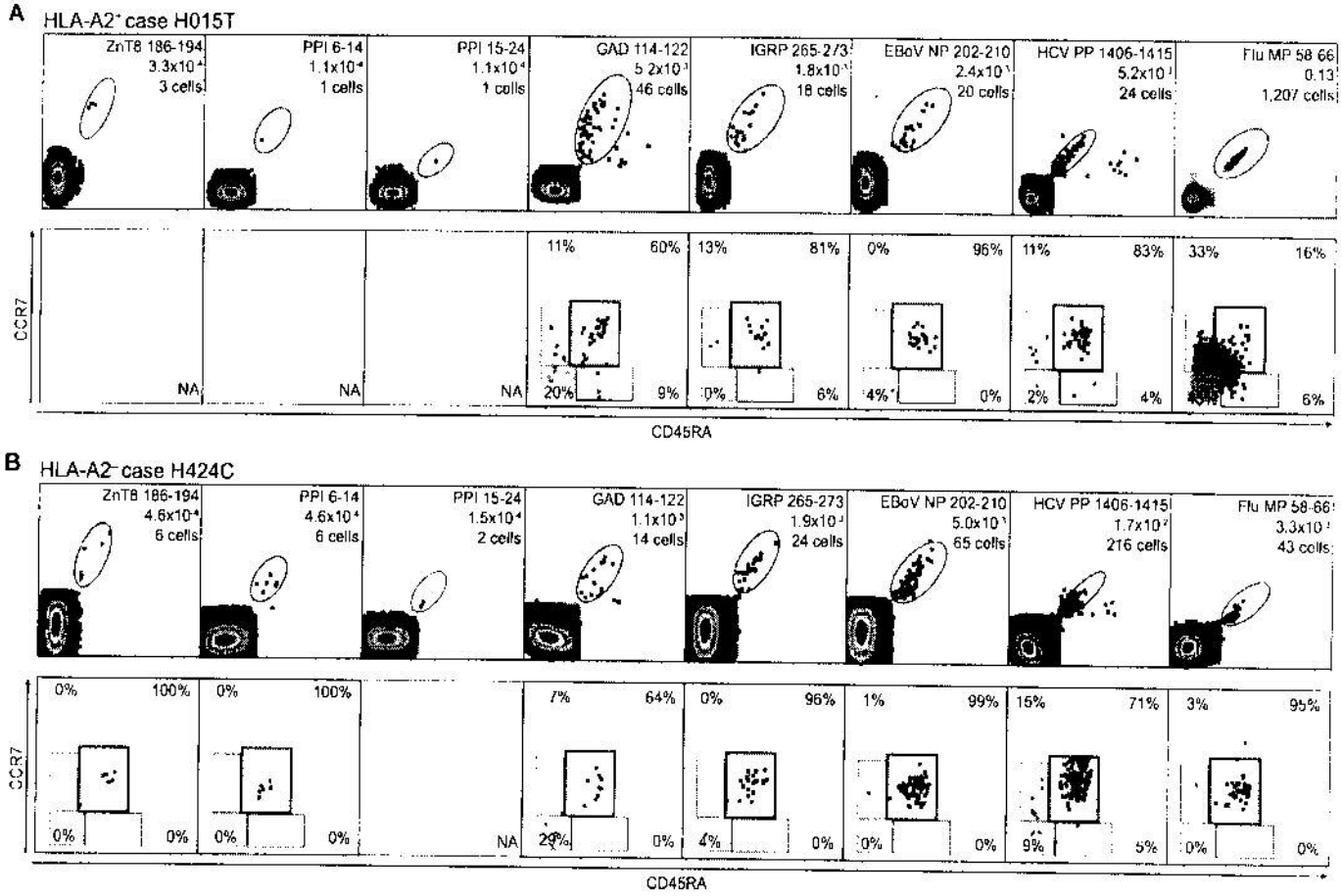

Fig. S12. Representative MMr and CD45RA/CCR7 dot plots for HLA-A2$^+$ and HLA-A2$^-$ healthy donors depicted in Fig. 6F-G. (**A**) MMr (top row) and CD45RA/CCR7 staining (bottom row) for each of the indicated epitopes for HLA-A2$^+$ case H015T. The corresponding frequency out of the total $0.9x10^6$ CD8$^+$ T cells acquired and the number of MMr$^+$ events counted are indicated in the top row. The second row shows the percent distribution of naïve (CD45RA$^+$CCR7$^+$; grey), central memory (CD45RA$^-$CCR7$^+$; blue), effector memory (CD45RA$^-$CCR7$^-$; green) and terminally differentiated EM CD45RA$^+$ cells (CD45RA$^+$CCR7$^-$; red) within each MMr$^+$ fraction, with percent cells indicated in each quadrant. NA, not available (<5 MMr$^+$ events counted). (**B**) The same representation is shown for HLA-A2$^-$ case H424C. A total of $1.3x10^6$ CD8$^+$ T cells was acquired.

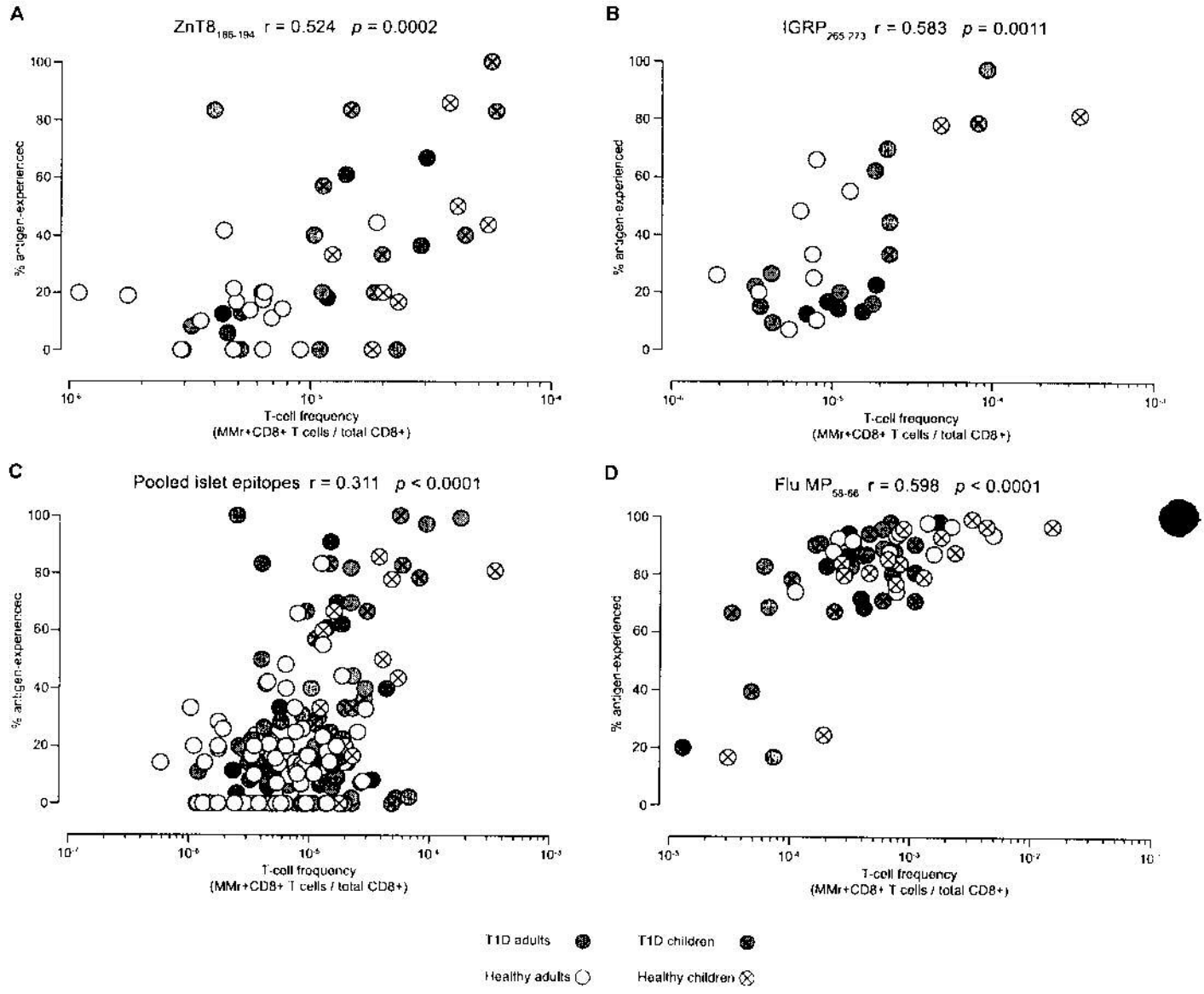

Fig. S13. Correlation between the frequency of $MMr^{+}CD8^{+}$ T cells and the Ag-experienced fraction within the same $MMr^{+}CD8^{+}$ population. (**A**) Correlation for $ZnT8_{186\text{-}194}$ $MMr^{+}CD8^{+}$ T cells. (**B**) Correlation for $IGRP_{265\text{-}273}$ $MMr^{+}CD8^{+}$ T cells. (**C**) Correlation for pooled $MMr^{+}CD8^{+}$ T cells recognizing all islet epitopes analyzed ($ZnT8_{186\text{-}194}$, $PPI_{6\text{-}14}$, $PPI_{15\text{-}24}$, $GAD_{114\text{-}122}$, $IA\text{-}2_{805\text{-}813}$, $IGRP_{265\text{-}273}$). (**D**) Correlation for Flu $MP_{58\text{-}66}$ $MMr^{+}CD8^{+}$ T cells. Graphs were obtained by compiling data presented in Fig. 5 for T1D patients (adults, grey circles; children, crossed grey circles) and age/sex-matched healthy donors (adults, white circles; children, crossed white circles). Values obtained by Spearman correlation analysis are shown for each graph.

Status	Donor	Age (yrs)	Gender (M/F)	T1D duration (days)	GADA	IA-2A	ZnT8A	Therapy	Sort strategy	Sorted wells	Growing wells	ZnT8 MMr+ wells	Cloning efficiency	Clones	Source cell
T1D	D220	60	M	3	+		+	Insulin	In vitro	100	5	3	3%	1	ND
														2	ND
														3	ND
T1D	D010R	12	M	8	-	+	-	Insulin	Ex vivo	50	10	2	4%	1D3	CD45RA+CCR7+
														(1E2)	CD45RA+CCR7+
T1D	D349V	62	F	6	+	+	+	Insulin	Ex vivo	87	1	1	1%	17B9	CD45RA+CCR7+
T1D	D267T	25	F	12	+	ND	-	Insulin	Ex vivo	50	7	1	2%	33B8	CD45RA+CCR7+
T1D	D351D	32	M	57	+	-	-	Insulin	Ex vivo	132	6	3	2%	18C3	CD45RA+CCR7+
														18D3	CD45RA+CCR7+
H	H017N	34	F	NA				None	In vitro	80	8	1	1%	A1	ND
H	H314C	24	M	NA	-	-	ND	None	Ex vivo	80	2	1	2%	6C4	CD45RA+CCR7+
H	H328C	29	M	NA	-	-	ND	None	Ex vivo	45	12	0	0%	NA	NA
									In vitro	119	28	3	2%	9E8	ND
														9G8	ND
														0B3	ND
H	H079D	30	F	NA	-		-	None	Ex vivo	260	7	1	0.4%	42D6	CD45RA+CCR7+
H	H034O	43	F	NA	-	-	-	None	Ex vivo	80	1	1	1%	14H9	ND

Table S1. Summary of $ZnT8_{186-194}$-reactive $CD8^+$ T-cell clones. Clones in parentheses could not be stabilized in long-term cultures and underwent more limited characterization. For those clones obtained after *ex-vivo* index sorting of $ZnT8_{186-194}$ MMr^+ cells, the surface phenotype of the source cell is indicated in the last column. NA, not applicable; ND, not determined; GADA, GAD aAbs; IA-2A, IA-2 aAbs; ZnT8A, ZnT8 aAbs.

Study group	Case ID	Age (years)	Gender (M/F)	T1D duration (Months)	HLA-A*02 status	IAA	GADA	IA-2A	ZnT8A	Therapy
T1D (n=10)	jdrfT1D1	21	M	3.6	-	+	+	+	+	Insulin
	jdrfT1D2	38	M	17.7	-	+	+	+	+	Insulin
	jdrfT1D3	50	F	34.6	-	+	+	-	-	Insulin
	sbirT1D3	25	M	25.7	-	+	-	+	-	Insulin
	sbirT1D4	44	M	10.2	-	-	-	-	-	Insulin
	sbirT1D5	16	M	17.2	+	-	-	-	-	Insulin
	sbirT1D6	20	F	15.4	+	+	+	-	-	Insulin
	sbirT1D7	25	F	10.7	+	-	+	+	+	Insulin
	sbirT1D8	41	M	8.3	+	-	+	-	-	Insulin
	sbirT1D9	17	M	8.3	+	+	+	-	-	Insulin
At-risk (n=7)	jdrfAB+ 2	44	F	NA	+	+	-	-	-	None
	jdrfAB+ 3	59	M	NA	-	+	+	-	-	None
	jdrfAB+ 4	29	M	NA	+	-	+	+	-	None
	jdrfAB+ 5	49	F	NA	+	-	+	+	-	None
	jdrfAB+ 6	53	M	NA	+	-	+	+	+	None
	jdrfAB+ 7	32	F	NA	-	-	+	-	-	None
	jdrfAB+ 9	17	F	NA	+	-	+	+	+	None
Healthy (n=12)	control1	24	F	NA	+	-	-	-	-	None
	control2	38	F	NA	-	-	-	-	-	None
	control3	22	F	NA	+	-	-	-	-	None
	sbirControl1	27	F	NA	+	-	-	-	-	None
	sbirControl3	22	M	NA	+	-	-	-	-	None
	sbirControl4	27	M	NA	+	-	-	-	-	None
	sbirControl5	25	F	NA	+	-	-	-	-	None
	sbirControl6	40	M	NA	+	-	-	-	-	None
	sbirControl7	33	M	NA	-	-	-	-	-	None
	sbirControl8	37	M	NA	+	-	-	-	-	None
	sbirControl9	21	M	NA	+	-	-	-	-	None
	sbirControl10	35	M	NA	+	-	-	-	-	None

Table S2. Characteristics of study subjects for *in-silico TRB* analyses. IAA, insulin aAbs; NA, not applicable.

Pediatric subjects - T1D

Case ID	Age (years)	Gender (M/F)	T1D duration (Months)	IAA	GADA	IA-2A	ZnT8A	Therapy
D001W	13	F	18	+	-	-	-	Insulin
D004W	15	F	13	ND	+	+	+	Insulin
D007W	10	F	30	ND	+	+	+	Insulin
D008W	11	M	6	ND	+	+	+	Insulin
D009W	10	F	5	ND	+	+	+	Insulin
D010W	17	M	15	ND	+	+	+	Insulin
D011W	10	M	5	ND	+	+	+	Insulin
D013W	10	M	13	ND	+	-	+	Insulin
D014W	14	M	18	ND	+	+	+	Insulin
D016W	18	M	19	ND	+	-	+	Insulin
D019W	8	M	12	+	-	-	-	Insulin
D027W	10	M	23	ND	+	+	+	Insulin
D028W	13	M	24	ND	-	+	+	Insulin
D001R	8	F	0.2	-	+	+	ND	Insulin
D006R	14	M	0.3	+	-	-	ND	Insulin
D016R	12	F	0.3	ND	+	-	ND	Insulin
N=16	12	38% F	15		75% +	63% +	65% +	100% insulin
	8-18	62% M	0.2-24		25% -	37% -	15% -	

Adult subjects - T1D

Case ID	Age (years)	Gender (M/F)	T1D duration (Months)	IAA	GADA	IA-2A	ZnT8A	Therapy
D015H	24	F	0.2	ND	+	+	+	Insulin
D026W	23	M	8.0	ND	+	+	+	Insulin
D267T	25	F	0.4	ND	+	ND	-	Insulin
D291V	33	M	0.2	ND	+	+	+	Insulin
D292V	28	M	0.6	ND	-	+	ND	Insulin
D296D	25	F	0.1	ND	+	+	ND	Insulin
D307D	23	M	1.2	ND	-	+	ND	Insulin
D322D	31	M	0.2	ND	+	+	+	Insulin
D323D	48	M	0.2	ND	-	-	-	Insulin
D324D	28	F	2.6	ND	+	+	+	Insulin
D328V	26	F	0.2	-	+	-	+	Insulin
D329D	23	M	0.1	ND	+	+	-	Insulin
D330D	25	F	0.1	ND	+	-	+	Insulin
D338D	31	M	0.3	ND	+	+	+	Insulin
D339V	29	M	0.1	ND	+	+	+	Insulin
D347D	42	M	1.0	ND	+	+	+	Insulin
D349D	62	F	0.2	ND	+	+	+	Insulin
D350D	44	F	0.2	ND	-	+	-	Insulin
D351D	32	M	1.9	ND	+	-	-	Insulin
D354V	54	F	0.2	ND	+	+	+	Insulin
D355D	28	M	0.2	ND	+	+	+	Insulin
D359D	25	F	0.2	ND	+	+	+	Insulin
D363V	58	F	0.4	ND	+	+	-	Insulin
N=23	28	48% F	0.2		83% +	82% +	70% +	100% insulin
	23-62	52% M	0.1-6		17% -	18% -	30% -	

Pediatric subjects - Healthy

H003W	11	M	NA	ND	-	-	-	None
H005W	17	M	NA	ND	-	-	-	None
H006W	10	F	NA	ND	-	-	-	None
H012W	10	M	NA	ND	-	-	-	None
H015W	13	M	NA	ND	-	-	-	None
H017W	13	F	NA	ND	-	-	-	None
H018W	9	M	NA	ND	-	-	-	None
H020W	14	M	NA	ND	-	-	-	None
H021W	12	F	NA	ND	-	-	-	None
H022W	11	M	NA	ND	-	-	-	None
H023W	10	M	NA	ND	-	-	-	None
H024W	17	M	NA	ND	-	-	-	None
H025W	10	F	NA	ND	-	-	-	None
H095M	14	M	NA	ND	ND	ND	ND	None
H100M	13	M	NA	ND	ND	ND	ND	None
H103M	16	F	NA	ND	ND	ND	ND	None
H113M	11	F	NA	ND	ND	ND	ND	None
N=17	12	35% F			0% +	0% +	0% +	100% none
	9-17	65% M			100% -	100% -	100% -	

Adult subjects - Healthy

H002W	23	M	NA	ND	-	-	-	None
H004N	42	M	NA	-	-	-	ND	None
H005N	36	F	NA	-	-	-	ND	None
H015T	30	M	NA	-	-	-	ND	None
H017N	34	F	NA	ND	-	ND	-	None
H034O	43	F	NA	-	-	-	ND	None
H079O	35	F	NA	-	-	-	ND	None
H087N	33	M	NA	-	-	-	ND	None
H109S	64	M	NA	ND	ND	ND	ND	None
H170S	37	F	NA	ND	-	ND	ND	None
H297S	27	M	NA	ND	-	ND	ND	None
H312C	34	M	NA	ND	-	ND	ND	None
H314C	24	M	NA	ND	ND	ND	ND	None
H315C	40	F	NA	ND	-	ND	ND	None
H316C	25	F	NA	ND	ND	ND	ND	None
H321C	30	F	NA	ND	ND	ND	ND	None
H328C	29	M	NA	ND	ND	ND	ND	None
H333O	23	M	NA	ND	ND	ND	ND	None
H353C	40	M	NA	ND	-	ND	ND	None
H354C	25	F	NA	ND	-	ND	ND	None
H356C	26	M	NA	ND	-	ND	ND	None
H372C	22	F	NA	ND	ND	ND	ND	None
N=22	32	45% F						100% none
	22-64	55% M						

Table S3. Characteristics of HLA-A2$^+$ study subjects for *ex-vivo* MMr studies. Individual clinical profiles of T1D pediatric subjects (top left; n=16), age/sex-matched healthy pediatric subjects (bottom left; n=17), T1D adults (top right; n=23) and age/sex-matched healthy adults (bottom right; n=22) are shown along with their distribution within each group (median and range for numerical variables). ND, not determined; NA, not applicable.

Case ID	Age (yrs)	Gender (M/F)	HLA-A/B	Predicted HLA binding affinity (nM)							
				ZnT8 186-194	PPI 6-14	PPI 15-24	GAD 114-122	IGRP 265-273	EboV NP 202-210	HCV PP 1406-1415	Flu MP 58-66
H015T ▽	32	M	A*02:01	355	13	234	23	16	10	41	16
			NA	–	–	–	–	–	–	–	–
			NA	–	–	–	–	–	–	–	–
			NA	–	–	–	–	–	–	–	–
H311C ○	33	M	A*02:01	355	13	234	23	16	10	41	16
			A*01:01	14759	19182	33558	7213	19192	16505	26256	22016
			B*15:01	10716	2679	6813	4816	1290	2288	2251	12092
			B*44:02	25029	17913	25941	18087	18349	14949	27487	24697
H314C ◇	24	M	A*02:01	355	13	234	23	16	10	41	16
			A*68:01	15512	29930	43713	31674	22468	26846	35191	22471
			B*07:02	7498	7405	17414	28460	11781	3812	6075	16630
			B*44:02	25029	17913	25941	18087	18349	14949	27487	24697
H356C □	28	M	A*02:01	355	13	234	23	16	10	41	16
			A*01:01	14759	19182	33558	7213	19192	16505	26256	22016
			B*08:01	12180	5071	31975	15488	14954	4951	17633	11752
			B*49:01	NA	NA	NA	NA	NA	NA	NA	NA
H372C △	24	F	A*02:01	355	13	234	23	16	10	41	16
			A*26:01	21758	23637	36297	23966	20711	23427	26585	19347
			B*18:01	21582	17880	39939	23844	13228	21410	33037	19695
			B*44:02	25029	17913	25941	18087	18349	14949	27487	24697
H018N ▽	35	F	A*02:05	NA	NA	NA	NA	NA	NA	NA	NA
			A*30:02	10619	2111	12271	2619	5559	1870	9148	11631
			B*18:01	21582	17880	39939	23844	13228	21410	33037	19695
			B*50:01	NA	NA	NA	NA	NA	NA	NA	NA
H279S ■	33	M	A*01:01	14759	19182	33558	7213	19192	16505	26256	22016
			A*66:01	9110	11692	39995	18633	9799	10023	37091	8751
			B*08:01	12180	5071	31975	15488	14954	4951	17633	11752
			B*41:02	NA	NA	NA	NA	NA	NA	NA	NA
H355C ●	34	M	A*03:01	18409	4379	15490	11720	6945	1985	9370	15303
			A*24:02	12287	1678	34034	18766	3617	41	36129	7558
			B*07:02	7498	7405	17414	28460	11781	3812	6075	16630
			B*35:02	NA	NA	NA	NA	NA	NA	NA	NA
H423C ◆	24	M	A*03:01	18409	4379	15490	11720	6945	1985	9370	15303
			A*23:01	11384	968	36359	17176	5503	100	32936	6184
			B*07:02	7498	7405	17414	28460	11781	3812	6075	16630
			B*15:01	10716	2679	6813	4816	1290	2288	2251	12092
H424C ▲	28	F	A*32:01	2093	727	35528	11017	32	12	9322	82
			A*32:01	2093	727	35528	11017	32	12	9322	82
			B*44:02	25029	17913	25941	18087	18349	14949	27487	24697
			B*44:02	25029	17913	25941	18087	18349	14949	27487	24697

Table S4. Characteristics of HLA-A2$^+$ and HLA-A2$^-$ healthy donors for *ex-vivo* MMr studies. Predicted HLA Class I peptide binding affinities were calculated using NetMHC 4.0 (http://www.cbs.dtu.dk/services/NetMHC/). HLA-A2 (A*02:01) and predicted affinity values compatible with peptide binding to the indicated HLA allotypes are highlighted in red. NA, not available.

	nPOD case	Sex	Age (yrs)	T1D T2D (yrs)	Positive aAbs	C-peptide (ng/ml)	ZnT8 MMr+		MelanA MMr+		CDR3β+
							Pa	PLN	Pa	PLN	PLN
T1D (n=9)	6070	F	23	7	IA-2/mIAA	<0.05	74	0	0	NA	NA
	6161	F	19	7	IA-2/mIAA	<0.05	124	1176	0	0	8-18-0
	6211	F	24	4	GAD/IA-2/ZnT8/mIAA	<0.05	30	60	0	54	0-0-0
	6212	M	20	5	mIAA	<0.05	0	0	NA	NA	14-0-0
	6237	F	18	12	GAD/mIAA	<0.05	267	0	0	NA	NA
	6242	M	39	19	IA-2/mIAA	<0.05	66	101	0	0	0-0-5
	6243	M	13	5	mIAA	0.42	0	209	NA	0	0-0-0
	6258	F	39	37	mIAA	<0.05	118	299	0	0	NA
	6325	F	20	6	GAD/IA-2	0.14	28	0	0	0	NA
aAb+ (n=9)	6080	F	69	NA	GAD/mIAA	1.84	55	50	25	61	NA
	6101	M	65	NA	GAD	26.18	0	0	NA	NA	NA
	6123	F	23	NA	GAD	2.01	0	0	NA	NA	NA
	6151	M	30	NA	GAD	5.49	28	NA	0	NA	NA
	6154	F	49	NA	GAD	<0.05	64	NA	0	NA	NA
	6171	F	4	NA	GAD	8.95	37	0	0	NA	NA
	6347	M	9	NA	mIAA	3.26	33	60	0	191	NA
	6388	F	25	NA	GAD/mIAA	1.38	34	35	0	0	NA
	6397	F	21	NA	GAD	12.8	42	189	0	0	NA
No diabetes (n=11)	6103	M	2	NA	—	0.98	55	0	0	NA	NA
	6179	F	20	NA	—	2.74	96	150	0	0	NA
	6182	M	3	NA	—	2.28	23	163	0	65	NA
	6227	F	17	NA	—	2.75	3	0	0	NA	NA
	6234	F	20	NA	—	6.89	6	0	0	NA	NA
	6254	M	38	NA	—	6.43	0	0	NA	NA	0-4-0
	6271	M	17	NA	—	11.47	0	0	NA	0	0-0-0
	6287	F	57	NA	—	4.75	4	0	0	NA	9-0-0
	6289	M	19	NA	—	8.05	0	0	NA	NA	0-0-0
	6357	M	5	NA	—	8.82	0	0	NA	NA	NA
	6366	F	21	NA	—	0.41	0	0	NA	NA	NA
T2D (n=3)	6028	M	33	17	—	22.40	0	0	NA	NA	NA
	6059	F	19	0.3	—	10.68	0	107	NA	0	NA
	6275	M	48	2	—	3.46	0	0	NA	NA	0-2-0
Other	6288	M	55	NA	—	12.96	211	87	0	0	250-0-0

Table S5. Characteristics of nPOD cases for *in-situ* ZnT8$_{186-194}$ MMr staining. The clinical caracteristics of each case are reported along with the counts ($x10^{-3}$) of ZnT8$_{186-194}$ and MelanA$_{26-35}$ MMr$^+$ cells/mm^2 pancreas (Pa) and PLN section area. Positive sections are marked in red. In several cases, the PLN CD8$^+$ T-cell repertoire was interrogated *in-silico* for the presence of immunodominant CDR3β aminoacid sequences retrieved from 3 ZnT8$_{186-194}$-reactive CD8$^+$ T-cell clones (Fig. 4D). The results of this *in-silico* search are reported in the last column, with numbers indicating the frequency of the 3 selected sequences (D010R 1E2, H1034O 141B9 and H328C 8E8, respectively) per 10^6 TCRs, and positive counts indicated in red. Case #6287 (presenting a circumscribed neuroendocrine tumor in the pancreatic pan-

body region; pan-tail region analyzed here) was classified as a non-diabetic control, while non-diabetic case #6288 was classified as 'other' based on a history of non-alcoholic cirrhosis and histological findings of chronic pancreatitis. NA, not applicable or not available; mIAA, micro-insulin aAbs.

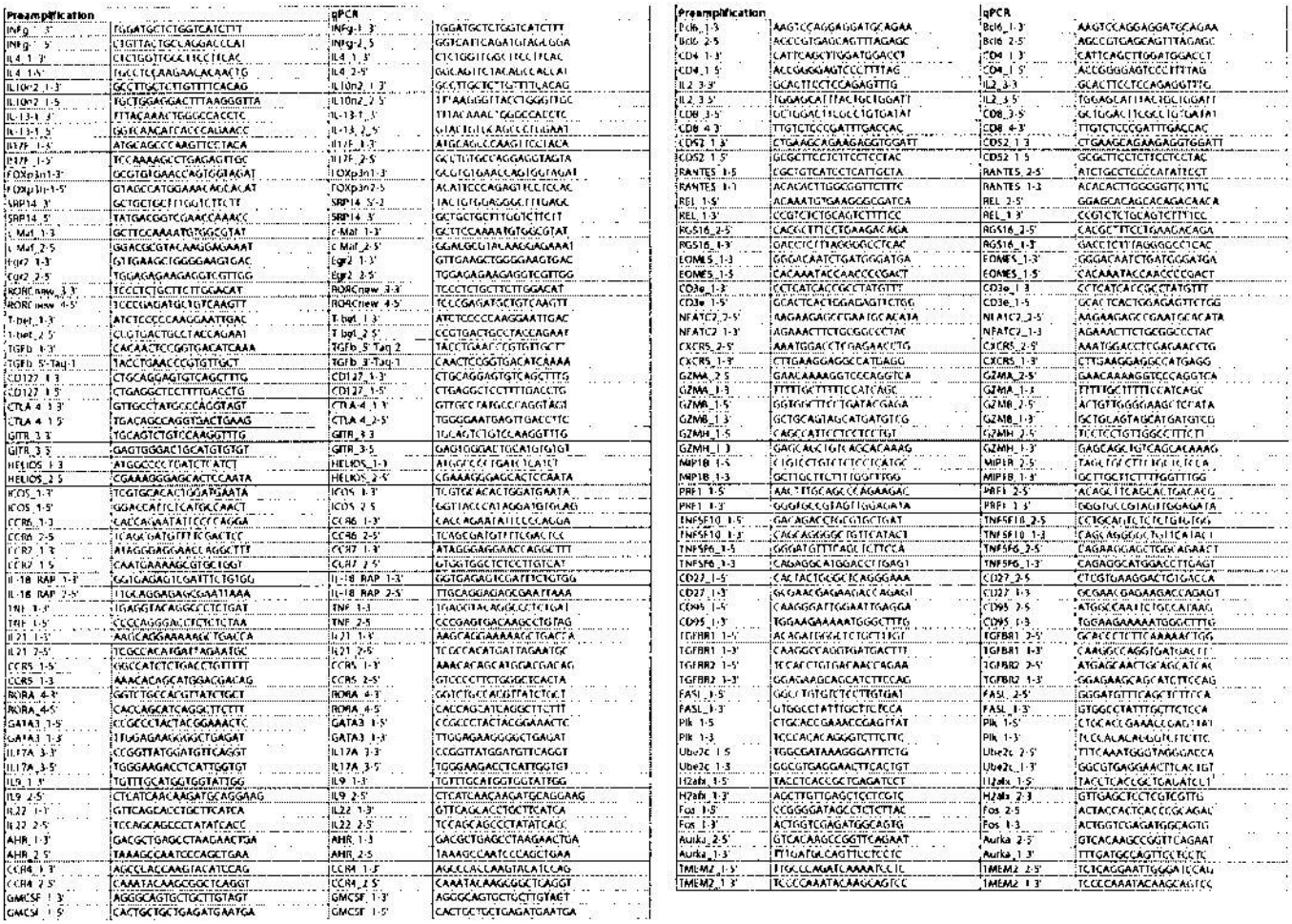

Preamplification		qPCR	
INFg_1_3'	TGGATGCTCTGGTCATCTTT	INFg_1_3'	TGGATGCTCTGGTCATCTTT
INFg_2_5'	CTGTTACTGCCAGGACCCAT	INFg_2_5'	GGTCATTCAGATGTAGCGGA
IL4_1_3'	CTCTGGTTGGCTTCCTTCAC	IL4_1_3'	CTCTGGTTGGCTTCCTTCAC
IL4_1_5'	TACCTCGAAGAACACAACTG	IL4_2_5'	GACAGTTCTACATCCACCAT
IL10rt2_1_3'	GCCTTGCTCTTGTTTTCACAG	IL10rt2_1_3'	GCCTTGCTCTTGTTTTCACAG
IL10rt2_1_5'	TGCTGGAGGACTTTAAGGGTTA	IL10rt2_2_5'	TTAAAGGGTTACCTGGGTTGC
IL-13_1_3'	TTTACAAACTGGGGCATCCTC	IL-13_1_3'	TTTACAAACTGGGGCATCCTC
IL-13_1_5'	GGGCATGATCACCCATAACC	IL-13_2_5'	GTATTGTTCAGCCCTTGAAT
IL17F_1_3'	ATGCAGCCCAAGTTCCTACA	IL17F_1_3'	ATGCAGCCCAAGTTCCTACA
IL17F_1_5'	TCCAAAAGCCTGAGAGTTGC	IL17F_2_5'	GCCTGTGCCAGGAGGTAGTA
FOXp3rt1-3'	GCGTGTGAACCAGTGGTAGAT	FOXp3rt1_3'	GCGTGTGAACCAGTGGTAGAT
FOXp3rt1-5'	GTAGCCATGGAAACAGCACAT	FOXp3rt2_5	ACATTCCCAGAGTTCCTCAC
SRP14_3'	GCTGCTGCTTTGGTCTCTCTT	SRP14_3'-2	TACTGTGGAGGGCTTTGAGC
SRP14_5'	TATGACGGTCGAACCAAACC	SRP14_3'	GCTGCTGCTTTGGTCTTCTT
c-Maf_1-3	GCTTCCAAAATGTGGCGTAT	c-Maf_1-3'	GCTTCCAAAATGTGGCGTAT
c-Maf_2-5	GGACGCGTACAAGGAGAAAT	c-Maf_2-5'	GGACGCGTACAAGGAGAAAT
Egr2_1-3'	GTTGAAGCTGGGGAAGTGAC	Egr2_1-3'	GTTGAAGCTGGGGAAGTGAC
Egr2_2-5'	TGGAGAGAAGAGGTCGTTGG	Egr2_2-5'	TGGAGAGAAGAGGTCGTTGG
RORCnew_3-3'	TCCCTCTGCTTCTTGGACAT	RORCnew_3-3'	TCCCTCTGCTTCTTGGACAT
RORCnew_4-5'	TCCCGAGATGCTGTCAAGTT	RORCnew_4-5'	TCCCGAGATGCTGTCAAGTT
T-bet_1-3'	ATCTCCCCCAAGGAATTGAC	T-bet_1-3'	ATCTCCCCCAAGGAATTGAC
T-bet_2-5'	CTGTCACTGCCTACCAGAAT	T-bet_2-5'	CCGTGACTGCCTACCAGAAT
TGFb_3-5'	CACAACTCCGGTGACATCAAA	TGFb_3-Taq-2	TACCTGAACCCGTGTTGCTT
TGFb_5'-Taq-1	TACCTGAACCCGTGTTGCT	TGFb_3-Taq-1	CAACTCCGGTGACATCAAAA
CD127_1-3	CTGCAGGAGTGTCAGCTTTG	CD127_1-3'	CTGCAGGAGTGTCAGCTTTG
CD127_1-5'	CTGAGGCTCCTTTTGACCTG	CD127_1-5'	CTGAGGCTCCTTTTGACCTG
CTLA-4_1-3'	GTTGCCTATGCCCAGGTAGT	CTLA-4_1-3'	GTTGCCTATGCCCAGGTAGT
CTLA-4_1-5'	TGACAGCCAGGTGACTGAAG	CTLA-4_2-5'	TGGGGAATGAGTTGACCTTC
GITR_3-3'	TGCAGTCTGTCCAAGGTTTG	GITR_3-3	TGCAGTCTGTCCAAGGTTTG
GITR_3-5'	GAGTGGGACTGCATGTGTGT	GITR_3-5	GAGTGGGACTGCATGTGTGT
HELIOS_1-3	ATGGCCCCTTCATCTCATCT	HELIOS_1-3	ATGGCCCCTGATCTCATCT
HELIOS_2-5	CGAAAGGGAGCACTCCAATA	HELIOS_2-5'	CGAAAGGGAGCACTCCAATA
ICOS_1-3'	TCGTGCACACTGGATGAATA	ICOS_1-3'	TCGTGCACACTGGATGAATA
ICOS_1-5'	GGGACCATTCTCATGCCAACT	ICOS_2-5	GGTTACCCATAGGATGTGAAG
CCR6_1-3	CACCAGAATATTCCCCAGGA	CCR6_1-3'	CACCAGAATATTCCCCAGGA
CCR6_2-5	TCAGCGATGTTTTCGACTCC	CCR6_2-5'	TCAGCGATGTTTTCGACTCC
CCR7_1-3	ATAGGGAGGAACCAGGCTTT	CCR7_1-3'	ATAGGGAGGAACCAGGCTTT
CCR7_1-5	CAATGAAAAGCGTGCTGGT	CCR7_2-5'	GTGGTGGCTCTCCTTGTCAT
IL-18_BAP_1-3'	GGTGAGAGTCGATTTCTGTGG	IL-18_BAP_1-3'	GGTGAGAGTCGATTTCTGTGG
IL-18_BAP_2-5'	TTGCAGGAGAAGCAAATTAAA	IL-18_BAP_2-5'	TTGCAGGAGAAGCAAATTAAA
TNF_1-3'	TGAGGTACAGGCCCTCTGAT	TNF_1-3	TGAGGTACAGGCCCTCTGAT
TNF_1-5'	CCCCAGGGACCTCTCTCTAA	TNF_2-5	CCCGAGTGACAAGCCTGTAG
IL21_1-3'	AAGCAGGAAAAAGCTGACCA	IL21_1-3'	AAGCAGGAAAAAGCTGACCA
IL21_2-5'	TCGCCACATGATTAGAATGC	IL21_2-5	TCGCCACATGATTAGAATGC
CCR5_1-5'	GGCCATCTCTGACCTGTTTT	CCR5_1-3'	AAACACAGCATGGACGACAG
CCR5_1-3	AAACACAGCATGGACGACAG	CCR5_2-5'	GTCCCCTTCTGGGCTCACTA
RORA_4-3'	GGTCTGCCACGTTATCTGCT	RORA_4-3'	GGTCTGCCACGTTATCTGCT
RORA_4-5'	CACCAGCATCAGGCTTCTTT	RORA_4-5'	CACCAGCATCAGGCTTCTTT
GATA3_1-5'	CCGCCCTACTACGGAAACTC	GATA3_1-5'	CCGCCCTACTACGGAAACTC
GATA3_1-3'	TTGGAGAAGGGGCTGAGAT	GATA3_1-3'	TTGGAGAAGGGGCTGAGAT
IL17A_3-3'	CCGGTTATGGATGTTCAGGT	IL17A_3-3'	CCGGTTATGGATGTTCAGGT
IL17A_3-5'	TGGGAAGACCTCATTGGTGT	IL17A_3-5'	TGGGAAGACCTCATTGGTGT
IL9_1_3'	TGTTTGCATGGTGGTATTGG	IL9_1-3'	TGTTTGCATGGTGGTATTGG
IL9_2-5'	CTCATCAACAAGATGCAGGAAG	IL9_2-5'	CTCATCAACAAGATGCAGGAAG
IL22_1-3'	GTTCAGCACCTGCTTCATCA	IL22_1-3'	GTTCAGCACCTGCTTCATCA
IL22_2-5'	TCCAGCAGCCCTATATCACC	IL22_2-5'	TCCAGCAGCCCTATATCACC
AHR_1-3'	GACGCTGAGCCTAAGAACTGA	AHR_1-3	GACGCTGAGCCTAAGAACTGA
AHR_2-5'	TAAAGCCAATCCCAGCTGAA	AHR_2-5	TAAAGCCAATCCCAGCTGAA
CCR4_1-3'	AGCCCACCAAGTACATCCAG	CCR4_1-3'	AGCCCACCAAGTACATCCAG
CCR4_2-5'	CAAATACAAGCGGCTCAGGT	CCR4_2-5'	CAAATACAAGCGGCTCAGGT
GMCSF_1-3'	AGGGCAGTGCTGCTTGTAGT	GMCSF_1-3'	AGGGCAGTGCTGCTTGTAGT
GMCSF_1-5'	CACTGCTGCTGAGATGAATGA	GMCSF_1-5'	CACTGCTGCTGAGATGAATGA

Preamplification		qPCR	
Bcl6_1-3	AAGTCCAGGAGGATGCAGAA	Bcl6_1-3'	AAGTCCAGGAGGATGCAGAA
Bcl6_2-5	ACCCGTGAGCAGTTTAGAGC	Bcl6_2-5'	ACCCGTGAGCAGTTTAGAGC
CD4_1-3'	CATTCAGCTTGGATGGACCT	CD4_1_3'	CATTCAGCTTGGATGGACCT
CD4_1_5'	ACCGAGGAGTCCCTTTTAG	CD4_1_5'	ACCGGGGAGTCCCTTTTAG
IL2_3-5'	GCACTTCCTCCAGAGGTTTG	IL2_3-3	GCACTTCCTCCAGAGGTTTG
IL2_3_5'	TGGAGCATTTACTGCTGGATT	IL2_3_5'	TGGAGCATTTACTGCTGGATT
CD8_3-5'	GCTGGACTTCGCCTGTCATAT	CD8_3-5'	GCTGGACTTCGCCTGTCATAT
CD8_4-3'	TTGTCTCCCGATTTGACCAC	CD8_4-3'	TTGTCTCCCGATTTGACCAC
CD52_1_3'	CTGAAGCAGAAGAGGTGGATT	CD52_1_3	CTGAAGCAGAAGAGGTGGATT
CD52_1_5'	GCGCTTCCTCTTCCTCCTAC	CD52_1-5	GCGCTTCCTCTTCCTCCTAC
RANTES_1-5	CGCTGTCATCCTCATTGCTA	RANTES_2-5'	ATCTGCCTCCCCATATTCCT
RANTES_1-3	ACACACTTGGCGGTTCTTTC	RANTES_1-3	ACACACTTGGCGGTTCTTTC
REL_1-5'	ACAAATGTGAAGGGCGATCA	REL_2-5'	GGAGCACAGCACACAGCAACA
REL_1-3'	CCGTCTCTGCAGTCTTTTCC	REL_1-3'	CCGTCTCTGCAGTCTTTTCC
RGS16_2-5'	CACGCTTCCTGAAGACAGA	RGS16_2-5'	CACGCTTCCTGAAGACAGA
RGS16_1-3'	GACCTCTTTAGGGGCCTCAC	RGS16_1-3'	GACCTCTTTAGGGGCCTCAC
EOMES_1-3	GGGACAATCTGATGGGATGA	EOMES_1-3'	GGGACAATCTGATGGGATGA
EOMES_1-5	CACAAATACCAACCCCGACT	EOMES_1-5'	CACAAATACCAACCCCGACT
CD3e_1-3'	CCTCATCACCGCCTATGTTT	CD3e_1-3	CCTCATCACCGCCTATGTTT
CD3e_1-5'	GCACTCACTGGAGAGTTCTGG	CD3E_1-5	GCACTCACTGGAGAGTTCTGG
NFATC2_2-5'	AGAAAGAGCCGAATGCACATA	NFATC2_2-5'	AGAAAGAGCCGAATGCACATA
NFATC2_1-3'	AGAAACTTCTGCGGCCCTAC	NFATC2_1-3	AGAAACTTCTGCGGCCCTAC
CXCR5_2-5'	AAATGGACCTCTGAGAACCTG	CXCR5_2-5'	AAATGGACCTCTGAGAACCTG
CXCR5_1-3'	CTTGAAGGAGGCCATGAGG	CXCR5_1-3'	CTTGAAGGAGGCCATGAGG
GZMA_2-5	GAACAAAAGGTCCCAGGTCA	GZMA_2-5'	GAACAAAAGGTCCCAGGTCA
GZMA_1-3	TTTTTGCTTTTTCCATCAGC	GZMA_1-3	TTTTTGCTTTTTCCATCAGC
GZMB_1-5'	GGTGAACTTCTTGATACGAGA	GZMB_2-5'	ACTGTTGGGGAAGCTCTATA
GZMB_1-3'	GCTGCAGTAGCATGATGTCG	GZMB_1-3'	GCTGCAGTAGCATGATGTCG
GZMH_1-5	CAGCCATTCCTCCTCCTGT	GZMH_2-5	TCCTCCTGTTGGCCTTTCTT
GZMH_1-3'	GAGCAGCTGTCAGCACAAAG	GZMH_1-3'	GAGCAGCTGTCAGCACAAAG
MIP1B_1-5	CTGTCCTGTCTCTCCTCATGC	MIP1B_2-5	TAGATCCTTTGCTCTCCA
MIP1B_1-3	GCTTGCTTCTTTGGTTTGG	MIP1B_1-3'	GCTTGCTTCTTTGGTTTGG
PRF1_1-5'	AACTTGCAGCCCAGAAGAC	PRF1_2-5'	ACAGCTTCAGCACTGACACG
PRF1_1-3'	GGGTCCCGTAGTTGGAGATA	PRF1_1_3'	GGGTCCCGTAGTTGGAGATA
TNFSF10_1-5'	GACAGACCTGCGTGCTGAT	TNFSF10_2-5	CCTGCATTCTCTCTGTGTGG
TNFSF10_1-3'	CAGCAGGGGCTGTTCATACT	TNFSF10_1-3	CAGCAGGGGCTGTTCATACT
TNFSF6_1-5	GGGATGTTTCAGCTCTTCCA	TNFSF6_2-5'	CAGAAGGAGCTGGCAGAACT
TNFSF6_1-3	CAGAGGCATGGACCTTGAGT	TNFSF6_1-3'	CAGAGGCATGGACCTTGAGT
CD27_1-5'	CACTACTGCGCTCAGGGAAA	CD27_2-5	CTCGTGAAGGACTGTGACCA
CD27_1-3'	GCGAACGAGAAGACCAGAGT	CD27_1-3	GCGAACGAGAAGACCAGAGT
CD95_1-5'	CAAGGGATTGGAATTGAGGA	CD95_2-5	ATGGCCAATCTGCCATAAG
CD95_1-3'	TGGAAGAAAAATGGGCTTTG	CD95_1-3	TGGAAGAAAAATGGGCTTTG
EGFBR1_1-5'	ACAGATTGGCTCTGCTTGCT	EGFBR1_2-5'	GCACCTCTTCAAAAACTGG
EGFBR1_1-3'	CAAGGCCAGGTGATGACTTT	EGFBR1_1-3'	CAAGGCCAGGTGATGACTTT
TGFBR2_1-5'	TCCACCTGTGACAACCAGAA	TGFBR2_2-5'	ATGAGCAACTGCAGCATCAC
TGFBR2_1-3'	GGAGAAGCAGCATCTTCCAG	TGFBR2_1-3'	GGAGAAGCAGCATCTTCCAG
FASL_1-5'	GGCTTGTGTCTCCTTGTGAT	FASL_2-5'	GGGATGTTTCAGCTCTTTCA
FASL_1-3'	GTGGCCTATTTGCTTCTCCA	FASL_1-3'	GTGGCCTATTTGCTTCTCCA
Plk_1-5	CTGCACCGAAACCGAGTTAT	Plk_1-5'	CTCCACCGAAACCGAGTTAT
Plk_1-3	TCCCACACAGGGTCTTCCTC	Plk_1-3'	TCCCACACAGGGTCTTCCTC
Ube2c_1-5	TGGCGATAAAGGGATTTCTG	Ube2c_2-5'	TTTCAAATGGGTAGGGACCA
Ube2c_1-3	GGCGTGAGGAACTTCACTGT	Ube2c_1-3'	GGCGTGAGGAACTTCACTGT
H2afx_1-5	TACCTCACCGCTGAGATCCT	H2afx_1-5'	TACCTCACCGCTGAUATCCT
H2afx_1-3'	AGCTTGTTGAGCTCCTCGTG	H2afx_2-3	GTTGAGCTCCTCGTCGTTG
Fos_1-5'	CCGGGGATAGCCTCTCTTAC	Fos_2-5	ACTACCACTCACCCGCAGAC
Fos_1-3'	ACTGGTCGAGATGGGCAGTG	Fos_1-3	ACTGGTCGAGATGGGCAGTG
Aurka_2-5'	GTCACAAGCCGGTTCAGAAT	Aurka_2-5'	GTCACAAGCCGGTTCAGAAT
Aurka_1-3'	TTTGATGCCAGTTCCTCCTC	Aurka_1_3'	TTTGATGCCAGTTCCTCCTC
TMEM2_1-5'	TTGCCCAGATCAAAATCCTC	TMEM2_2-5'	TCTCAGGAATTGGGATCCAG
TMEM2_1_3'	TCCCCAAATACAAGCAGTCC	TMEM2_1_3'	TCCCCAAATACAAGCAGTCC

Table S6. Primers used for gene expression analysis of the individual ZnT8$_{186\text{-}194}$ MMr^{+}CD8^{+} T cells depicted in Fig. S9A.

Members of the ImMaDiab Study Group.

Jean-Claude Carel, Nadia Tubiana-Rufi, Laetitia Martinerie, Amélie Poidvin, Evelyne Jacqz-Aigrain, Laurence Corvez, Véronique Berruer (Robert Debré Hospital, Paris);
Jean-François Gautier, Baz Baz (Saint Louis Hospital, Paris);
Fabrizio Andreelli, Chloé Amouyal, Sophie Jaqueminet, Olivier Bourron, Agnès Hartemann (Pitié-Salpêtrière Hospital, Paris);
Amal Lemoine-Yazigi, Danièle Dubois-Laforgue (Cochin Hospital, Paris);
Florence Travert, Michel Marre (Bichat Hospital, Paris);
Philippe Chanson, Claire Briet (Kremlin-Bicêtre Hospital, Paris);
Pierre-Jean Guillausseau, Leila Ait-Bachir (Lariboisière Hospital, Paris);
Carole Collet, Frédéric Beziaud, Gwenaelle Petit-Aubert (Versailles André Mignot Hospital, Le Chesnay);
Sophie Christin-Maitre, Bruno Fève, Camille Vatier (Saint Antoine Hospital, Paris);
Najiba Lahlou (Laboratory of Hormonology, Cochin Hospital, Paris);
Prissile Bakouboula, Caroline Elie, Hélène Morel, Jean-Marc Treluyer (Clinical Research Unit Paris Centre Descartes, Paris);
Marie-Claude Gagnerault, Claire Maillard, Anna Jones (INSERM U1016, Cochin Institute, Paris).